BRIGHTNESS DISTRIBUTIONS IN COMPACT AND NORMAL GALAXIES

Thesis by

John Kormendy

In Partial Fulfillment of the Requirements
for the Degree of
Doctor of Philosophy

California Institute of Technology
Pasadena, California

1976

(Submitted April 9, 1976)

To my parents

ACKNOWLEDGEMENTS

It is a great pleasure to thank my adviser, Dr. W. L. W. Sargent, for suggesting this study of compacts, for continued practical support in its execution, for excellent advice on everything from the filling of liquid-cell filters to the philosophy of science, and, not least of all, for his patience.

I am grateful to Dr. H. W. Babcock and the Staff Members of Caltech and the Hale Observatories for very generous allotments of observing time over five years.

Discussions with many people have been helpful in directing my thinking and in answering specific questions about results. I would particularly like to thank Drs. K. C. Freeman and I. R. King for holding a sort of preliminary final examination for me last November. I also thank Dave Burstein, John Huchra, and Drs. P. Goldreich, J. Gunn, D. Richstone, M. Schmidt, L. Searle, A. Toomre, and especially Drs. A. Sandage and F. Schweizer for very helpful conversations.

I am most grateful to Dr. I. King and the Berkeley Astronomy Department for letting me use their PDS microdensitometer. It would have been impossible to finish in even an unreasonable time without it. Dr. S. Schoolman and

Mr. R. Kron kindly introduced me to the use of the machine. Early measurements, particularly of the calibration masks, were made using the Caltech microphotometer. I am grateful to Dr. T. Williams for letting me use his scanning program, and to the Wizards Larry Blakée, Martin Olsiewski and Bud Smith for their efforts to keep the Raytheon on the air. Earle Emery kindly contributed several mechanical items. Finally, I thank Drs. S. and G. Knapp for lending me the University of Maryland *Anglotron* to measure position angles of galaxies.

I am deeply indebted to Dr. I. King for allowing me to use his unpublished photometry of elliptical galaxies, and for letting me do to it many of the things he was probably interested in doing himself. Almost none of Papers II and III would have been possible without these data. Thanks are also due to Dr. A. Sandage, Dr. L. Searle, Mr. D. Rabin and Dr. T. Williams for data in advance of publication, and to Mr. J. Huchra and Drs. H. Arp, K. Y. Lo and W. Sargent for obtaining several important observations for me.

In a rare moment of weakness, Doug Richstone volunteered to read the initial manuscripts of Papers I and II. However, his critical faculties recovered very promptly, and I thank him very much for his comments.

A great many friends have helped make the last 5-1/2 years a rewarding experience. An incomplete list includes, most especially, François and Linda Schweizer, and Chip Arp, John Bahcall, Bob Brucato, Jay Elias, Richard Green, Eduardo Hardy, Paul Hickson, John Hoessel, John Huchra, Jorge Melnick, Bill Quirk, Doug Richstone, Greg Shields, Trinh Thuan, Barry Turnrose, and Chris Wilson.

I would like to thank Marilynne Rice and Sharon Hage for typing almost the whole of this thesis. Helen Holloway kindly typed the two long tables in Paper I.

I am most grateful to Caltech and to the National Research Council of Canada for financial support.

Finally, I cannot adequately express my gratitude to my parents for their continued moral and practical support over many years. It is only a small gesture to dedicate this thesis to them.

ABSTRACT

A study is made of three problems on luminosity distributions in galaxies: the nature of red compact galaxies, the systematic properties of spheroids, and the effect of decomposing observed profiles into spheroid and disk components.

Photographic brightness profiles are measured and discussed for sixteen compact and four normal galaxies, with the following results.

(i) Red compacts are qualitatively E and S0 galaxies.

(ii) Their central and mean surface brightnesses are generally normal. Only II Zw 67 and VII Zw 421 are noticeably compact.

(iii) Profile components which Sandage, in the Hubble Atlas, called lenses occur with great frequency and strength. They are the "large, nearly uniform brightness halos" described by Zwicky. VII Zw 793 has an exceptionally strong lens, which must be a disk because it shows spiral structure.

(iv) II Zw 67 and VII Zw 421 seem to be prototypes of a class of very luminous, early-type objects with dominant spheroid-like lenses, and spectra characteristic of metal-poor stars.

(v) Lenses are a distinct and independent component in galaxy profiles. They seem to be morphologically intermediate between spheroids and disks.

A systematic study of galaxy spheroids is made by fitting the de Vaucouleurs $r^{1/4}$-law to the profiles of sixteen compact and nineteen normal galaxies. The results are as follows.

(i) Ellipticals with massive neighbors have bright outer halos not possessed by more isolated objects. Possible tidal explanations are considered.

(ii) The brightness and radius parameters are related by $B_{oV} = 3.02 \log r_o + 19.74$ B mag arcsec^{-2} (μ). Here r_o varies from 1.0 to 14.1 kpc, and B_{oV} from 19.8 to 23.3 Bμ. Brighter galaxies tend to have larger r_o and fainter B_{oV}, with considerable scatter.

(iii) Some compacts are truly compact in having abnormally small r_o and bright B_{oV} for their absolute magnitude; most are just intrinsically faint.

(iv) The $B_{oV}(\log r_o)$ relation can be used to determine distances. We show that the Virgo cluster is closer than its redshift distance by $\delta(m-M) \leq 0^m.07 \pm 0^m.23$, a null result supporting the uniform Hubble flow advocated by Sandage and Tammann.

Detailed comparisons are made of how profile models due to de Vaucouleurs, Hubble and King fit galaxies. We show that the above results are model independent.

Finally, exponential disk parameters are derived for seven S0 compacts and for NGC 7457. The central disk brightness $B(0)_c$ is generally normal, but is unusually faint in two objects. Scale lengths are ~ 7 kpc, at the long end of the distribution found in normal galaxies. Spheroids clearly contribute significantly to the disk parameters. We therefore decompose the profiles into their underlying components. The disks, actually lenses in these objects, are shown to have a (possibly complete) inner brightness cutoff, where they enter the dominant part of the spheroid. Parameters of the underlying distributions are poorly determined, because there is considerable freedom in their relative strength. However, spheroids, and the above results on spheroids, are little affected by decomposition. In contrast, disks become significantly fainter.

Motivated by this, we use model galaxies to investigate the spheroid contribution to $B(0)_c$ derived for a composite profile. Exponentials with $B(0)_c$ = 20-25 B_μ are added to spheroids with a wide range of parameters. These reproduce very well the distribution

of $B(0)_c$ observed for normal galaxies. Thus the near universality of $B(0)_c = 21.65 \pm 0.30$ B_{μ}, observed by Freeman for 28 of 36 galaxies, is largely due to the contribution of the spheroid. Real disks can be much fainter. Measurements of galaxies with no spheroid are found to be consistent with this conclusion.

TABLE OF CONTENTS

CHAPTER 1

SURFACE PHOTOMETRY OF RED COMPACT GALAXIES

I. INTRODUCTION

The existence of several independent components in galaxy brightness profiles is well known. Their characteristics have been reviewed by de Vaucouleurs (1959), Sandage (1961), Freeman (1975), and others. In this series of papers, we will consider several aspects of the study of component profile shapes and parameter systematics.

It is convenient to adopt the language of simple analytic fitting functions. Thus spheroids have been described by functions due to Hubble (1930) and de Vaucouleurs (1948), the King (1966) model, and many others. A comparison of some of these functions, and a preliminary study of their characteristic parameters, will be made in Papers II and III (Kormendy 1976a,b). In the present paper, we will use the de Vaucouleurs relation, $\log I(r) \propto r^{1/4}$. Galaxy disks generally fall off exponentially in brightness (de Vaucouleurs 1959). A detailed study of disk structure has been made by Freeman (1970). We will consider some further aspects in Paper IV (Kormendy 1976c).

In the Hubble Atlas, Sandage (1961, see also Freeman 1975) described a possible third component in S0 and other early-type galaxies. Between the spheroid and disk there often appeared a distinct zone of slowly decreasing brightness, which he called a lens. However, there is too little

published data to allow modelling or parameter studies. In particular, we do not know whether to consider lenses as independent components, or as (not necessarily small) perturbations, like spiral structure, on the disk. It will turn out that lenses are prominent in the galaxies studied here.

To separate the characteristics of several partially superposed profile components, it is useful to study extreme cases. Zwicky (1971) has suggested that compact galaxies have unusual structure. For instance, he frequently used the phrase "compact core with large, nearly uniform brightness halo." Therefore, in this paper we will present photoelectric UBVR photometry, major and minor axis brightness profiles, and some spectroscopic data on selected red compact galaxies. Our purpose is to investigate how much they are quantitatively extreme, or even qualitatively peculiar.

Zwicky (1971) defined as compact any galaxy or part of a galaxy whose surface brightness exceeds 20 mag arcsec^{-2} (hereafter "μ"), in some wavelength range. However, at optical wavelengths essentially all spheroids reach a much higher brightness. Hence, we also ask whether these galaxies are quantitatively more compact than normal objects.

The galaxy sample is described in § II. Basic data are listed, including six new redshifts. In § III we present UBVR photometry of 26 compact and 16 normal galaxies, to consider overall colors. Photographic surface photometry of 16 compacts and 4 comparison galaxies is then described in § IV, and the data are presented in § V. In § VI we discuss the galaxies, divided into similar groups. In § VII their compactness is considered quantitatively in terms of central and mean surface brightness. Finally, § VIII provides a list of results.

II. THE GALAXY SAMPLE

To isolate a dynamical problem, we work on red and neutral compacts. Sargent (1970) has shown that these have spectra like those of elliptical galaxies. They consist of stars, with no visible emission lines. The objects chosen were bright, generally with $m_p \leq 14.6$, and regular in structure. Patchy or double objects were avoided. Two were called "very compact" by Zwicky (1971), and approximately half had "compact cores and nearly uniform brightness halos." All objects were chosen by examining Palomar Observatory Sky Survey prints. The sample is not statistically representative, though it covers the range of types observed, subject to the above restrictions.

The normal galaxies were chosen partly to allow some independent verification of the photometry. Thus M87 has been measured by King (1975); NGC 3379 by Dennison (1954), Miller and Prendergast (1962), and Burkhead and Kalinowski (1974); and NGC 524 by Hodge and Steidl (1976). Also, NGC 3379 has been used as a standard E galaxy in many applications. Finally, NGC 524 and NGC 7457 are normal S0's with strong and weak spheroids respectively.

The surface photometry galaxies are listed in Table 1. Columns 1 and 2 give the Zwicky and NGC numbers. The next two columns list 1950.0 positions. Morphological types are

TABLE 1

SURFACE PHOTOMETRY GALAXIES

Galaxy	NGC	α	δ	Type[1]	m_{pg}	V_o	Source[2]	PA[3]	Plates[4]	Q[5]
V Zw 114	679	1 46.8	35 32	(S0)	13.1	5153	1	...	0602	14
VI Zw 111	736	1 53.8	32 48	E1(*)	13.6	4494	12	125°	0300	24
V Zw 257	984	2 31.9	23 12	(S0)(*)	14.5	4427	1	86°	0400	43
II Zw 42	...	6 00.4	7 50	(E0)	16.0	5201	134	...	0500	35
I Zw 21	...	9 43.3	46 00	(S0)*	14.9	4922	34	...	1311	11
VII Zw 303	3065	9 57.6	72 25	SA(r)0*	12.9	2179	2	...	1021	22
VII Zw 352	...	10 53.3	60 57	(S0)(*)	15.7	9118	1	61°	1030	43
VII Zw 421	...	11 42.8	59 15	(S0)(*)	13.5	2575	1	19°	1211	14
I Zw 38	4486B	12 28.0	12 46	E0	14.5	1496	23	85°	1401	25
II Zw 67[6]	4853	12 56.2	27 51	E1,(S0)(*)	14.2	7556	6	86°	1302	24
I Zw 86	5603	14 21.1	40 36	(E0)(*)	14.0	5779	1	...	1041	35
I Zw 118A	IC 4562	15 34.3	43 39	(E0?)	13.8	5897[7]	334	...	3142	25
I Zw 118B	...	"	"	(E0)vc	15.3	" [7]	"	...	3142	35
I Zw 144	6126	16 19.6	36 30	(E1)	14.5	9834	1	...	2141	35
I Zw 178	...	17 16.6	48 31	(E0)vc(*)	15.2	8765	34	19°	1040	45
VII Zw 793	6654	18 25.2	73 09	(R')SB(s)0*	12.7	1509	2	176°,[8] 10-1/2°	1012	22
...	524	1 22.1	9 16	SA(rs)0+	11.5	2494	12	...	0500	14
...	3379	10 45.2	12 51	E^+1	9.6	769	5	111.5°	2401	25
M87	4486	12 28.3	12 40	E0-1P	10.4	1196	5	155°	1401	25
...	7457	22 58.6	29 53	SA(rs)0^-?	12.3	747	2	130°	1012	42

NOTES TO TABLE 1

(1) Type is the Revised Morphological Type according to de Vaucouleurs and de Vaucouleurs (1964). If enclosed in parentheses, the type is determined from the profile shape. An appended * indicates the Zwicky description "compact core, large nearly uniform halo." Parentheses indicate that "uniform" was not specified. "Very compact" is denoted vc.

(2) Sources of velocities:

(1) This paper

(2) Humason, Mayall and Sandage (1956)

(3) Zwicky (1971)

(4) Sargent (1970)

(5) De Vaucouleurs and de Vaucouleurs (1964)

(6) Rood, Page, Kintner and King (1972)

(3) Position angles of NGC 3379 and M87 were taken, respectively, from Miller and Prendergast (1962) and Arp and Bertola (1971). Other values were measured with the University of Maryland Anglotron, kindly made available by Drs. S. and G. Knapp.

(4) The four numbers are, respectively, the number of plates taken with the Mount Wilson 60-inch Cassegrain (8".3 mm^{-1}), Mount Wilson 100-inch

Newtonian (16".2 mm^{-1}), Mount Wilson 60-inch Newtonian (27" mm^{-1}), and Palomar Schmidt (67".5 mm^{-1}).

(5) Quality of the profile:

1 = Very good. Can be used for studies of profile shapes. All features should be real.

2 = Good.

3 = Fair. Parameters should be determined moderately well.

4 = Poor. Only approximate parameters derivable.

5 = Not detected.

The two numbers refer to spheroid and disk respectively. The central 1-2 arcsec, and the outermost $\sim$ 1/2 μ, are generally less accurate than the overall classification.

(6) In the Coma cluster.

(7) Mean value for I Zw 118A and B.

(8) Position angles of disk and bar major axis, respectively.

given in column 5, and Zwicky's photographic magnitudes in column 6. Column 7 gives the value, and column 8 the source of the radial velocity, corrected to the center of the galaxy. Column 9 lists major axis position angles, north through east. Column 10 gives the number of measured plates taken with each of four telescopes. The last column gives an estimate of the quality of the profile. This will be discussed in § V.

Figure 1 shows photographs of the galaxies. For many objects, isodensity tracings made with the Berkeley PDS microdensitometer are also shown. These will be discussed in § VI.

Redshifts were required for six objects. Spectra were taken with the one- and two-stage image-tube spectrograph and the Palomar 60-inch telescope. The dispersion was 144 $\mathring{A}$ mm^{-1}. Two spectra were obtained for each object except I Zw 144. All spectra were measured and reduced using standard techniques, and should yield redshifts accurate to ~ 70 km s^{-1}.

FIGURE 1

Photographs and isodensity tracings of S0 compacts. The prints are made from blue Palomar Observatory Sky Survey plates, unless otherwise noted, and have north up and east at the left. All photographs have a scale of 4.5 arcsec mm^{-1}. Top row, left-right: I Zw 21 (IIIa-J Schmidt plate), VII Zw 303 (IIIa-J Schmidt plate), isodensity tracing of VII Zw 303, enlarged 4.6 times from the print; second row, left-right: V Zw 114, V Zw 257, isodensity tracing of V Zw 257, enlarged 1.9 times from the print; third row, left to right: VI Zw 111, VII Zw 352, isodensity tracing of VII Zw 352, enlarged 7.6 times from the print.

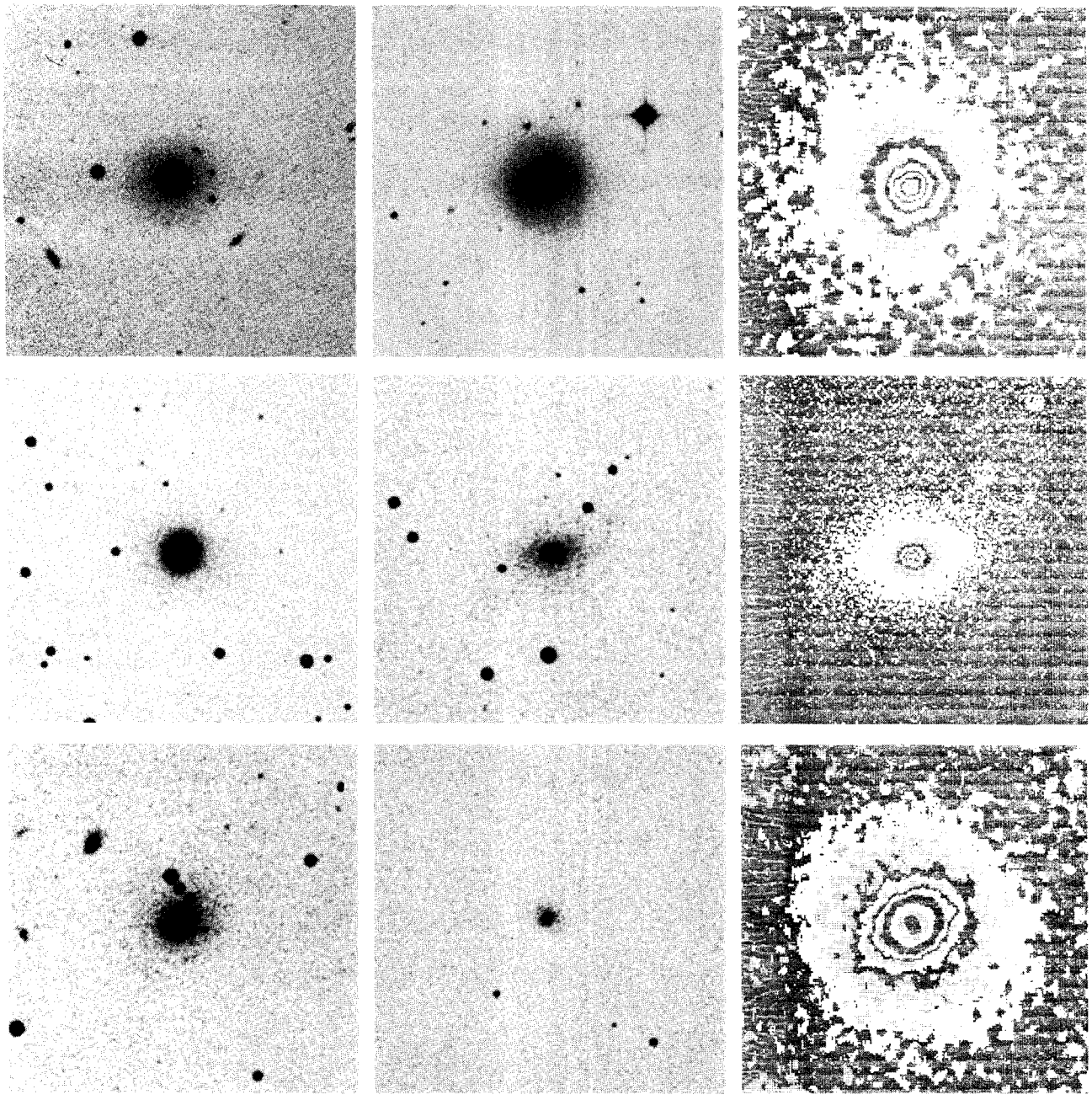

FIGURE 1 (Continued)

The peculiar S0 compacts. VII Zw 793 is shown in the top row; the isodensity tracing is enlarged 1.5 times from the print. The second row shows VII Zw 421, with the isodensity tracing similarly enlarged by a factor of 3.0. The third row shows II Zw 67, with a isodensity tracing enlarged 4.4 times from the print. The latter two photographs are deep IIIa-J plates taken with the Palomar Schmidt.

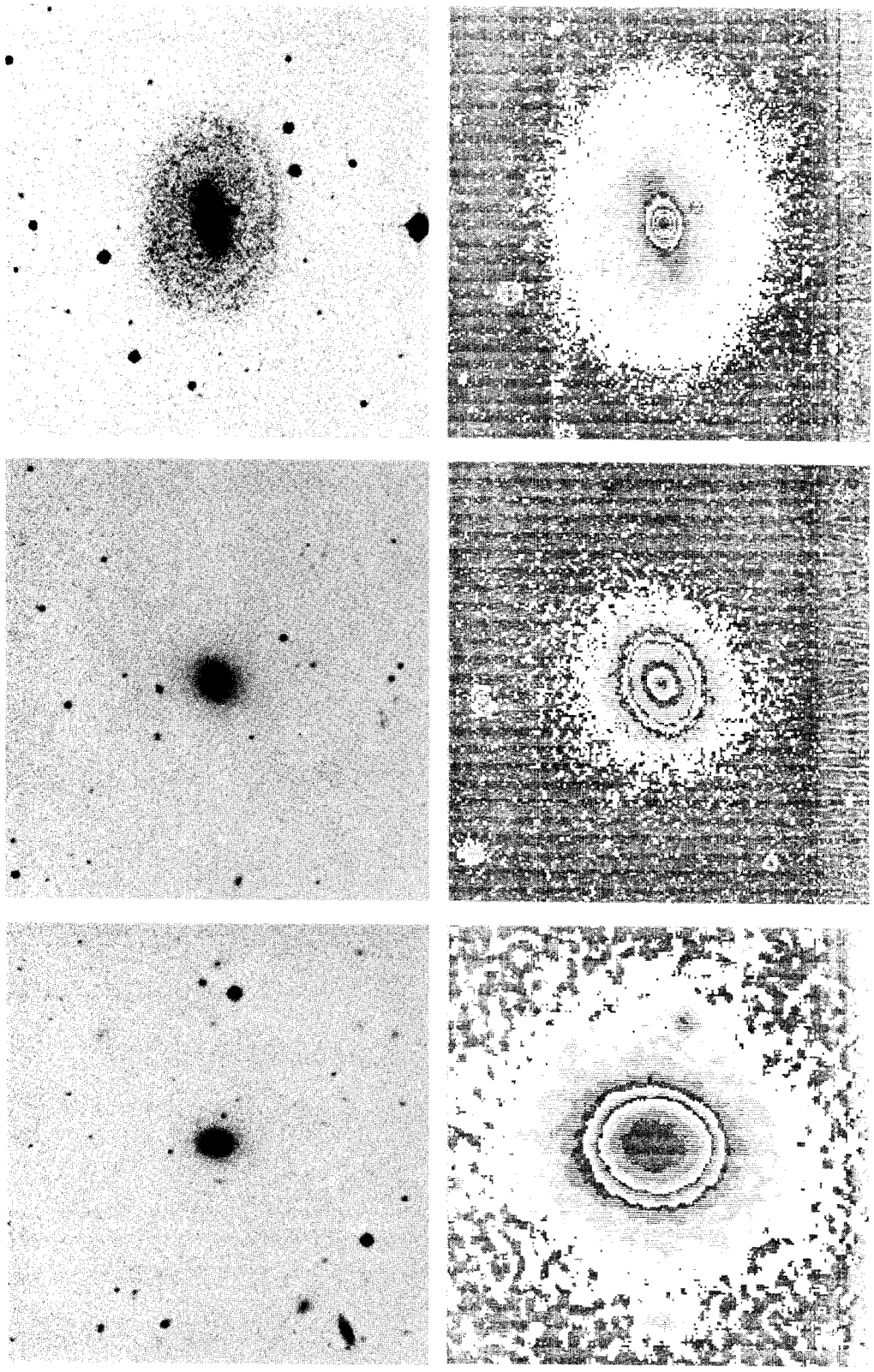

FIGURE 2 (Continued)

The elliptical compacts. Top row, left to right: I Zw 118B and A (IIIa-J plate), I Zw 144 (127-02 plate), I Zw 86; second row, left to right: II Zw 42, I Zw 178 and I Zw 38 (IIIa-J plate).

FIGURE 4 (lower)

Spectrum of VII Zw 421, taken with the Palomar 60-inch telescope, at a dispersion of 144 $\mathring{A}\ mm^{-1}$. The Balmer absorption spectrum is virtually as strong as Ca II H and K.

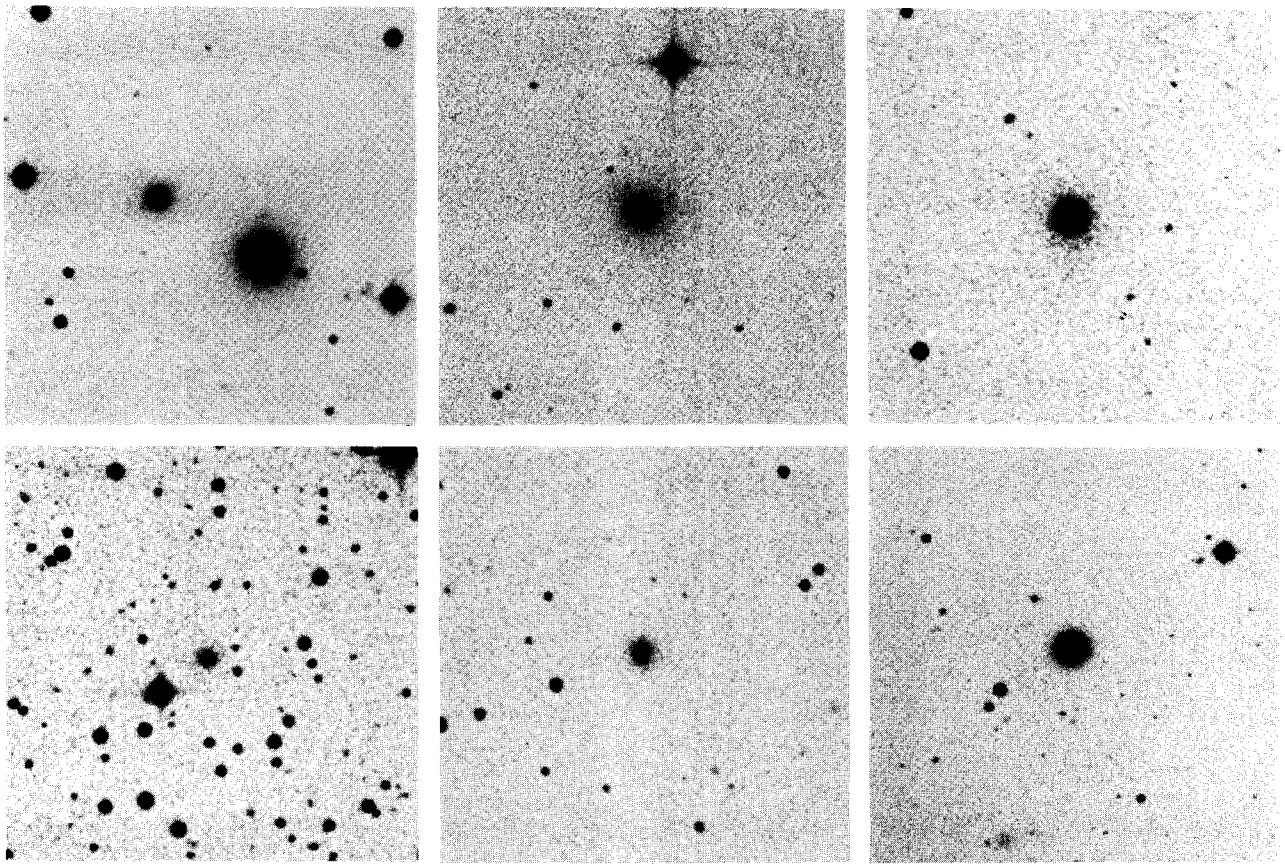

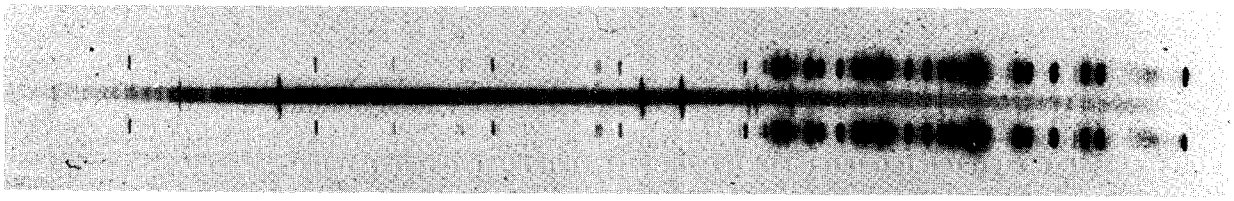

III. PHOTOELECTRIC PHOTOMETRY

Photoelectric magnitudes will be needed in § IV for profile zero points. In this § we will list these data, and briefly compare the colors of compact and normal galaxies.

Measurements were made with the Palomar 60-inch telescope and two-tube photometer, and pulse-counting electronics. Sandage's (1973) photometric system was used, as defined by standard filters and the S20 photocathodes of ITT FW-130 tubes. Ten to twenty measurements of six to twelve standard stars were made each night. A few observations were also made with a one-tube photometer and the 100-inch telescope. A systematic correction of $0^m.10$ was required to bring the resulting V magnitudes into accord with Palomar data.

Table 2 lists data for 26 compact and 16 normal galaxies. Estimated accuracies are $\pm\ 0^m.04$ - $0^m.06$ in V, $\pm\ 0^m.03$ - $0^m.05$ in U-B, and $\pm\ 0^m.02$ - $0^m.04$ in B-V and V-R, depending on the number n of measurements made on different nights. This is confirmed when the data are compared to values listed in de Vaucouleurs and de Vaucouleurs (1964). The most reliably determined galaxies in common, NGC 524, 3379 and 4853, show a mean deviation in the sense (de Vaucouleurs-Kormendy) of $-0^m.023 \pm 0^m.022(\sigma)$. Measure-

TABLE 2

S20 PHOTOELECTRIC PHOTOMETRY

Object	Aper[1]	V	U-B	B-V	V-R	n	Notes
V Zw 52	20.9	13.57	0.61	1.04	0.92	3	
	41.1	13.12	0.63	1.05	0.92	3	
V Zw 114	20.9	13.39	0.61	1.06	0.94	3	
	41.1	12.96	0.60	1.04	0.92	3	
VI Zw 111	29.0	13.12	0.54	1.03	0.91	3	
	41.1	12.88	0.55	1.01	0.90	3	
II Zw 188	20.9	14.23	0.68	1.19	1.07	4	
	114.6	13.14	0.41	1.01	0.96	4	
	annulus	13.64	0.30	0.93	0.89		
VI Zw 26	29.0	13.67	0.35	0.90	0.84	1	
V Zw 257	20.9	14.06	0.64	1.18	1.08	3	
	29.0	13.79	0.63	1.16	1.07	3	
III Zw 52	81.4	13.20	0.70	1.19	1.06	2	
II Zw 42	29.0	14.93	0.50	1.15	1.09	3	
I Zw 15	14.5	14.29	0.81	1.27	1.24	1	
	20.9	14.14	0.65	1.25	1.21	1	
	57.5	13.75	0.49	1.11	1.11	1	
I Zw 21	19.6	14.36	0.58	0.99	0.87	1	2
	20.9	14.31	0.44	0.97	0.87	4	
	34.6	14.10	0.57	0.96	0.85	1	2
	41.1	14.01	0.42	0.95	0.86	4	
VII Zw 303	20.9	13.19	0.48	0.98	0.92	3	
	41.1	12.82	0.46	0.97	0.89	3	
VII Zw 421	19.6	13.47	0.31	0.73	0.76	1	2
	20.9	13.41	0.31	0.74	0.76	2	
	34.6	13.24	0.31	0.73	0.75	1	2
	41.1	13.23	0.28	0.74	0.76	2	

TABLE 2 (Continued)

Object	Aper[1]	V	U-B	B-V	V-R	n	Notes
VII Zw 16	41.1	11.99	-0.20	0.74	0.78	1	3
	81.4	11.51	-0.15	0.78	0.82	1	
VII Zw 18	29.0	13.09	0.70	1.12	1.01	1	
VII Zw 148	41.1	14.44	0.39	0.97	0.88	2	
VII Zw 159	57.5	13.94	0.52	1.13	0.97	1	
VII Zw 352	19.6	15.20	0.60	1.03	0.91	1	2
	41.1	14.90	0.50	1.07	0.91	4	
I Zw 38	20.9	13.55	0.57	0.99	0.87	2	
	29.0	13.51	0.57	0.99	0.87	1	
	41.1	13.50	0.60	0.99	0.91	2	
II Zw 67	20.9	13.93	0.21	0.75	0.76	2	
	24.3	13.80	0.26	0.79	0.76	1	4
	41.1	13.75	0.20	0.76	0.76	2	
I Zw 86	29.0	13.58	0.49	0.99	0.89	1	
I Zw 118A	19.6	13.50	0.58	1.02	0.90	1	
	20.9	13.49	0.49	1.01	0.88	1	
I Zw 118B	11.0	14.80	0.95	1.02	0.90	1	
	24.3	14.68	0.60	1.00	0.86	1	4
VII Zw 657	29.0	13.06	0.56	1.02	0.90	1	
I Zw 144	29.0	14.00	0.49	1.00	0.87	3	
VII Zw 793	29.0	13.00	0.54	1.00	0.90	2	
	81.4	12.27	0.49	1.01	0.89	2	
NGC 68	14.5	14.81	0.47	1.06	0.96	5	5
NGC 128	29.0	12.63	0.58	1.04	0.91	2	
	41.1	12.41	0.58	1.04	0.90	2	

TABLE 2 (Continued)

Object	Aper[1]	V	U-B	B-V	V-R	n	Notes
M 32	20.9	10.03	0.46	0.95	0.87	2	
	29.0	9.72	0.46	0.94	0.87	1	
	41.1	9.47	0.46	0.95	0.86	2	
NGC 524	20.9	12.44	0.66	1.11	1.00	3	
	29.0	12.05	0.64	1.09	0.99	3	
	41.1	11.74	0.64	1.08	0.97	3	
	57.5	11.40	0.62	1.07	0.96	3	
	81.4	11.14	0.61	1.06	0.95	3	
NGC 1201	20.9	12.19	0.54	1.00	0.89	1	
	41.1	11.74	0.53	0.96	0.88	2	
NGC 2685	19.6	12.70	0.46	0.98	0.87	1	2
	20.9	12.75	0.45	0.97	0.89	4	
	41.1	12.28	0.41	0.95	0.89	4	
	114.6	11.71	0.33	0.91	0.86	3	
	annulus	12.69	0.23	0.84	0.81		6
NGC 3032	20.9	13.28	0.00	0.59	0.71	2	
	41.1	12.91	0.04	0.65	0.73	3	
	57.5	12.70	0.07	0.67	0.73	2	
NGC 3081	20.9	13.45	0.30	0.96	0.90	1	
	57.5	12.70	0.34	0.95	0.92	1	
	annulus	13.44	0.38	0.94	0.94		
NGC 3115	20.9	10.87	0.62	1.00	0.90	1	
	29.0	10.57	0.58	1.00	0.91	2	
	41.1	10.31	0.58	1.00	0.90	3	
NGC 3245	57.5	11.62	0.45	0.93	0.86	2	
NGC 3379	20.9	11.21	0.58	1.00	0.89	2	
	29.0	10.90	0.57	1.00	0.88	2	
	41.1	10.66	0.56	0.99	0.89	2	
	57.5	10.41	0.56	0.98	0.88	2	
NGC 7331	41.1	11.00	0.56	1.04	0.99	3	
	114.6	10.18	0.42	0.99	0.98	3	
NGC 7332	20.9	12.08	0.46	0.92	0.84	3	
	57.5	11.44	0.43	0.90	0.82	3	
NGC 7457	41.1	12.43	0.40	0.90	0.84	3	
	57.5	12.08	0.39	0.91	0.84	3	

NOTES TO TABLE 2

1. Aperture diameters in arcsec.
2. Measured on Mount Wilson 100-inch telescope. The V magnitude has been corrected by $+0^{m}.10$.
3. See Hodge (1974).
4. Mount Wilson 100-inch telescope measurement kindly made by J. Huchra.
5. Raw photometry used by Kormendy and Sargent (1974).
6. Annulus between 41".1 and 114".6 diameter apertures.

ments of NGC 3065, 6654 and 7457 deviate by $-0^m.17$ to $+0^m.43$. However, there is reason to doubt either the photometry used in the above reference, or the applicability of standard magnitude-aperture growth curves to galaxies with peculiar profiles.

Figure 2 is a two-color diagram of the data. All galaxies have been corrected for K reddening by $0^m.012$ (V/1000 km s^{-1}) in both colors, where V is the observed velocity (de Vaucouleurs 1961). Corrections for galactic reddening have also been applied. These are $E_{U-B} = 0^m.038$ csc b^{II} and $E_{B-V} = 0^m.050$ csc b^{II}, corresponding to our adopted absorption of $0^m.20$ csc b^{II}. Three boxes illustrate the distribution of normal galaxies, as follows (cf. Huchra 1976a). The center line is the relation calculated by Huchra (1976b) for all galaxies with colors listed in de Vaucouleurs and de Vaucouleurs (1964):

$$(U-B)_o = 1.33(B-V)_o - 0.78 \quad . \qquad (1)$$

The boxes are 0.2 mag wide, thus including most of the observations. The lower right-hand side is common to all three. It is the average line for E and S0 galaxies which includes all but one object in the distribution. The upper left sides enclose 80% of the ellipticals (heavy solid line)

FIGURE 2

Two-color diagram for compact and normal galaxies. Colors within outer annuli are shown for II Zw 188 (upper) and NGC 2685 (see Table 2). The boxes show the distribution of normal galaxies, and are defined in the text.

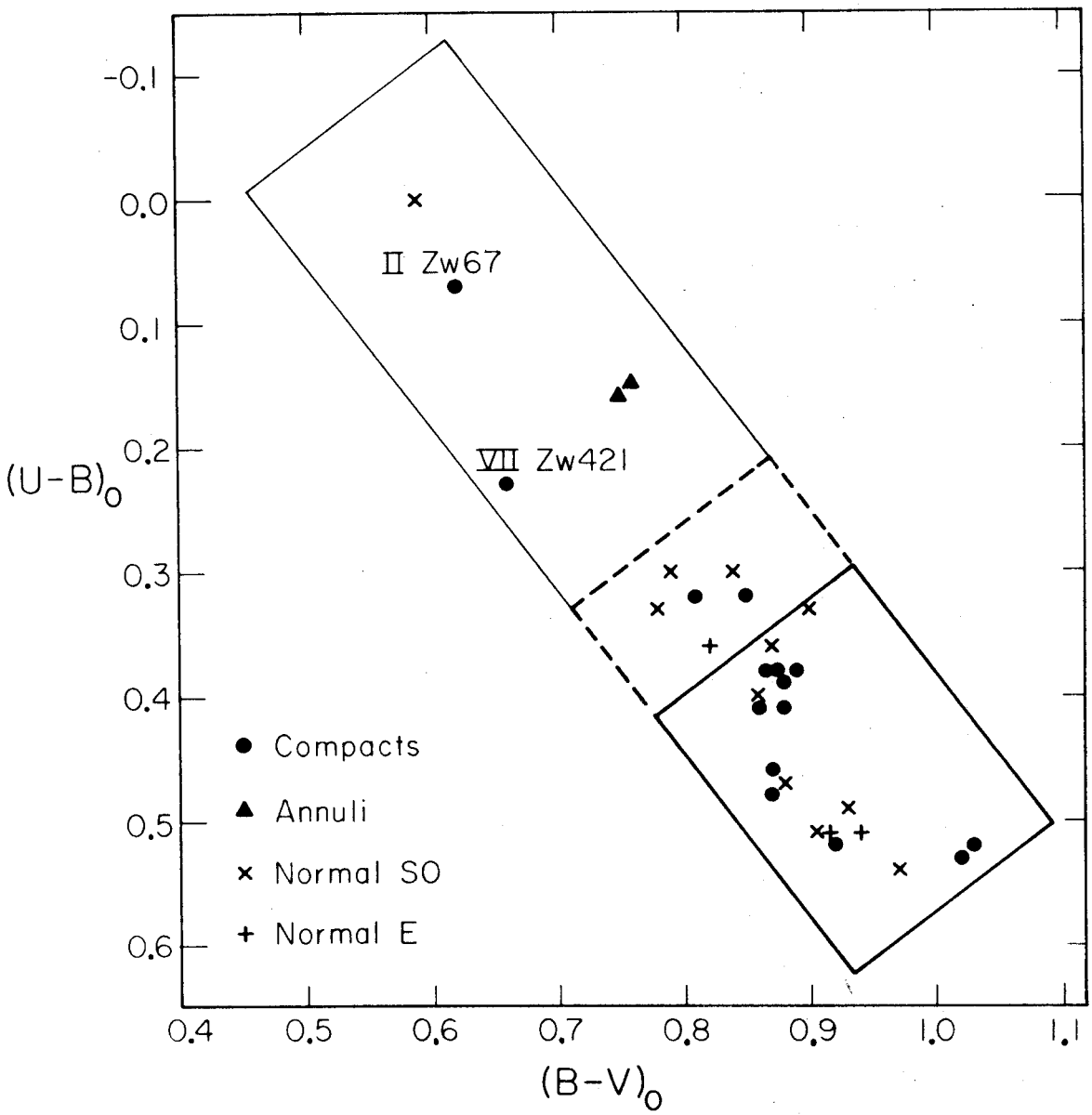
-0.1
0.0
0.1
0.2
0.3
0.4
0.5
0.6
(U-B)o
II Zw67
VII Zw421
Compacts
Annuli
Normal SO
Normal E
0.4
0.5
0.6
0.7
0.8
0.9
1.0
1.1
(B-V)o

and S0's (dashed). The upper left side of the largest box is defined in the same way as the lower right side. These definitions are similar to ones used in Huchra's (1976a) study of the colors of normal and Markarian galaxies.

Figure 2 confirms Sargent's (1970) result that red compacts have the normal colors of E and S0 galaxies. Table 2 shows that they also have small color gradients similar to those in normal galaxies.

A number of compacts have outer detached rings. Examples include II Zw 188 and I Zw 133. The rings seem to be slightly patchy, but not made up of H II regions, and often have sharp edges. They do not seem to consist of almost-azimuthal spiral arms, like the ring in NGC 3081 (Sandage 1961). A nearby galaxy with a similar ring is the very peculiar NGC 2685 (see Sandage 1961). Annular measurements listed in Table 2 isolate the ring in II Zw 188, the inner "helix" in NGC 2685, and part of the ring in NGC 3081. As expected, the latter has the same colors as the rest of the galaxy. The former are considerably bluer, as shown in Figure 2. This agrees with Zwicky's (1971) estimates from Sky Survey plates. An investigation of the spectra of these rings would be of considerable interest.

IV. PHOTOGRAPHIC PHOTOMETRY: OBSERVATION AND REDUCTION

To study the different profile components ideally requires plates from three telescopes. Most of the galaxy is measured on medium-scale plates taken with the Mount Wilson 100-inch and 60-inch Newtonians. Also, for 15 of 20 galaxies, plates of the nuclei were obtained at 8.3 arcsec mm^{-1}, in seeing $\lesssim$ 1 arcsec, at the 60-inch Cassegrain focus. Finally, we require deep IIIa-J plates taken with the Palomar Schmidt telescope. Unfortunately, limiting plates were obtained for only eight galaxies. Since the Mount Wilson sky is very bright, typically $\sim$ 21-21$\frac{1}{2}$ B_J, with B-V $\simeq$ 0.7, the photometry often does not go very faint. This is the most serious limitation in the data. Table 1 lists the number of plates of each galaxy taken with each telescope.

The bandpass used is defined by IIIa-J or 124-01 (= 103a-J) plates and a Wr 4 filter. Denoted by G, it covers the approximate range 4600 - 5400 Å. It is used because fine-grain IIIa-plates for deep exposures, and fast 103a-plates for work at f/16 are available in the same system. There is also a well-known dark window at G in the night-sky spectrum. Finally, it is still possible to relate the system to photoelectrically determined zero points via the relation

$$B-G = 0.65(B-V), \quad -0.2 \leq B-V \leq 1.4 \quad , \qquad (2)$$

determined by Kormendy and Bahcall (1974, see also Thuan and Gunn 1976).

Eight plates of four galaxies were also taken in the R system defined by 127-01 or 098-04 plates and a RG1 filter (6200-6900 Å). The only color gradient noticeable was a suggestion that the central 1-2 arcsec might be red (cf. § III). Such data were discarded, and otherwise R and G plates were averaged together.

Palomar Schmidt plates were calibrated with a sensitometer projecting twelve spots separated by $\sqrt{2}$ in intensity. These relative intensities have been verified previously (Kormendy 1973), and are confirmed again below.

Mount Wilson plates were calibrated with a contact print through a transmission mask exposed onto Kodak 649-F emulsion. All exposures were made using the Mount Wilson preflash unit (Miller 1964), to give uniform illumination. The two masks used range over 0.7 and 2.6 orders of magnitude in transmission T, with fourteen steps each. They were calibrated against the Palomar sensitometer. Each mask was measured twice. Six plates were taken for each measurement, with two exposures each of the mask and the spots. All plates were 103a-D with a Wr4 filter. The

first set was developed for 4 min in D19, and the second for 7 min in MWP-2. The resulting very different characteristic curves were each determined to $\lesssim$ 2%, confirming the accuracy of the spot sensitometer. Similarly, the two mask measurements agreed to $\sim$ 2%. Thus the masks are well enough determined to serve as calibration standards.

For all calibrations, an incandescent light bulb was used with Wratten neutral density filters and the filter used in the telescope. Plates were calibrated in the darkroom, usually immediately before or after the telescope exposure, and for a period 0.7 - 1.2 times as long. Most were developed on the following afternoon, so the two exposures were the same age to $\lesssim\lesssim$ 25%. Plates were processed 8-9 min in MWP-2 developer, using a standard plate rocker (Miller 1971).

Ninety-six of the 100 plates were measured with the Photometric Data Systems microdensitometer in the Berkeley Astronomy Department of the University of California. The others were processed similarly using the Caltech Digital Microphotometer. Preliminary measurements showed that calibrations of plates from the same box and observing run, and with similar exposures, were identical within errors. Therefore, plates were measured together in appropriate

groups of 1-7, without changing any measuring optics or electronic settings. Their calibrations were then averaged.

A galaxy measurement consisted of two or three scans each along the major and minor axis, and separated by 1°-10°, depending on the ellipticity. Round galaxies were measured at 4-6 equally spaced orientations. Each scan reached well into the sky on both sides of the galaxy. Measuring slits ranged from 0.2 arcsec square to ~ 2 x 7 arcsec, small enough not to average different densities. Thirty-one plates were later remeasured with larger slits to reach fainter limiting magnitudes. An interactive programming system was used for the initial processing, to remove stars and plate flaws, and to find the sky levels and galaxy center.

Calibrations were reduced on a computer, but averaged by hand. The characteristic curves were partially linearized used the opacitance $\omega = 1/T - 1$ (de Vaucouleurs 1967), and a polynomial of the form

$$\log \text{intensity} = \sum_{i=o}^{n} a_i (\log \omega)^{i/2} \quad , \; n \simeq 6 \quad . \qquad (3)$$

Galaxy scans were averaged in photographic density, and intensity reduced using the above. The sky intensity was

then subtracted, and the radial magnitude profile $\mu(r)$ plotted against log r.

The different μ(log r) plots for each axis of each galaxy were shifted together in μ to minimize the scatter, and then averaged by hand. Note that this was done in log r coordinates, to prevent any prejudice in favor of an exponential or a de Vaucouleurs law. Thus real conclusions can be drawn about whether these functions fit the data.

Ellipticities measured on isodensity tracings were used to help fit the major and minor axis profiles together. Mostly this affects only the central several arcseconds. Basically the two axis measurements are independent, and therefore ellipticity profiles cannot be derived from the data.

Zero points were obtained by integrating the elliptical profiles within the circular apertures of the photometry in § III. Results for different apertures were averaged.

V. THE BRIGHTNESS PROFILES

The data are presented in Table 3 and Figures 3a-g. The Table lists for each galaxy the logarithm of the radius in arcsec, and the average major and minor axis profiles. The Figures show the individual profile segments from each plate, matched together as described earlier. The only editing is a truncation at each end, where the deviations from average become too large (variously 0.05 - 0.2 μ). A few plates have been discarded, because the sky was too underexposed to be measured, or because a calibration failed.

It is difficult to estimate the accuracy of photographic photometry, since the errors are usually systematic rather than statistical. Most errors are measured by the spread in the profile segments in Figure 3, and are small. There is enough redundancy that the rare bad calibration is easily recognized and discarded. Cumulative errors introduced in matching the profile segments can be estimated by experimenting with the fitting procedure. A profile quality is given in Table 1, separately for spheroid and disk. Estimated accuracies for Q = 1-2 are $\pm$ 0.03 - 0.06 μ, and for Q = 3-4, $\pm \sim$ 0.05 - 0.1 μ or slightly more. The data are worse than this in the central arcsecond and at the faint end. For instance,

TABLE 3

BRIGHTNESS PROFILES

V Zw 114		VI Zw 111		
log r	μ_G	log r	μ_G(maj)	μ_G(min)
-0.30	17.78	-0.30	17.44	17.44
-0.20	17.81	-0.20	17.51	17.51
-0.10	17.87	-0.10	17.63	17.63
0.0	17.95	0.0	17.76	17.76
0.10	18.07	0.10	17.95	17.95
0.18	18.20	0.18	18.14	18.16
0.26	18.36	0.26	18.36	18.42
0.34	18.56	0.34	18.60	18.69
0.42	18.80	0.42	18.88	19.01
0.50	19.08	0.50	19.14	19.31
0.58	19.39	0.58	19.40	19.61
0.66	19.75	0.66	19.67	19.92
0.74	20.13	0.74	19.95	20.21
0.82	20.50	0.82	20.24	20.52
0.90	20.86	0.90	20.54	20.83
0.98	21.26	0.98	20.90	21.19
1.06	21.68	1.06	21.29	21.59
1.14	22.12	1.10	21.50	21.79
1.18	22.37	1.14	21.73	21.98
1.22	22.60	1.18	21.97	22.18
1.26	22.80	1.22	22.17	22.37
1.30	23.00	1.26	22.36	22.57
1.34	23.20	1.30	22.55	22.72
1.38	23.37	1.34	22.72	22.88
1.42	23.54	1.38	22.85	23.03
1.46	23.72	1.42	22.97	23.19
1.50	23.91	1.46	23.10	23.36
1.54	24.11	1.50	23.29	23.55
1.58	24.33	1.54	23.53	23.77
1.62	24.57	1.56	23.70	23.90
1.66	24.82	1.58	23.87	24.05
1.70	25.10	1.60	24.07	24.23
1.74	25.43			

TABLE 3 (continued)

V Zw 257			II Zw 42	
log r	μ_G(maj)	μ_G(min)	log r	μ_G
-0.30	18.29	18.29	-0.30	18.57
-0.20	18.37	18.37	-0.22	18.64
-0.10	18.46	18.46	-0.14	18.73
0.0	18.56	18.57	-0.06	18.84
0.10	18.71	18.77	0.0	18.95
0.18	18.85	18.99	0.06	19.08
0.26	19.05	19.26	0.10	19.19
0.34	19.28	19.54	0.14	19.31
0.42	19.51	19.84	0.18	19.43
0.50	19.79	20.14	0.22	19.56
0.58	20.08	20.46	0.26	19.70
0.66	20.39	20.78	0.30	19.84
0.74	20.72	21.13	0.34	20.01
0.82	21.08	21.49	0.38	20.18
0.86	21.27	21.65	0.42	20.35
0.90	21.42	21.82	0.46	20.54
0.94	21.56	21.94	0.50	20.74
0.98	21.68	22.03	0.54	20.97
1.02	21.80	22.13	0.58	21.18
1.06	21.90	22.26	0.62	21.40
1.10	21.97	22.41	0.66	21.60
1.14	22.04	22.57	0.70	21.83
1.18	22.12	22.73	0.74	22.06
1.22	22.23	22.90	0.78	22.27
1.26	22.36		0.82	22.48
1.30	22.51		0.86	22.68
1.34	22.65		0.90	22.87
1.38	22.81		0.94	23.10
1.42	22.96		0.98	23.33
1.46	23.15		1.00	23.44
1.50	23.33			
1.54	23.53			

TABLE 3 (continued)

I Zw 21		VII Zw 303	
log r	μ_G	log r	μ_G
-0.60	17.89	-0.60	17.06
-0.40	17.92	-0.40	17.11
-0.30	17.96	-0.20	17.22
-0.24	18.00	-0.10	17.30
-0.20	18.04	0.0	17.44
-0.12	18.14	0.10	17.63
-0.04	18.28	0.20	17.90
0.0	18.37	0.28	18.16
0.04	18.47	0.36	18.44
0.12	18.71	0.44	18.77
0.20	18.98	0.52	19.11
0.28	19.27	0.60	19.41
0.36	19.59	0.68	19.74
0.44	19.94	0.76	20.09
0.52	20.26	0.84	20.46
0.60	20.59	0.92	20.85
0.68	20.94	1.00	21.25
0.76	21.34	1.08	21.68
0.84	21.74	1.12	21.91
0.92	22.18	1.16	22.10
1.00	22.62	1.18	22.19
1.04	22.82	1.20	22.26
1.08	23.00	1.24	22.38
1.12	23.17	1.28	22.47
1.16	23.31	1.32	22.56
1.20	23.44	1.36	22.66
1.24	23.55	1.40	22.77
1.28	23.65	1.44	22.92
1.32	23.76	1.48	23.10
1.36	23.87	1.52	23.32
1.40	24.02	1.56	23.56
1.44	24.18	1.60	23.84
1.48	24.37	1.64	24.19
1.50	24.47	1.66	24.35
1.52	24.63	1.68	24.56
1.54	24.79	1.70	24.82
1.56	25.00		

TABLE 3 (continued)

VII Zw 352			VII Zw 421		
log r	μ_G(maj)	μ_G(min)	log r	μ_G(maj)	μ_G(min)
-0.60	18.41	18.41	-0.60	17.04	17.04
-0.50	18.42	18.42	-0.50	17.06	17.06
-0.40	18.45	18.45	-0.40	17.09	17.09
-0.30	18.53	18.53	-0.30	17.13	17.13
-0.20	18.64	18.64	-0.20	17.20	17.20
-0.10	18.79	18.79	-0.10	17.30	17.30
0.0	18.97	18.97	-0.04	17.40	17.40
0.08	19.17	19.17	0.04	17.56	17.56
0.16	19.45	19.45	0.12	17.72	17.76
0.20	19.63	19.63	0.20	17.92	18.01
0.24	19.85	19.85	0.28	18.16	18.29
0.28	20.09	20.09	0.36	18.44	18.57
0.32	20.32	20.30	0.44	18.75	18.87
0.36	20.56	20.49	0.52	19.05	19.20
0.40	20.83	20.68	0.56	19.19	19.41
0.44	21.08	20.85	0.60	19.33	19.63
0.48	21.28	21.05	0.64	19.47	19.89
0.52	21.49	21.25	0.68	19.62	20.15
0.56	21.74	21.44	0.72	19.75	20.39
0.60	21.94	21.63	0.76	19.89	20.69
0.64	22.09	21.85	0.80	20.02	21.02
0.68	22.22	22.05	0.84	20.20	21.32
0.72	22.35	22.21	0.88	20.47	21.65
0.76	22.46	22.37	0.92	20.81	21.95
0.80	22.57	22.57	0.96	21.19	22.21
0.84	22.70	22.73	1.00	21.57	22.45
0.88	22.83	22.88	1.04	22.00	22.69
0.92	22.97	23.04	1.08	22.33	22.90
0.96	23.13	23.21	1.12	22.66	23.09
1.00	23.29	23.44	1.16	22.96	23.28
1.04	23.48	23.69	1.20	23.18	23.44
1.08	23.68	23.96	1.24	23.40	23.60
1.10	23.82		1.28	23.59	23.77
1.12	23.98		1.32	23.79	23.96
1.14	24.17		1.36	24.00	24.14
			1.40	24.21	24.35
			1.44	24.49	24.67
			1.46	24.64	24.83
			1.48	24.82	24.98

TABLE 3 (continued)

I Zw 38			II Zw 67		
log r	μ_G(maj)	μ_G(min)	log r	μ_G(maj)	μ_G(min)
-0.60	17.23	17.23	-0.60	17.90	17.90
-0.50	17.24	17.24	-0.40	17.94	17.94
-0.40	17.27	17.27	-0.30	17.99	17.99
-0.30	17.31	17.31	-0.20	18.07	18.07
-0.20	17.37	17.37	-0.10	18.17	18.17
-0.12	17.44	17.44	0.0	18.28	18.28
-0.04	17.53	17.53	0.10	18.42	18.42
0.04	17.64	17.64	0.20	18.61	18.61
0.12	17.79	17.79	0.28	18.79	18.80
0.20	17.98	17.98	0.36	19.02	19.03
0.28	18.23	18.23	0.44	19.25	19.32
0.32	18.38	18.38	0.52	19.50	19.58
0.38	18.53	18.53	0.56	19.60	19.72
0.40	18.70	18.70	0.60	19.69	19.88
0.44	18.88	18.89	0.64	19.78	20.10
0.48	19.06	19.10	0.68	19.89	20.36
0.52	19.22	19.31	0.72	20.03	20.63
0.56	19.40	19.53	0.76	20.24	20.92
0.60	19.58	19.78	0.80	20.53	21.21
0.64	19.79	20.02	0.84	20.86	21.54
0.68	20.03	20.28	0.88	21.21	21.88
0.72	20.31	20.58	0.92	21.57	22.19
0.76	20.61	20.88	0.96	21.91	22.54
0.80	20.92	21.17	1.00	22.28	22.86
0.84	21.25	21.50	1.04	22.61	23.19
0.88	21.61	21.84	1.08	22.91	23.46
0.92	21.97	22.18	1.12	23.15	23.69
0.96	22.33	22.53	1.16	23.37	23.90
1.00	22.69	22.87	1.20	23.61	24.09
1.04	23.07	23.21	1.24	23.87	24.25
1.08	23.43	23.55	1.28	24.11	24.43
1.12	23.79	23.90	1.32	24.36	24.62
1.16	24.16	24.26	1.36	24.62	24.83
1.20	24.57	24.67	1.40	24.88	25.05
1.22	24.81	24.86	1.44	25.17	25.31
1.24	25.04	25.07	1.48	25.47	25.63
1.26	25.28	25.29	1.52	25.84	

TABLE 3 (continued)

I Zw 86		I Zw 118 A	
log r	μ_G	log r	μ_G
-0.60	17.76	-0.60	17.42
-0.50	17.77	-0.50	17.43
-0.40	17.77	-0.40	17.46
-0.30	17.79	-0.30	17.51
-0.20	17.83	-0.20	17.56
-0.10	17.92	-0.10	17.66
0.0	18.04	0.0	17.80
0.04	18.09	0.10	18.01
0.12	18.23	0.20	18.25
0.20	18.40	0.28	18.48
0.28	18.63	0.36	18.75
0.36	18.92	0.44	19.05
0.44	19.25	0.52	19.40
0.52	19.60	0.60	19.75
0.60	19.95	0.68	20.12
0.68	20.31	0.76	20.47
0.76	20.70	0.80	20.64
0.84	21.07	0.84	20.80
0.92	21.47	0.88	20.96
1.00	21.88	0.92	21.13
1.08	22.33	0.96	21.28
1.16	22.80	1.00	21.44
1.24	23.22	1.04	21.59
1.32	23.64	1.08	21.76
		1.12	21.95
		1.16	22.15
		1.20	22.38
		1.24	22.62
		1.28	22.86
		1.32	23.10
		1.36	23.30
		1.40	23.50
		1.44	23.71
		1.48	23.93
		1.50	24.05
		1.52	24.24
		1.54	24.45

TABLE 3 (continued)

I Zw 118 B		I Zw 178		
log r	μ_G	log r	μ_G(maj)	μ_G(min)
-0.60	17.99	-0.60	17.98	17.98
-0.50	18.01	-0.50	17.99	17.99
-0.40	18.04	-0.40	18.02	18.02
-0.30	18.11	-0.30	18.04	18.04
-0.20	18.19	-0.20	18.09	18.09
-0.10	18.31	-0.10	18.15	18.15
0.0	18.49	-0.04	18.20	18.20
0.04	18.58	0.04	18.32	18.32
0.08	18.67	0.12	18.49	18.49
0.12	18.78	0.16	18.61	18.61
0.16	18.90	0.20	18.75	18.75
0.20	19.04	0.24	18.88	18.88
0.24	19.19	0.28	19.02	19.02
0.28	19.36	0.32	19.17	19.18
0.32	19.55	0.36	19.31	19.35
0.36	19.76	0.40	19.47	19.52
0.40	19.99	0.44	19.63	19.73
0.44	20.21	0.48	19.79	19.95
0.48	20.45	0.52	19.96	20.18
0.52	20.68	0.56	20.14	20.41
0.56	20.93	0.60	20.32	20.66
0.60	21.14	0.64	20.50	20.87
0.64	21.36	0.68	20.68	21.08
0.68	21.59	0.72	20.90	21.30
0.72	21.81	0.76	21.10	21.53
0.76	22.06	0.80	21.32	21.75
0.80	22.30	0.84	21.54	21.95
0.84	22.56	0.88	21.77	22.18
0.88	22.82	0.92	22.02	22.42
0.92	23.08	0.96	22.27	22.68
0.96	23.32	1.00	22.52	22.92
1.00	23.53			
1.04	23.72			
1.08	23.92			
1.12	24.13			
1.16	24.33			
1.20	24.54			
1.24	24.81			

TABLE 3 (continued)

I Zw 144		VII Zw 793			
log r	μ_G	log r	μ_G(maj)	μ_G(bar)	μ_G(min)
-0.60	18.22	-0.60	17.13		17.13
-0.40	18.24	-0.50	17.14		17.14
-0.30	18.28	-0.40	17.16		17.16
-0.20	18.34	-0.30	17.20		17.20
-0.10	18.44	-0.20	17.28		17.28
0.0	18.59	-0.10	17.39		17.39
0.10	18.81	0.0	17.52		17.52
0.20	19.09	0.10	17.74		17.74
0.28	19.34	0.20	18.00		18.00
0.36	19.63	0.28	18.23		18.23
0.44	19.95	0.36	18.49		18.53
0.52	20.24	0.44	18.76		18.87
0.60	20.53	0.52	19.06		19.21
0.68	20.82	0.60	19.38		19.57
0.76	21.12	0.68	19.69		19.94
0.84	21.43	0.76	20.02		20.28
0.92	21.77	0.84	20.32		20.62
1.00	22.13	0.92	20.63		21.00
1.08	22.48	1.00	20.91	20.91	21.42
1.16	22.83	1.08	21.22	21.16	21.84
1.24	23.20	1.16	21.53	21.39	22.21
1.32	23.56	1.20	21.68	21.48	22.37
1.40	23.95	1.24	21.83	21.57	22.48
		1.28	21.98	21.54	22.56
		1.32	22.14	21.50	22.61
		1.36	22.26	21.63	22.65
		1.40	22.36	21.84	22.70
		1.44	22.44	22.13	22.75
		1.48	22.52	22.43	22.76
		1.52	22.60	22.60	22.81
		1.56	22.69		22.88
		1.60	22.79		22.98
		1.64	22.85		23.12
		1.68	22.89		23.44
		1.72	22.96		23.95
		1.76	23.07		24.47
		1.80	23.24		
		1.82	23.41		
		1.84	23.64		
		1.86	23.89		
		1.88	24.17		
		1.90	24.56		

TABLE 3 (continued)

NGC 524		NGC 3379		
log r	μ_G(maj)	log r	μ_G(maj)	μ_G(min)
-0.30	17.76	-0.60	16.19	16.19
-0.20	17.78	-0.50	16.19	16.19
-0.10	17.81	-0.40	16.20	16.20
0.0	17.86	-0.30	16.22	16.22
0.10	17.92	-0.20	16.25	16.25
0.20	18.01	-0.10	16.28	16.28
0.30	18.13	0.0	16.33	16.33
0.40	18.29	0.10	16.39	16.39
0.50	18.46	0.20	16.50	16.50
0.58	18.63	0.30	16.66	16.66
0.66	18.82	0.40	16.85	16.85
0.74	19.05	0.50	17.09	17.09
0.82	19.28	0.60	17.37	17.37
0.90	19.53	0.68	17.61	17.61
0.98	19.76	0.76	17.89	17.89
1.06	19.98	0.84	18.15	18.16
1.14	20.21	0.92	18.43	18.45
1.22	20.45	1.00	18.71	18.76
1.30	20.71	1.08	19.03	19.08
1.38	21.04	1.16	19.38	19.43
1.42	21.23	1.24	19.70	19.79
1.46	21.44	1.32	20.03	20.13
1.50	21.62	1.40	20.32	20.41
1.54	21.79	1.48	20.57	20.68
1.58	21.93	1.56	20.81	20.97
1.62	22.07	1.64	21.11	21.32
1.66	22.23	1.72	21.47	21.73
1.70	22.38	1.80	21.86	22.16
1.74	22.57	1.88	22.29	22.61
1.78	22.78	1.96	22.74	23.06
1.82	23.03	2.04	23.18	23.48
1.86	23.25	2.12	23.61	23.95
1.90	23.49	2.20	24.06	24.44
1.92	23.64	2.28	24.55	

TABLE 3 (continued)

M 87			NGC 7457		
log r	μ_G(maj)	μ_G(min)	log r	μ_G(maj)	μ_G(min)
-0.60	17.00	17.00	-0.60	17.55	17.55
-0.40	17.02	17.02	-0.50	17.57	17.57
-0.30	17.03	17.03	-0.40	17.62	17.62
-0.20	17.07	17.07	-0.30	17.69	17.69
-0.10	17.12	17.12	-0.20	17.78	17.78
0.0	17.17	17.17	-0.10	17.90	17.90
0.10	17.24	17.24	0.0	18.05	18.05
0.20	17.32	17.32	0.10	18.23	18.27
0.30	17.41	17.41	0.20	18.44	18.50
0.40	17.50	17.50	0.30	18.66	18.76
0.50	17.61	17.61	0.40	18.87	19.04
0.60	17.73	17.73	0.50	19.09	19.35
0.70	17.87	17.87	0.60	19.33	19.66
0.80	18.03	18.03	0.70	19.55	19.96
0.90	18.24	18.24	0.80	19.78	20.22
1.00	18.49	18.49	0.90	20.02	20.49
1.08	18.72	18.72	1.00	20.21	20.72
1.16	18.98	18.98	1.08	20.38	20.94
1.24	19.26	19.26	1.16	20.55	21.19
1.32	19.55	19.55	1.24	20.74	21.50
1.40	19.84	19.84	1.32	20.97	21.82
1.48	20.16	20.17	1.40	21.19	22.17
1.56	20.47	20.52	1.48	21.43	22.52
1.64	20.79	20.90	1.52	21.56	22.70
1.72	21.13	21.29	1.56	21.72	22.93
1.80	21.48	21.67	1.60	21.89	23.18
1.88	21.84	22.06	1.64	22.07	23.46
1.96	22.20	22.47	1.68	22.25	23.74
2.04	22.58	22.93	1.72	22.42	24.03
2.12	22.95	23.38	1.76	22.60	24.30
2.20	23.33	23.80	1.80	22.78	24.62
2.28	23.66	24.22	1.84	22.99	25.07
2.36	24.01	24.68	1.88	23.27	
2.44	24.36	25.13	1.92	23.53	
2.52	24.72		1.96	23.80	
2.60	25.01		2.00	24.13	
			2.04	24.56	
			2.08	25.02	

FIGURE 3

Brightness profiles of the program galaxies are shown against the fourth root of the radius. In this coordinate system, de Vaucouleurs' (1948) law is a straight line. Each line is one measurement of one plate. Major and minor axis profiles are shown for elliptical objects. For VII Zw 793, the bar major axis (top), disk major axis, and minor axis (bottom) are shown. The points in Figures 3a and b are discussed in the text.

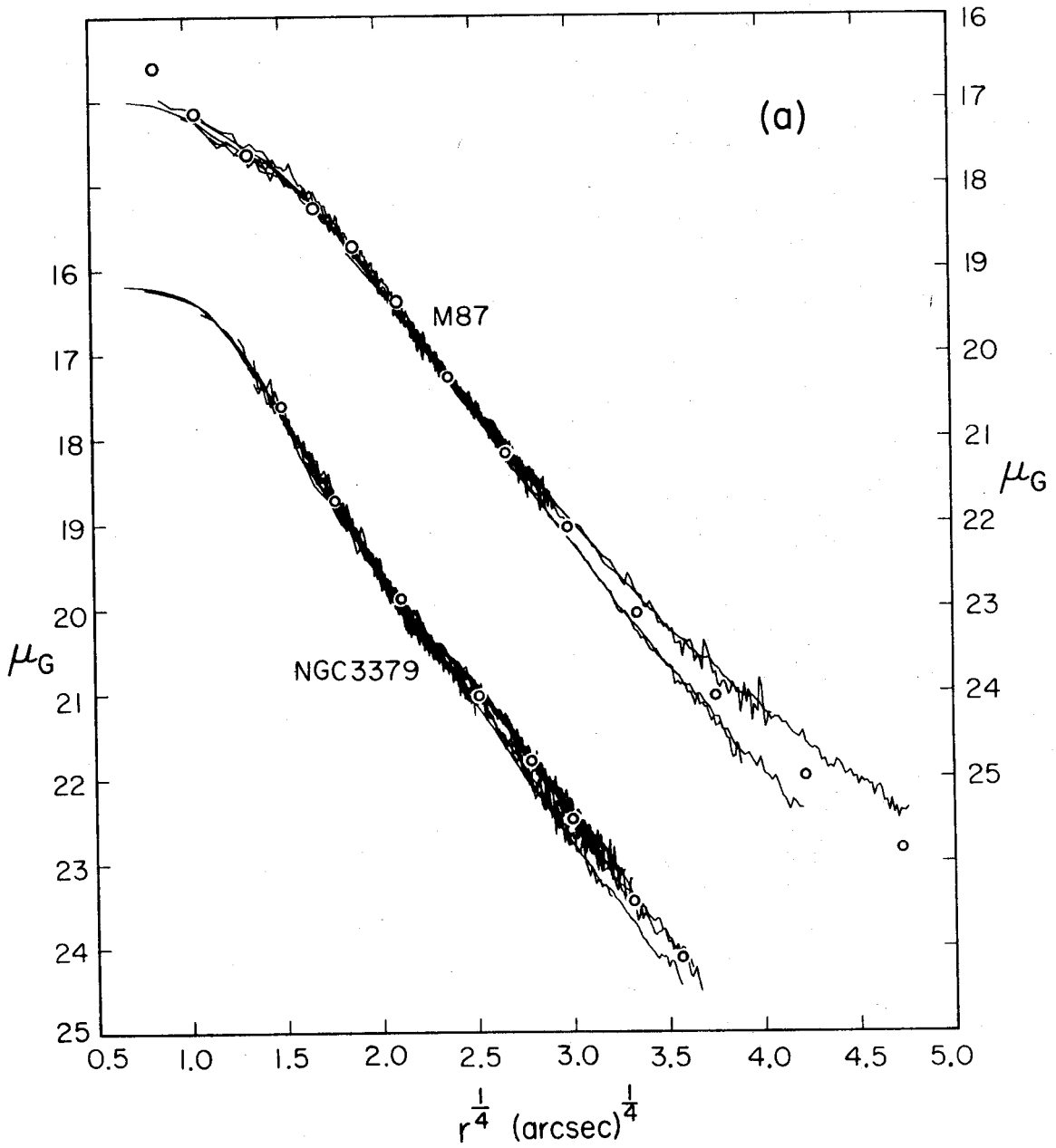
(a)
M87
NGC3379
μ_G
$r^{\frac{1}{4}}$ (arcsec)$^{\frac{1}{4}}$
0.5
1.0
1.5
2.0
2.5
3.0
3.5
4.0
4.5
5.0
16
17
18
19
20
21
22
23
24
25

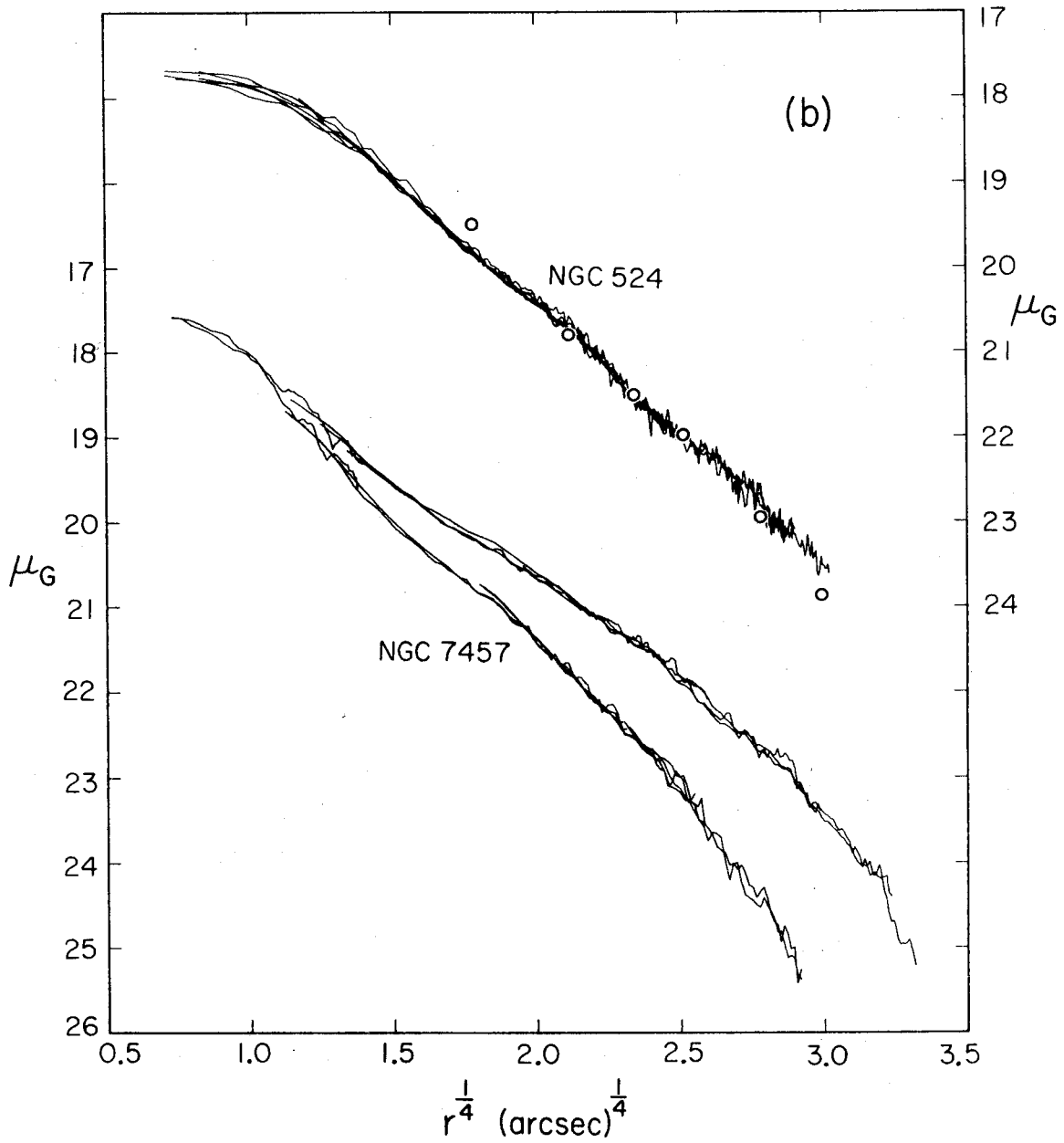
(b)
NGC 524
NGC 7457
μ_G
$r^{\frac{1}{4}}$ (arcsec)$^{\frac{1}{4}}$
17
18
19
20
21
22
23
24
25
26
0.5
1.0
1.5
2.0
2.5
3.0
3.5

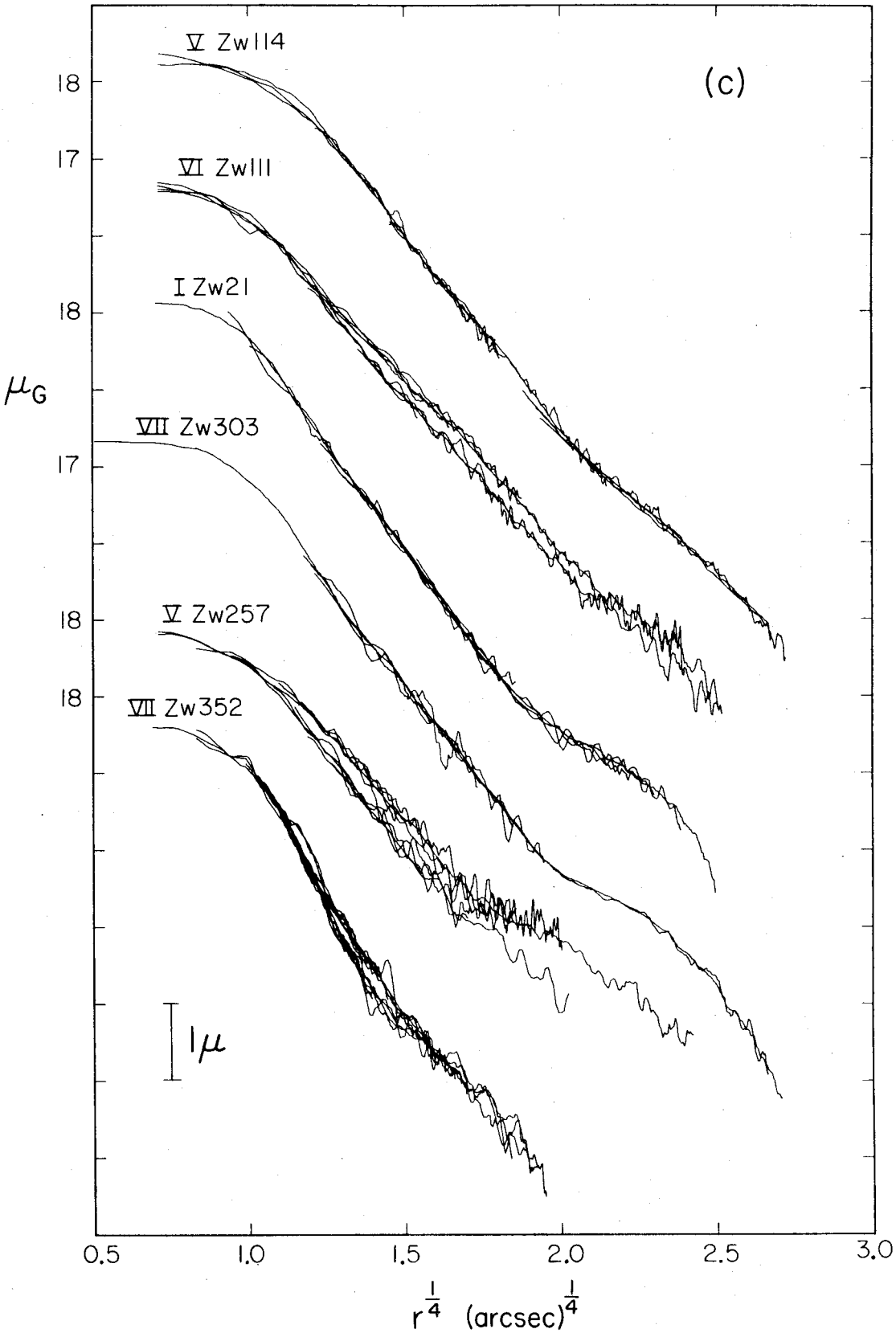
V Zw114
(c)
VI Zw111
I Zw21
VII Zw303
V Zw257
VII Zw352
18
17
18
17
18
18
μ_G
1μ
0.5
1.0
1.5
2.0
2.5
3.0
$r^{\frac{1}{4}}$ (arcsec)$^{\frac{1}{4}}$

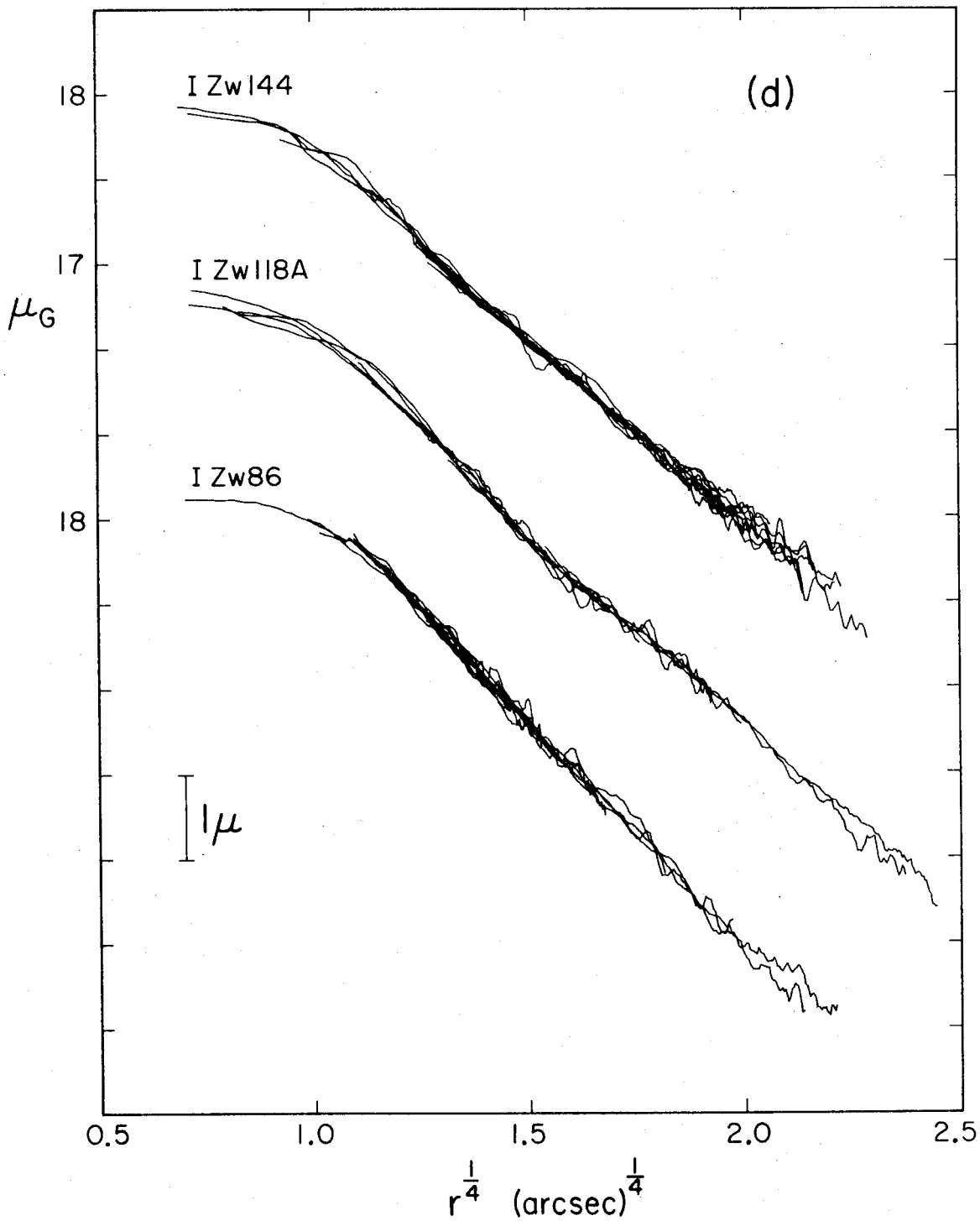
I Zw144
(d)
I Zw118A
I Zw86
18
17
18
μ_G
1μ
0.5
1.0
1.5
2.0
2.5
$r^{\frac{1}{4}}$ (arcsec)$^{\frac{1}{4}}$

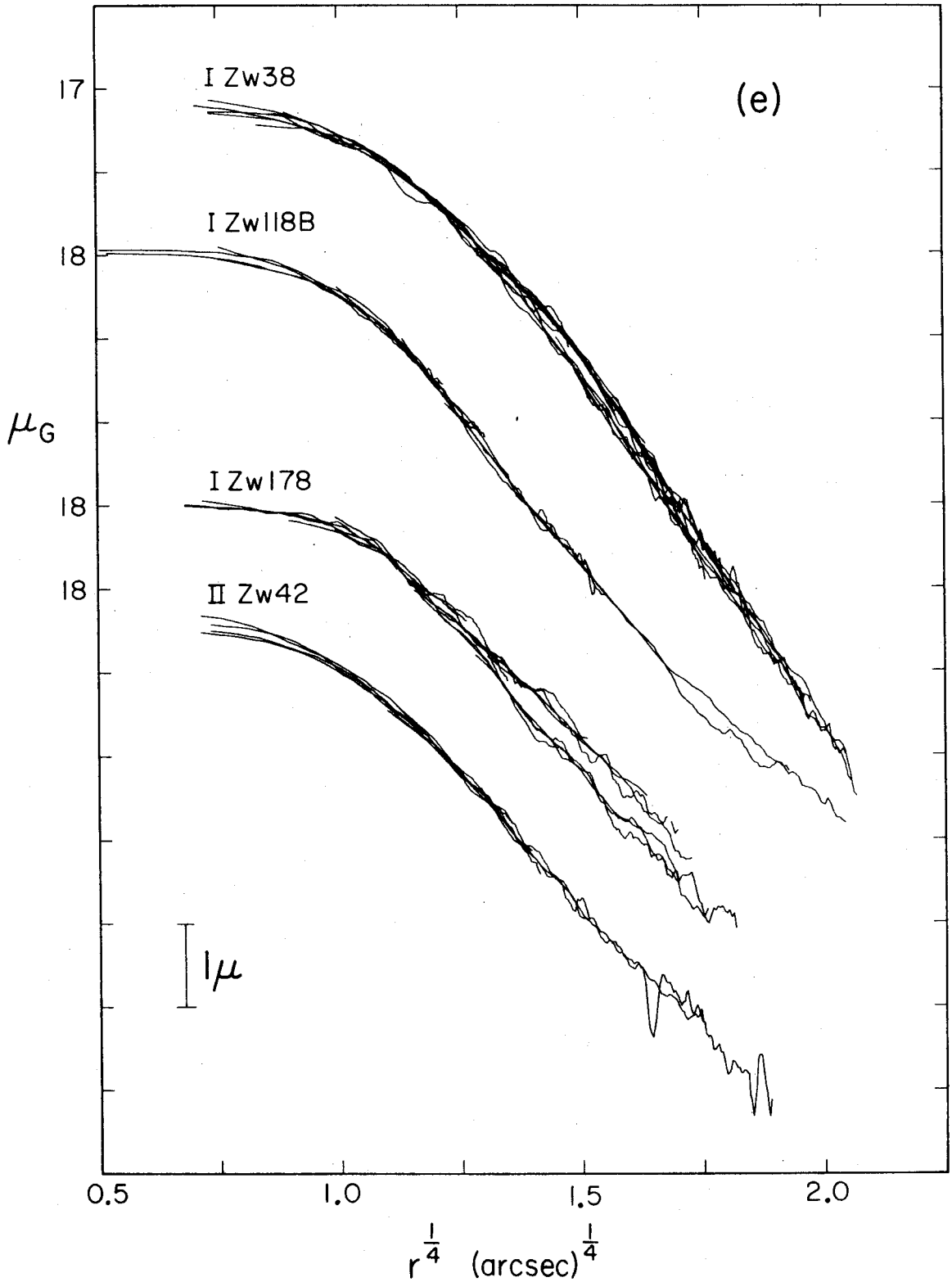
I Zw38
(e)
I Zw118B
I Zw178
II Zw42
17
18
18
18
μ_G
1μ
0.5
1.0
1.5
2.0
$r^{\frac{1}{4}}$ (arcsec)$^{\frac{1}{4}}$

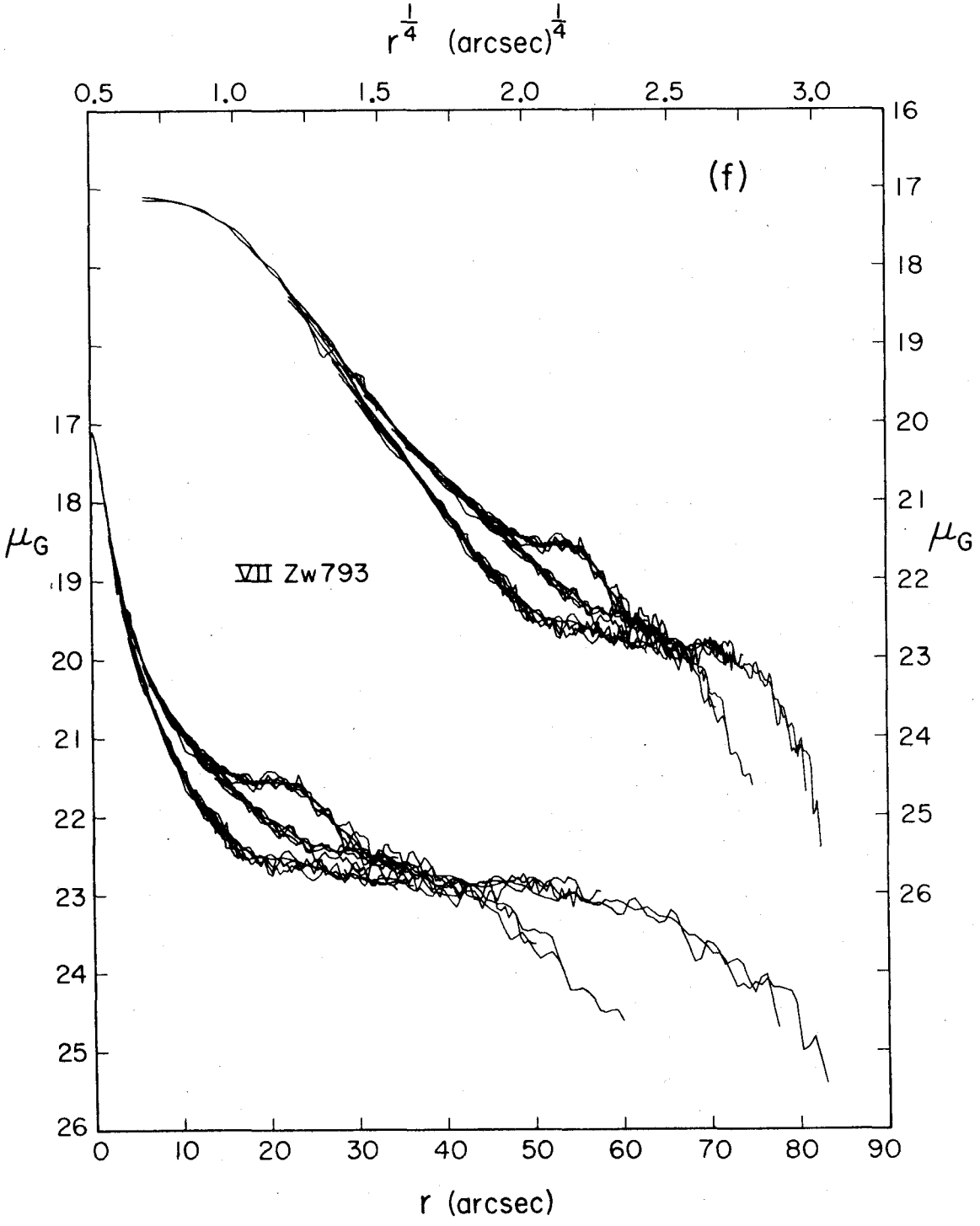
$r^{\frac{1}{4}}$ (arcsec)$^{\frac{1}{4}}$
0.5
1.0
1.5
2.0
2.5
3.0
(f)
VII Zw793
μ_G
μ_G
r (arcsec)
0
10
20
30
40
50
60
70
80
90
16
17
18
19
20
21
22
23
24
25
26

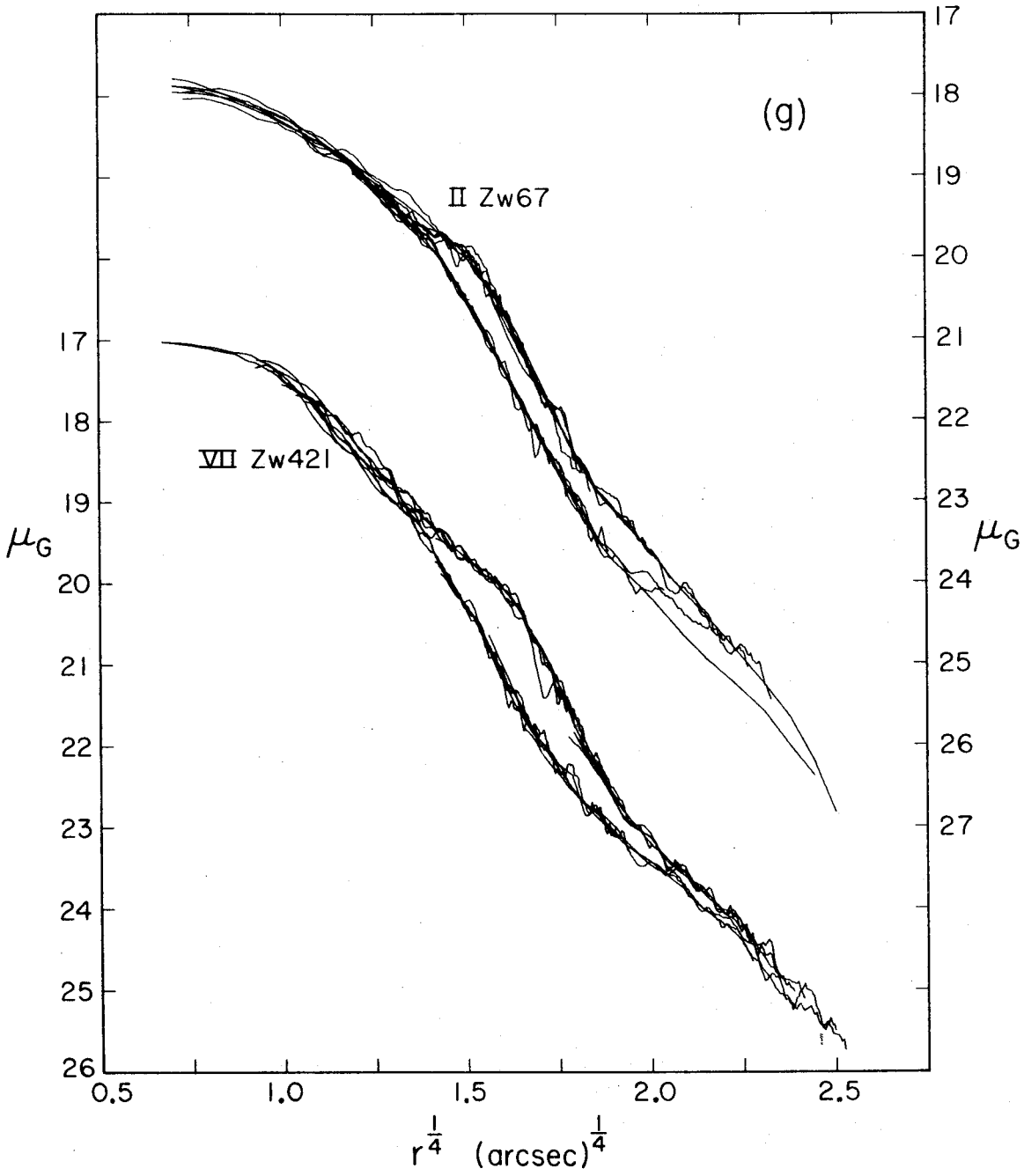
(g)
II Zw67
VII Zw421
μ_G
μ_G
17
18
19
20
21
22
23
24
25
26
27
0.5
1.0
1.5
2.0
2.5
$r^{\frac{1}{4}}$ (arcsec)$^{\frac{1}{4}}$

the existence of a cutoff in VII Zw 793 is certain, but the outermost point could be in error by 0.25 μ.

Another check comes from averaging, for different galaxies, the mean deviation of zero points obtained from different photoelectric apertures. This average is $0^m.016$ for measurements made on the same night, and $0^m.027$ otherwise. These are not larger than the photoelectric errors alone.

Finally, we can compare the present data with previous observations. NGC 3379 has been observed both photographically (Dennison 1954) and photoelectrically (Miller and Prendergast 1962; Burkhead and Kalinowski 1974). The various measurements agree well. The points in Figure 3a show Burkhead and Kalinowski's east-west B profile, converted to G using their B-V values and relation (2). Since east-west is nearly along the major axis, we see that the agreement in zero point and profile shape is excellent. King (1975) has measured the profile of M87 at 45° to the major axis. This is also shown in Figure 3a, with a zero point derived from de Vaucouleurs and de Vaucouleurs' (1964) B(0). The zero points are the same by construction, but the shapes can be compared, and agree very well. (In the central arcsecond, King (1975) has included part of the jet.) Finally, Figure 3b shows

Hodge and Steidl's (1976) photoelectric B profile of NGC 524, converted to G using their colors. The zero points agree very well, but the shapes begin to diverge at 23 Gμ. However, our data agree in detail with measurements by Johnson (1961), including the brightness enhancements at 20 and 45 arcsec. At the limit of our data, the profiles agree to 0.1 μ. Since no Schmidt plate is available, this is considered adequate.

VI. DISCUSSION OF INDIVIDUAL GALAXIES

a) The "Normal" Ellipticals

M87 and NGC 3379 were chosen more as photometric standard galaxies than because they are normal. M87 has an unusually low central concentration; that is, a very large core radius. It is the only galaxy in the sample in which a de Vaucouleurs law breaks down at small radii before seeing becomes important. The mean profile satisfies an $r^{1/4}$-law in the range $1.6 \leq r^{1/4} \leq 3.6$, and then gradually grows brighter than the $r^{1/4}$-law. Similarly, NGC 3379's profile turns upward strongly with respect to a de Vaucouleurs law at $r^{1/4} = 2.3$. We will suggest in Paper II that this is strong tidal distension produced by the close neighbors NGC 3384 and 3389. NGC 3379 also has a very compact core, and the highest central surface brightness in the present sample.

b) The "Normal" S0 Galaxies

NGC 7457 is an $S0_1$ galaxy chosen from the Hubble Atlas (Sandage 1961). It has a weak spheroid, which is only poorly measured on one plate. The disk is strong and exponential to the limits of the data.

NGC 524 is an $S0_2$, also chosen from the Hubble Atlas. It has a very strong spheroid, which is essentially a

giant elliptical galaxy. Within a diameter of D(0) (de Vaucouleurs and de Vaucouleurs 1964), the absolute B magnitude is -21.63, equal to that of M87, and remarkably high for an S0 galaxy. The profile satisfies a de Vaucouleurs law well, except for brightness enhancements at 20 and 45 arcsec. These are well determined and real; both were observed by Johnson (1961), and the outer one also by Hodge and Steidl (1976). An examination of the Hubble Atlas plate, kindly made available by Dr. A. Sandage, clearly shows that the outer feature is an S0 disk, with very faint spiral structure. The inner feature is probably a lens. It is noteworthy how small a perturbation---here less than 0.2 μ--results when (normal?) lenses and disks are added to a giant elliptical spheroid. A much larger deviation from a de Vaucouleurs law was detected at large radii by Johnson (1961). This will be discussed further in Paper II.

c) The S0 Compacts: Lens Components

Approximately six of the compacts have central spheroids following the de Vaucouleurs law and disks which appear mostly exponential. They are S0 galaxies. Figure 3c shows their profiles. Note that V Zw 114 and VI Zw 111 deviate so little above a de Vaucouleurs law that the existence of a disk is not certain. VI Zw 111, especially,

might only have a tidal halo (see Paper II).

I Zw 21 and VII Zw 303 are prototype core-halo compacts. A de Vaucouleurs law fits the cores very well. The halo in I Zw 21 is exponential to a few percent, but only over ~ 1 scale length before it begins to cut off. In VII Zw 303 there is a narrow shallow region, followed by a steeper decline. Possibly both halos are the shallow portions of extreme Type II exponentials (Freeman 1970). However, the profiles and photographs in Figure 1 strongly suggest that they are lens components of unusual prominence.

We adopt as defining characteristics of lenses the following (cf. Sandage 1961; Freeman 1975): (i) clear differentiation from spheroid and exponential disk, if visible; (ii) a shallow brightness gradient, possibly exponential, but only over $\lesssim$ 1 scale length, so other functions might work as well, and (iii) a sharp and steep outer cutoff. These are suggested by the present galaxies and ones in the above references. However, many other galaxies with a wide range of morphological types also have inner disks that look like lenses. Examples include the NGC 2841 class of spirals (Sandage 1961). It is not known whether all of these are to be identified as the same component (i.e., whether they have a unique origin and similar dynamics). A general interpretation of non-

exponential disks awaits the accumulation of more photometry. However, the identification of lens components in the present galaxies is fairly certain.

VII Zw 303 = NGC 3065 is discussed in the Hubble Atlas. The above lens is referred to there as the "outer envelope." The "lens" is not visible here; possibly it is not resolved by our small-scale plates, but more probably it was produced by a photographic effect (the toe of the characteristic curve). The "internal absorption ring" may be real, but is not visible at the scale of the Schmidt plates.

The other objects, V Zw 257 and VII Zw 352, seem to be more normal S0's. They have weak spheroids, like NGC 7457. The disks are exponential to the limit of the photometry, but may be lenses, since that limit is not very faint.

d) The E Compacts

The compacts illustrated in Figures 3d and e are elliptical galaxies. Except for I Zw 38, they have de Vaucouleurs profiles, sometimes with outer halos like that in M87. I Zw 118A has a brightness enhancement at 15 arcsec, which appears similar to the ones in NGC 524, and which may be a faint disk inside the spheroid. Some

of the other galaxies could have disks beyond the rather bright limit of the photometry.

The dispersion of profile segments is unusually large for I Zw 144 because the ellipticity of the galaxy has been ignored. Note also that the "very compact" galaxies I Zw 118B and I Zw 178 are similar to the other objects.

e) I Zw 38 = NGC 4486B: Tidal Limiting

I Zw 38 (Zwicky 1964) is a close companion of M87. Rood (1965) has shown that it has a tidally limited profile. Tidal effects in I Zw 38 have also been discussed by Faber (1973) and de Vaucouleurs (1974). Since no previous photometry is published, the profile is illustrated in Figure 3e. A de Vaucouleurs law fits badly, and the tidal cutoff is noticeable. The galaxy somewhat resembles a King (1966) globular cluster model with $\log (r_{tidal}/r_{core}) = 1.25$. A similar model described NGC 5846A (King and Kiser 1973). This model, and a plot of $\sqrt{\text{intensity}}$ versus $1/r$ (King 1962), both imply limiting radii of 27 arcsec. This agrees well with Rood's (1965) value of 30 arcsec. As emphasized by King and Kiser (1973), such tidally limited objects should probably be regarded as distinct from other compacts.

f) VII Zw 793: A Strong Lens

This is one of the most unusual galaxies in the sample. There is a compact $r^{1/4}$-law spheroid, and a faint bar. Surrounding this is a very large halo which drops by only ~ 1 μ in more than 35 arcsec of the major axis. The isodensity tracing illustrates it well. The halo has a sharp outer edge, beyond which the brightness drops steeply. The shallow part of the profile is moderately exponential, but only over 1/2 scale length, so that an exponential disk interpretation is meaningless. Rather, this is a lens of extraordinary prominence. Further, the weak spiral structure evident in Figure 1 implies that the lens is flattened like a disk. It would be of great interest to search for an exponential outer envelope. Deeper photometry of this object is in progress.

g) VII Zw 421 and II Zw 67: Possibly Metal-Poor Lens-Dominated Galaxies

These galaxies seem to be prototypes of a new class of objects. They are dominated by a very strong lens[1],

---

[1] I am indebted to Dr. K. C. Freeman for suggesting the lens interpretation.

shown in Figure 3g, with the usual nearly flat top and steep outer decline. There is a central spheroid which becomes brighter than the lens by ~ 2 μ. The outer exponential envelope is identified as an S0 disk. The overall profile resembles that of NGC 1553 (Freeman 1975).

The ellipticity in VII Zw 421 reaches a maximum in the lens, and then decreases toward zero in the disk. If the disk is really almost face-on, then the lens seems to be slightly ellipsoidal. Alternatively, the disk could be non-circular (as in many barred galaxies). However, neither the profile nor the photographs are consistent with the "lens" being a normal bar.

The spectra of these objects are also peculiar. VII Zw 421 (Figure 4) shows the Balmer series in absorption essentially as strong as Ca II H and K. At least eight Balmer lines are visible. Normal strong metal lines such as Fe λ4383 and Mg I λ5175 are weak or absent. No emission lines are detected. A SIT spectrum kindly obtained by Dr. H. C. Arp using the Hale telescope shows that II Zw 67 has a similar but less extreme spectrum. Note that the peculiarities clearly occur in the spheroid (the lens is underexposed). Possibly the galaxies are dominated by young stars. However, the spectra resemble more those of metal-poor globular clusters. An accurate

metal line index cannot be obtained for VII Zw 421 because the G band is masked by night sky emission at λ4358, and because most other indicators are absent. However, we can use the relative strength of H and K and the adjacent hydrogen lines. Comparing to spectra of globular clusters in our galaxy (Williams 1976) and in M31 (Searle and Rabin 1976) shows that only in M15 are the hydrogen lines nearly as strong as H and K. M15 has the lowest line index L = -1 on van den Bergh's (1969) scale of -1 to 15. Similarly, using the metal lines also, II Zw 67 has L $\simeq$ 6. Neither galaxy is intrinsically faint; in fact, II Zw 67 is nearly as bright as M87 (see Paper II). Thus there are giant, morphologically early (E or S0) galaxies which may be metal-poor (or possibly young). Other objects with similar spectra are listed by Zwicky (1964) and Sargent (1970). A more detailed study of these objects is planned.

VII. ARE COMPACTS COMPACT?

We have shown that the profiles of most compacts are qualitatively normal. In this § we ask whether they are quantitatively compact. We will compare compacts to four normal giant elliptical and S0 galaxies from the present sample, and 16 more measured and kindly made available by Dr. I. R. King (1976, see also Papers II and III).

Figure 5 compares the central surface brightnesses, B_o. Since no correction for seeing has been made, the central brightness decreases with decreasing resolution. Thus B_o is well correlated with the corrected velocity V_o. It should be strongly emphasized that the correlation contains no information about cosmology or galactic evolution. Then, omitting the most deviant point (V Zw 257), fifteen compacts are adequately described by the straight line $B_o = 17\overset{\mu}{.}17 + 0\overset{\mu}{.}149\ V_o/1000\ \text{km s}^{-1}$. The dispersion about the line is $0\overset{\mu}{.}24(\sigma)$. Twenty normal galaxies are <u>brighter</u> than this relation by $0\overset{\mu}{.}18 \pm 0\overset{\mu}{.}55(\sigma)$. Thus none of the compacts are unusual in terms of central brightness. In their central parts, all the galaxies greatly exceed the 20 μ required by Zwicky's (1971) definition of compactness. On the other hand, the definition suggests that a more global brightness measurement would be more appropriate.

FIGURE 5

Central surface brightness in B_{μ} versus the corrected velocity of recession V_o. Fifteen of sixteen compacts (filled circles) are described by the straight line $B_o = 17^{\mu}.17 \pm 0^{\mu}.149\ (V_o/1000\ \text{km s}^{-1})$. This is produced by atmospheric seeing, and the resulting decrease of resolution with increasing distance. Normal galaxies are shown as crosses.

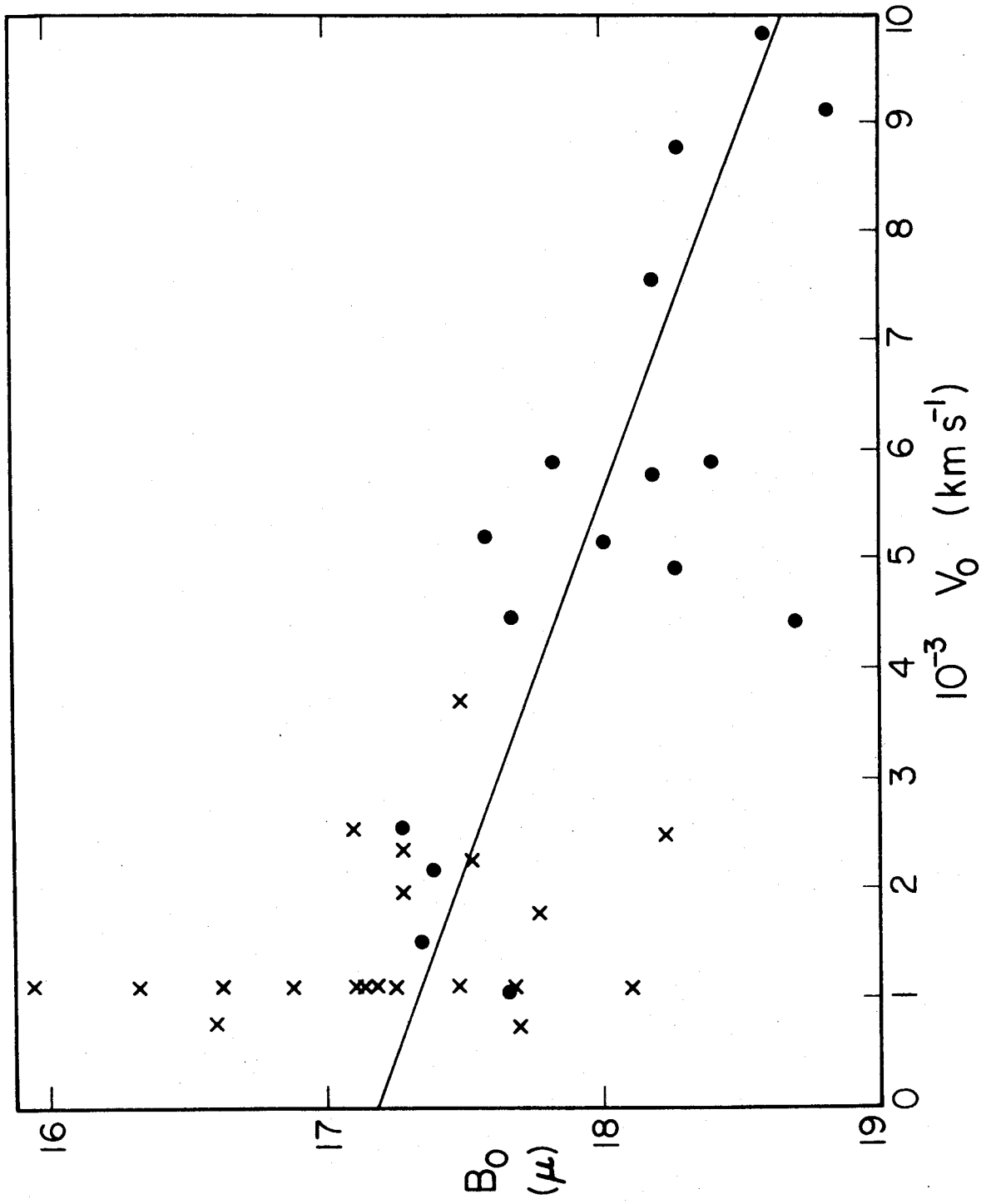
16
17
18
19
B_0 (μ)
0
1
2
3
4
5
6
7
8
9
10
10^{-3} V_0 (km s^{-1})

Figure 6 shows the mean surface brightness within the 23.0 B_{μ} contour, as seen from outside our galaxy ($A_B = 0.2 \csc b^{II}$). It is plotted against the absolute magnitude within the same contour. This isophote would correspond to de Vaucouleurs and de Vaucouleurs' (1964) diameter D(0) if there were no absorption. Again, most compacts appear normal. VII Zw 793 seems faint because the 23 B_{μ} isophote includes the lens, which has a strong effect because of its shallow gradient. It is otherwise not more diffuse than the other objects. Only II Zw 67 and VII Zw 421 are significantly compact. I Zw 38 also has a high mean brightness, but cannot be compared directly to the normal galaxies because it is so much less luminous. Over larger magnitude ranges, $\langle \mu_B \rangle_o$ may depend on M_B (cf. Oemler 1974). Evidently most compacts are quantitatively normal in terms of global photometric parameters. We will show in Paper II that this is essentially confirmed when a more detailed examination is made of characteristic parameters of the profiles.

FIGURE 6

Mean B surface brightness within the 23.0 B_{μ} isophote as seen outside our galaxy, plotted against absolute magnitude within the same contour. Compacts are shown as filled circles, and normal galaxies as crosses.

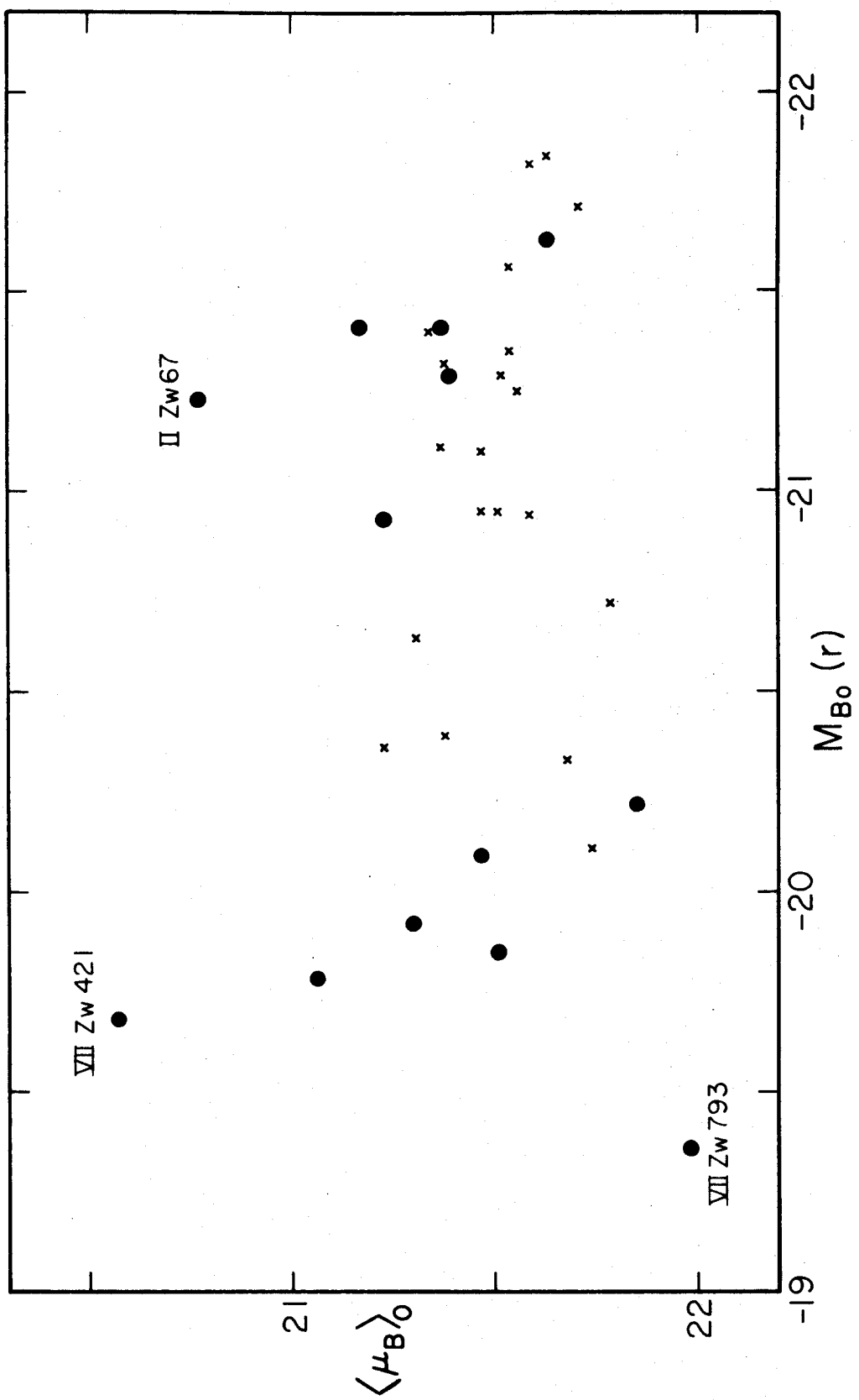
II Zw67
VII Zw421
VII Zw793
21
22
-19
-20
-21
-22
$\langle \mu_B \rangle_0$
M_{B_0} (r)

VIII. SUMMARY OF RESULTS

We have presented major and minor axis G brightness profiles, photoelectric photometry, and spectroscopic data for sixteen red compact and four normal galaxies. Detailed studies of profile shapes and parameter systematics will be made in future papers. Major results of the present, mostly qualitative, discussion are summarized below.

(1) Brightness distributions in the compacts surveyed consist of the same components found in ordinary galaxies: spheroids following the $r^{1/4}$-law, lenses with as-yet unmodelled profiles, and (probably) exponential disks. Compacts are therefore E and S0 galaxies.

(2) Their central surface brightnesses, and mean brightnesses within the 23 B_{μ} contour are mostly normal. The exceptions are VII Zw 421 and II Zw 67, whose mean brightnesses are abnormally high by ~ 1-1/2 μ. Compacts also have the normal UBVR colors of early type galaxies. Thus they are generally not compact in terms of global photometric properties.

(3) The "large nearly uniform brightness halos" frequently described by Zwicky are lens com-

ponents (Sandage 1961) of unusual prominence. Lenses occur between the spheroid and any exponential disk, and are characterized by shallow brightness gradients and sharp, steep outer cutoffs. Often the shallow portions are very exponential, but only over a short range ($\lesssim$ 1 scale length).

(4) Particularly worth noting among the strong-lens compacts is VII Zw 793. Here the lens is almost completely uniform, and dominates the galaxy. The existence of weak spiral structure implies it is a disk. No exponential disk is visible on the present short exposures. It would be interesting to know whether, when the lens is a disk, it co-exists with or takes the place of an outer exponential.

(5) Most peculiar in the present sample are VII Zw 421 and II Zw 67. They appear to be prototypes of a special class of objects. Even more than VII Zw 793, they are dominated by lenses, but here the lenses have high surface brightness and resemble spheroids. They are clearly distinct from the real spheroid and outer exponential disk. Also characteristic

of these objects are spectra consisting of Ca II H and K and strong Balmer absorption, but only weak metal lines. They are similar to globular cluster spectra with the lowest van den Bergh (1969) metal line indices ($L \simeq -1$ for VII Zw 421; $L \simeq 6$ for II Zw 67). Thus these are high luminosity, early type galaxies which may be metal poor.

(6) Lenses seem to be distinct components in brightness distributions, which can be varied in strength almost independently of the rest of the galaxy. They seem further to be morphologically intermediate between spheroids and disks. Thus the lens in VII Zw 793 is clearly a disk, while those in VII Zw 421 and II Zw 67 resemble spheroids. In fact, their outer cutoffs follow a de Vaucouleurs law well enough that if the flat portions were even smaller, or the galaxies farther away, the lenses would be indistinguishable from spheroids. On the other hand, the evidence is not yet strong enough to imply an origin for lenses intermediate between that for spheroids and disks.

Most compacts are qualitatively peculiar only in their tendency to have prominent lens components, although this is partly a selection effect in the choice of objects. Further investigation requires a quantitative study of the photometric structure parameters. This is the subject of the remaining papers in this series.

REFERENCES

Arp, H., and Bertola, F. 1971, Ap. J., 163, 195.

Burkhead, M. S., and Kalinowski, J. K. 1974, A. J., 79, 835.

Dennison, E. W. 1954, Ph.D. thesis, University of Michigan.

de Vaucouleurs, G. 1948, Ann. d'Astrophys., 11, 247.

_____. 1959, Hdb. d. Phys., 53, 311.

_____. 1961, Ap. J. Suppl., 5, 233.

_____. 1967, Publ. Dept. Astron. Univ. Texas, Ser. II, 2, No. 3.

_____. 1974, in The Formation and Dynamics of Galaxies (IAU Symposium No. 58), ed. J. R. Shakeshaft (Boston: D. Reidel), p. 1.

de Vaucouleurs, G., and de Vaucouleurs, A. 1964, Reference Catalogue of Bright Galaxies (Austin: University of Texas Press).

Faber, S. M. 1973, Ap. J., 179, 423.

Freeman, K. C. 1970, Ap. J., 160, 811.

_____. 1975, in Dynamics of Stellar Systems (IAU Symposium No. 69), ed. A. Hayli (Boston: D. Reidel), p. 367.

Hodge, P. 1974, Ap. J. (Letters), 191, L21.

Hodge, P., and Steidl, P. 1976, A. J. (in press).

Hubble, E. 1930, Ap. J., 71, 231.

Huchra, J. P. 1976a, in preparation.

_____. 1976b, private communication.

Humason, M. L., Mayall, N. U., and Sandage, A. R. 1956, A. J., 61, 97.

Johnson, H. M. 1961, Ap. J., 133, 314.

King, I. 1962, A. J., 67, 471.

_____. 1966, ibid, 71, 64.

_____. 1975, private communication.

King, I. R., and Kiser, J. 1973, Ap. J., 181, 27.

Kormendy, J. 1973, A. J., 78, 255.

_____. 1976a,b,c, in preparation.

Kormendy, J., and Bahcall, J. N. 1974, A. J., 79, 671.

Kormendy, J., and Sargent, W. L. W. 1974, Ap. J., 193, 19.

Miller, R. H., and Prendergast, K. H. 1962, Ap. J., 136, 713.

Miller, W. C. 1964, Pub. A.S.P., 76, 433.

_____. 1971, A.A.S. Photo Bulletin, Issue No. 4, 3.

Oemler, A. 1974, Ap. J., 194, 1

Rood, H. J. 1965, A. J., 70, 689 (A).

Rood, H. J., Page T. L., Kintner, E. C., and King, I. R. 1972, Ap. J., 175, 627.

Sandage, A. 1961, The Hubble Atlas of Galaxies (Washington: Carnegie Institution of Washington).

_____. 1973, Ap. J., 183, 711.

Sargent, W. L. W. 1970, Ap. J., 160, 405.

Searle, L., and Rabin, D. 1976, private communication.

Thuan, T. X., and Gunn, J. E. 1976, submitted to Pub. A.S.P.

van den Bergh, S. 1969, Ap. J. Suppl., 19, 145.

Williams, T. B. 1976, private communication.

Zwicky, F. 1964, Ap. J., 140, 1467.

_____. 1971, Catalogue of Selected Compact Galaxies and of Post-Eruptive Galaxies (Guemligen: F. Zwicky).

CHAPTER 2

STRUCTURE PARAMETERS OF THE SPHEROIDAL COMPONENT

I. INTRODUCTION

In this paper, we will make a preliminary study of the systematic properties of galaxy spheroids. The problems considered will be the homogeneity of the shapes of their brightness profiles, and the ranges of, and relevant correlations between their characteristic parameters. We will also continue an investigation of red compact galaxies, begun in Paper I (Kormendy 1976a), by comparing them, in the above context, to normal galaxies. In the past, the only papers on the general properties of spheroids have been based on poor data or on statistical mean parameters (eg., Fish 1964, Gudehus 1973; see also de Vaucouleurs 1974). In large part, this was due to a lack of data. We are very fortunate in having access to a sample of 17 elliptical galaxies measured and kindly made available by Dr. I. R. King (1975). These, together with 15 red compacts from Paper I, provide a sample large enough for the present preliminary study. However, it should be remembered that the sample is still small, probably not representative of all objects, and limited in luminosity range.

A large number of simple analytic fitting functions have been used to model spheroid profiles. These include ones by Hubble (1930), de Vaucouleurs (1948, 1953), Baum (1955), King (1962), and Abell amd Mihalas (1966). We will also so classify the King (1966) dynamical model, since

it is similarly general and easy to use. In an Appendix, we will compare how the functions of Hubble and de Vaucouleurs, and the King (1966) model describe galaxies. It will turn out that they all basically measure the same quantities. However, the de Vaucouleurs law is the most convenient, and marginally the most accurate. It will be used in the discussion which follows.

A recurring theme in this paper will be the suggestion that ellipticals with close neighbors are tidally distended. This emerges from a consideration in § II of the homogeneity of profile shapes. In § III, we will discuss the parameters derived by fitting de Vaucouleurs laws to the galaxies. Section IV provides a list of conclusions.

Nine of the King galaxies required profile zero points. Fortunately, all 17 objects had B(0) values listed in de Vaucouleurs and de Vaucouleurs (1964). We have integrated King's mean profiles to radii of 1/2 D(0) and identified the result with B(0). This yields zero points accurate to $\leq 0^m.1$, which is adequate for our purposes.

A Hubble constant of $H_0 = 50$ km s^{-1} Mpc^{-1}, and a galactic absorption of $0^m.20$ csc b^{II} are used throughout.

II. TIDAL DISTENSION IN ELLIPTICAL GALAXIES

In the course of matching de Vaucouleurs laws to the King ellipticals, it became clear that some galaxies were fit very well, while others were fit very badly. That is, the profiles did not all have the same shape. Some of the non-$r^{1/4}$ galaxies, like NGC 4406 and NGC 4649, were noticed to have close massive neighbors. Some that were well fit, like NGC 4472, were dynamically isolated. This suggested a possible tidal effect.

Accordingly, and without looking at the profiles further, the galaxies were divided into three groups, according to the degree of possible tidal influence by neighbors.

T3: These are galaxies with at least one companion of comparable or greater luminosity within several diameters.

T1: There are no neighbors of any importance, so the objects should be dynamically isolated.

T2: An intermediate group was required where the degree of tidal influence is unclear. It includes galaxies at moderate distances from much brighter objects, and very luminous galaxies with much fainter companions.

The results of this classification are given in Table 1 (§ III).

An examination of the data showed that the non-$r^{1/4}$ law profiles were all T3 or T2. Even here, the inner portions were described by a de Vaucouleurs law over $\geq$ 4 mag arcsec^{-2} (hereafter μ). Since tidal effects are largest at large radii, this inner range was fit. In contrast, de Vaucouleurs laws could be fit to the whole of T1 profiles. The tidal effect can then be illustrated by scaling the galaxies to have a common de Vaucouleurs law, with r_0 = 10 kpc and B_{0V}= 22 B μ (see § III for a definition of the parameters). The galaxies are plotted in Figure 1, grouped by tidal class. This illustrates the main conclusion of this §, namely that <u>ellipticals with nearby companions of comparable luminosity have bright envelopes above the extrapolation of a de Vaucouleurs law fit to the inner parts. These envelopes are greatly reduced or absent in isolated galaxies</u>.

In Figure 1, there is some residual curvature even in T1 profiles. If our interpretation of how to model tidal halos has been overenthusiastic, then r_0 will be too large, and B_{0V}too faint, in undisturbed galaxies. The effect is small, and will be evaluated in the Appendix. However, Figure 1 emphasizes the halos by construction. We will therefore also, in the Appendix, test for their presence using Hubble and King models. We will show that these support the above conclusion.

FIGURE 1

Surface brightness versus the fourth root of the radius, for King ellipticals scaled to have a common de Vaucouleurs law (dashed lines). The different tidal classes have been separated by 3 μ intervals. This illustrates the tidal halos possessed by T3 galaxies.

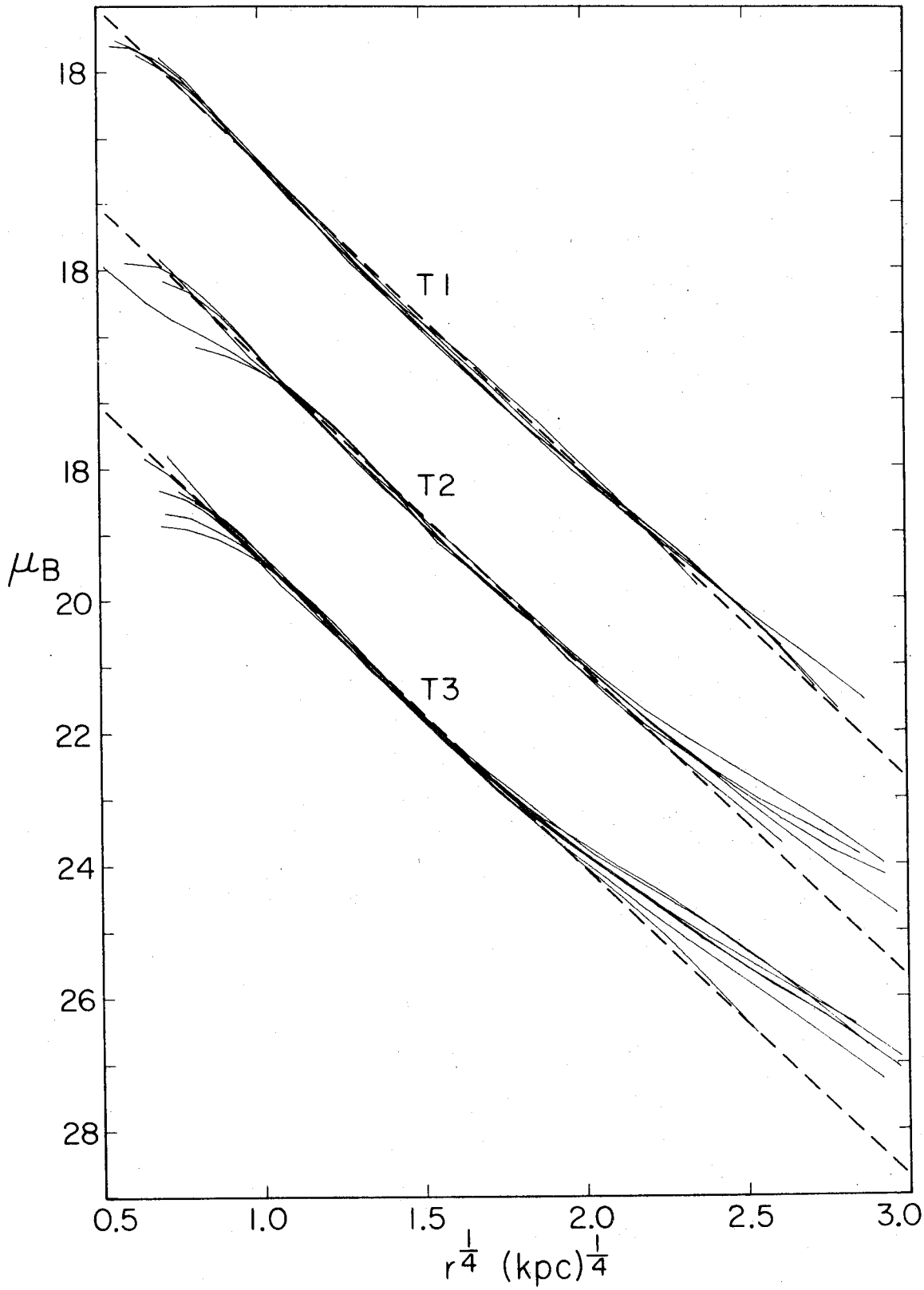
18
18
18
20
22
24
26
28
μ_B
T1
T2
T3
0.5
1.0
1.5
2.0
2.5
3.0
$r^{\frac{1}{4}}$ (kpc)$^{\frac{1}{4}}$

Note that one T3 galaxy fits a de Vaucouleurs law well. This is NGC 7626, the second brightest galaxy in a loose cluster. However, one exception is not a problem, since projection effects will always make a few galaxies seem closer to neighbors than they really are. More embarrassing would be a T1 object with a large halo, and this is not observed.

How do the halos arise? The simplest possibility is that the gravitational potential fields are instantaneously distended by tidal forces. When two similar galaxies are brought close together, their potential wells grow and become elongated along the line joining them. This process is reversible as long as stellar orbital periods are much shorter than the encounter timescale. However, at the limits of the present photometry, the stellar orbital periods are several times 10^8 years, entirely comparable to the interaction time. Thus stars will also gain energy at the expense of the galactic orbit. This will increase the size of any tidal halo. If the galaxies are bound to each other, stars at these radii will be shared, in complicated orbits in a common outer potential well. This would produce a strong merging of the outer isophotes, as observed by Arp and Bertola (1971), and Kormendy and Bahcall (1974). If the galaxies are not bound, the heating will probably be less, and some stars will escape. Such collisions of

galaxies have been studied by Richstone (1975). A similarly detailed calculation of the magnitude of the above effects is beyond the scope of this paper. However, there seems to be ample opportunity to produce the observed halos.

Note that the processes discussed above will have a very different effect, namely tidal stripping, if one galaxy is much less massive than the other. As the small galaxy approaches, and the potential barrier between the objects gets smaller, the outer stars try to equally populate all of the phase space accessible to them. Since a large new region belonging to the massive galaxy has become accessible, the victim will escape without these stars, because they don't happen to be anywhere nearby. Tidal stripping is a well known phenomenon, observed by Rood (1965), King and Kiser (1973), Paper I, and others.

One other comment is worth making. According to King (1975), the data have been corrected for profile overlap. Tidal halos seem to exist despite this correction. Kormendy and Sargent (1974) used the absence of such distortions to conclude that NGC 68 was not a member of VV 166. Similar contamination corrections were made there. Thus the results of that paper are not invalidated.

III. PARAMETERS OF THE DE VAUCOULEURS RELATION

The de Vaucouleurs (1948, 1953) law has the form

$$\log (I/I_{0V}) = -3.33\ [(r/r_0)^{1/4} - 1], \text{ in intensity units,} \quad (1)$$

where r_0 is the radius that contains half the light of the model, and I_{0V} is the surface brightness at that radius. To minimize effects of the three-dimensionality of spheroids, we use the profile at 45° to the major axis. Mean profiles were calculated for galaxies from Paper I, assuming the isophotes are elliptical. The King (1975) data were already mean profiles. De Vaucouleurs laws were then fit to all the galaxies as discussed in § II. The parameters are listed in Tables 1 and 2.

The fits for normal galaxies are very good, as illustrated in Figure 1. A similar figure is not shown for compacts, because the excellent quality of the fits is easily seen in Figure 3 of Paper I, where the profiles are plotted against $r^{1/4}$. In S0 compacts, equation (1) is satisfied to a few percent from the seeing disk to the start of the lens, generally 4-5 μ. Elliptical compacts are entirely similar. Note that several also have tidal halos. All this is true despite the fact that the profiles were averaged in log r coordinates, in Paper I, increasing our confidence that the de Vaucouleurs law adequately describes the data.

TABLE 1

PARAMETERS OF THE SPHEROIDS OF NORMAL GALAXIES

NGC	Type[1]	Distance (Mpc)	Source[2]	$-M_B$[3]	T	B_{0V}	r_0(kpc)	B_{0H}	a(kpc)	B_{0M}	a_M(kpc)	n	B_{0K}	r_C(kpc)	$\log(\frac{r_t}{r_c})$
2300	E^+2	47	1,4	21.22	3	21.93	5.6	16.49	0.47	16.48	0.37	1.78	17.18	0.46	2.25
4261	E2-3	45	2	21.65	2	22.49	8.9	17.08	0.77	16.97	0.65	1.92	17.56	0.71	2.25
4365	E3	22	3	20.76	2	23.25:	9.2:	17.55	0.64	17.48	0.52	1.84	18.07	0.57	2.25
4374	E^+1	22	3	21.12	3	21.59	4.4	16.69	0.52	16.56	0.44	1.90	17.13	0.46	2.20
4382	$SAS(s)0^+P$	22	3	21.50	3	20.78	2.7	15.26	0.22	14.89	0.12	1.67	16.12	0.24	$\geq$ 2.25
4406	E^+3	22	3	21.19	3	22.28	6.3	16.93	0.57	16.77	0.38	1.73	18.11:	0.76:	> 2.25:
4472	E2	22	3	22.10	1	22.57:	12.5:	17.25	1.08	16.70	0.65	1.85	17.31	0.76	> 2.25
4486	E0-1P	22	3	21.64	2	22.08:	7.3:	16.59	0.60	17.33	1.03	2.11	18.21	1.15	1.80
4552	E0	22	3	20.64	2	21.02	2.6	15.86	0.26	15.84	0.25	1.99	17.12	0.40	2.00
4589	E2	40	4	20.87	1	22.58	7.1	17.23	0.63	17.19	0.59	1.97	17.61:	0.48:	$\geq$ 2.25:
4621	E5	22	3	20.66	2	21.71	3.7	16.80	0.43	16.71	0.37	1.92	16.84:	0.27:	$\geq$ 2.25:
4636	E^+0-1	22	3	20.94	1	23.31:	11.0:	17.47:	0.65:	17.38	0.44	1.66	17.95	0.58	$\geq$ 2.25
4649	E2	22	3	21.64	3	21.28	4.7	16.31	0.53	16.27	0.51	1.99	17.34	0.61	2.00
4697	E6	22	3,4	21.39	1	22.17	7.1	16.49	0.50	16.53	0.51	1.98	17.01	0.42	$\geq$ 2.25
5846	E0	36	4	21.27	3	22.54	7.8	17.37	0.79	17.36	0.70	1.88	17.95	0.69	2.25
6703	S0	51	4	21.33	1	22.53:	8.4:	17.32	0.78	17.29	0.75	1.98	17.40	0.50	$\geq$ 2.25
7626	E1	76	4,5	21.78	3	23.01	14.2	17.96	1.49	18.24	2.19	2.23	17.78	0.83	$\geq$ 2.25
524	$SA(rs)0^+$	49	6	21.59	2	23.21	13.9	18.00	1.39	17.77	0.91	1.76	18.36:	1.10:	> 2.25:
3379	E^+1	17	4,7	20.59	3	20.87	2.08	15.84	0.23	15.79	0.19	1.82	16.60	0.22	2.25
4486	E0-1P	22	3	21.64	2	22.09	7.1	16.77	0.65	17.27	1.10	2.17	17.98:	0.98:	2.00:

NOTES TO TABLE 1

[1] Morphological types are taken from de Vaucouleurs and de Vaucouleurs (1964).

[2] Distances are derived using H_0 = 50 km s^{-1} Mpc^{-1} and individual or group velocities from the following sources:

(1) Average velocity of NGC 2300 and 2276, from (4),below, and from Zwicky and Herzog (1968).

(2) $\langle V_0 \rangle$ = 2253 ± 57 km s^{-1} for five galaxies in the "W-a" cloud discussed by de Vaucouleurs (1961, see Table 4).

(3) $\langle V_0 \rangle$ = 1111 ± 75 km s^{-1} for the Virgo cluster (Sandage and Tammann 1974; see also de Vaucouleurs 1961).

(4) De Vaucouleurs and de Vaucouleurs (1964).

(5) $\langle V_0 \rangle$ = 3804 km s^{-1} for NGC 7611, 7617, 7619, 7623 and 7626, as listed in (4).

(6) Paper I.

(7) $\langle V_0 \rangle$ = 862 km s^{-1} for NGC 3379, 3384 and 3389, as listed in (4).

[3] The absolute magnitude corresponds to B(0) as listed in de Vaucouleurs and de Vaucouleurs (1964).

TABLE 2

DE VAUCOULEURS PARAMETERS FOR COMPACT GALAXIES

Galaxy	Type[1]	Distance	$-M_B$[2]	T	B_{0V}	r_0(kpc)
V Zw 114	(S0)	103	21.32	1	20.90	3.6
VI Zw 111	E1	90	21.21	3	21.76	5.1
V Zw 257	(S0)	89	20.24	1	22.21:	3.6:
II Zw 42	(E0)	104	20.51	1	19.90	1.7
I Zw 21	(S0)	98	19.87	1	21.53	2.5
VII Zw 303	SA(r)0	46	19.70	3	20.95	1.6
VII Zw 352	(S0)	182	20.02	1	20.01:	1.3:
VII Zw 421	(S0)	52	19.71	1	(19.6)[3]	(0.9)[3]
II Zw 67	E1;(S0)	138[4]	21.25	2	(19.7)[3]	(2.0)[3]
I Zw 86	(E0)	116	20.89	3	21.12	3.3
I Zw 118 A	(E0P?)	118[5]	21.36	3	21.21	4.0
I Zw 118 B	E0 vc	118[5]	19.74	3	19.80	1.1
I Zw 144	(E1)	197	21.54	1	22.89	11.7
I Zw 178	(E2)vc	175	21.31	1	20.41	2.8
VII Zw 793	(R')SB(s)0	30	19.13	1	21.16	1.3

[1]Morphological types are taken from de Vaucouleurs and de Vaucouleurs (1964), unless in parentheses, in which case these are our own estimates. Zwicky's (1971) "very compact" is denoted vc.

[2]These are absolute magnitudeswithin the observed 23.0 B μ contour, corresponding to the definition in Table 1.

[3]Very approximate overall fits were made to give indicative scale factors.

[4]Distance from Rood et al. (1974).

[5]Distance determined using mean velocity of A and B.

In the Table, colons indicate uncertainty.

Next we consider the parameters. Some experimentation suggests that the most relevant correlation is that between B_{0V} and r_0, shown in Figure 2. The parameter range observed is as follows.

$$
\begin{aligned}
B_{0V} &\begin{cases} \text{Normal Galaxies:} & 20.8 \leq B_{0V} \leq 23.3 \quad B\ \mu \\ \text{Compacts} & : \quad 19.8 \leq B_{0V} \leq 21.8 \quad B\ \mu \\ \text{All} & : \quad 19.8 \leq B_{0V} \leq 23.3 \quad B\ \mu \end{cases} \\
r_0 &\begin{cases} \text{Normal Galaxies:} & 1.9 \text{ kpc} \leq r_0 \leq 14.1 \text{ kpc} \\ \text{Compacts} & : \quad 1.0 \text{ kpc} \leq r_0 \leq 5.1 \text{ kpc} \\ \text{All} & : \quad 1.0 \text{ kpc} \leq r_0 \leq 14.1 \text{ kpc} \end{cases}
\end{aligned}
\tag{2}
$$

In the above, we have neglected V Zw 257, which is poorly determined, and VII Zw 421, whose fit is only very approximate, to give some idea of its size. Also, I Zw 144 is clearly a misidentified normal galaxy at large distance.

There is a good correlation between the parameters. For 19 normal galaxies, it has the form

$$B_{0V} = 3.02 \log r_0 + 19.74\ \mu \ , \tag{3}$$

with a dispersion of only 0.28 μ. The thirty normal and compact galaxies together give essentially the same result, with a dispersion 0.1 μ larger than the above. The parameter along this line is absolute magnitude M_B. Lines of constant M_B satisfy

$$B_{0V} = 5 \log r_0 + \text{constant} \ . \tag{4}$$

FIGURE 2

B_{0V} versus log r_0 for de Vaucouleurs law fits to compact (small symbols) and normal (large symbols) galaxies. The heavy line is the relation for normal galaxies, given at upper right. Average absolute magnitude ticmarcs are defined by equation (5). Also shown is a typical line of constant M_B, defined by the labelled galaxies.

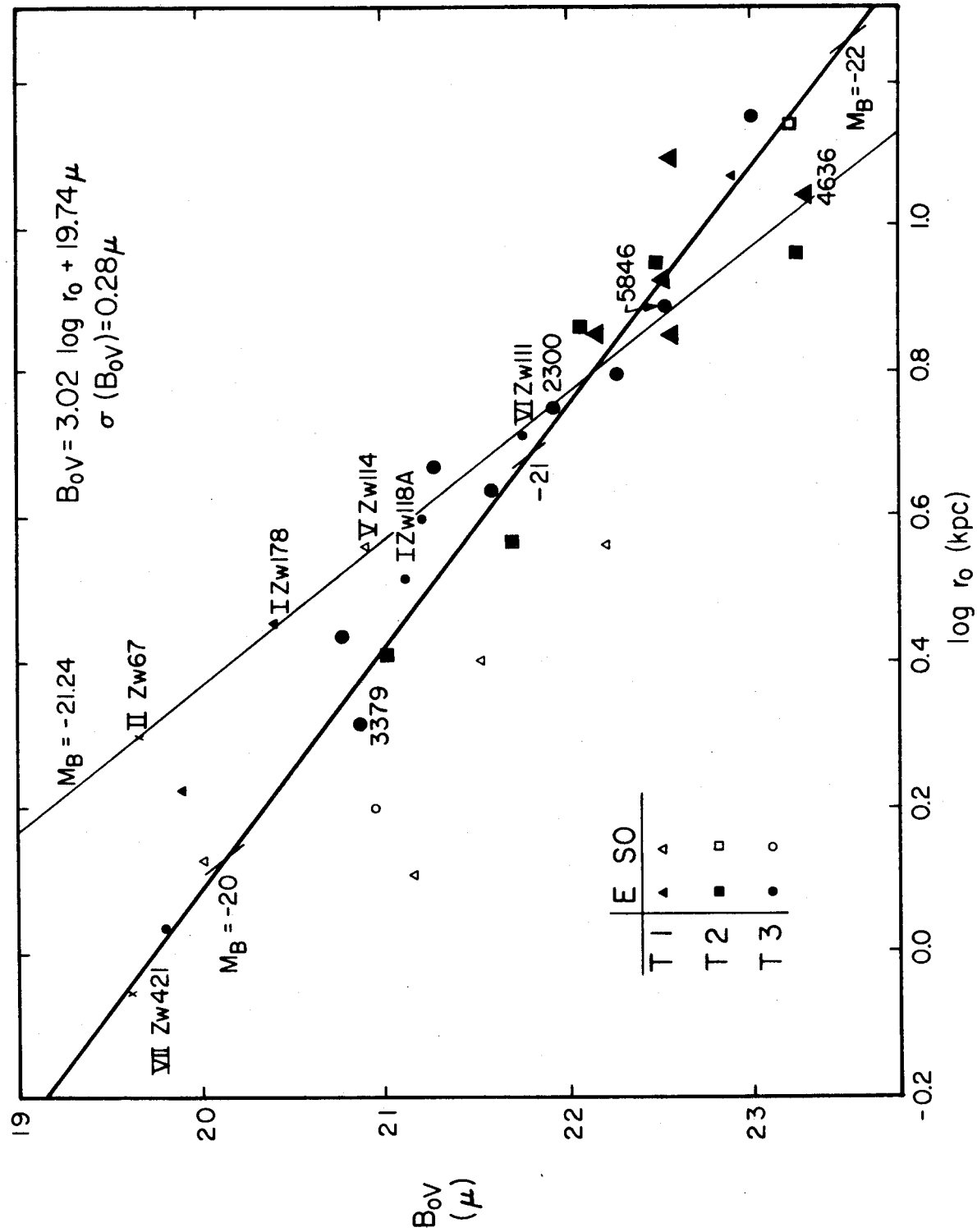
$B_0V = 3.02 \log r_0 + 19.74\mu$
$\sigma(B_0V) = 0.28\mu$
$M_B = -21.24$
$M_B = -20$
$M_B = -22$
-21
II Zw67
IZw178
VZw114
IZw118A
VIIZw111
2300
5846
4636
3379
VII Zw421
E SO
T 1
T 2
T 3
19
20
21
22
23
B_0V (μ)
-0.2
0.0
0.2
0.4
0.6
0.8
1.0
log r_0 (kpc)

One such line is shown. Since it is not strongly inclined to $B_{0V}(\log r_0)$, a range in observed galaxy models at any M_B does not greatly increase the scatter about the parameter relation. Put another way, it is difficult to extract the distribution of possible models from any errors.

As expected, compact galaxies are at the small-r_0, bright-B_{0V} end of the $B_{0V}(\log r_0)$ relation. However, there is considerable overlap in the two distributions. For instance, NGC 3379 is entirely similar to an average compact. Most compacts are small only because they have a low luminosity, but a few actually have abnormally small r_0 and bright B_{0V} for their absolute magnitude. This is well illustrated by the eight galaxies defining the line $\langle M_B \rangle = -21.24 \pm 0.13(\sigma)$ in Figure 2. (The absolute magnitude M_B is defined below.) From an approximate model, the most compact of these is the very peculiar object II Zw 67 (Paper I). Next is I Zw 178, called "very compact" by Zwicky (1971). The remaining compacts are increasingly more normal. Finally, the most diffuse objects are three ordinary ellipticals from King (1975). Note that these galaxies, all of which have the same M_B, span almost the complete parameter range observed. Thus Zwicky's classification is sometimes successful. On the other hand, most compacts are not unusual (see also Paper I).

Note that four S0 compact spheroids, which certainly appear as compact as the rest, are actually abnormally diffuse for their M_B. An important question is whether S0 spheroids are generally more diffuse than ellipticals.

The existence of a B_{0V} (log r_0) relation implies that each parameter correlates individually with M_B. To illustrate this, we will use an absolute magnitude based on B(0), as listed in de Vaucouleurs and de Vaucouleurs (1964). Then for normal galaxies, M_B is independent of the profiles. An equivalent M_B is calculated for compacts by integrating the profile to the 23 B μ contour (see the above reference). This defining isophote is also appropriate because it is usually just interior to any tidal halo or S0 disk.

Figures 3(a) and (b) show B_{0V} and 5 log r_0 plotted against M_B. The scatter is large, because B_{0V}(log r_0) is nearly parallel to lines of constant M_B. However, the correlations are present. The lines shown are not fit to the points, but are calculated from equations (3) and (5), below. They describe the average way in which brighter galaxies have larger r_0 and fainter B_{0V} (i.e., are "more diffuse"). It would be interesting to know whether cD galaxies, which are exceptionally bright and exceptionally diffuse, satisfy B_{0V}(log r_0). This would help to determine whether cD galaxies originate in a different way than normal galaxies.

FIGURE 3

Correlations of the de Vaucouleurs parameters with absolute magnitude. The meaning of the symbols is the same as in Figure 2. The mean relations shown are defined by equations (3) and (5). The scatter is large, representing the range of possible galaxy models at each M_B (also any modelling errors). Since B_{0V} and r_0 together must define M_B very precisely (see Figure 4), the deviations are generally of equal amounts and in opposite directions in the two panels.

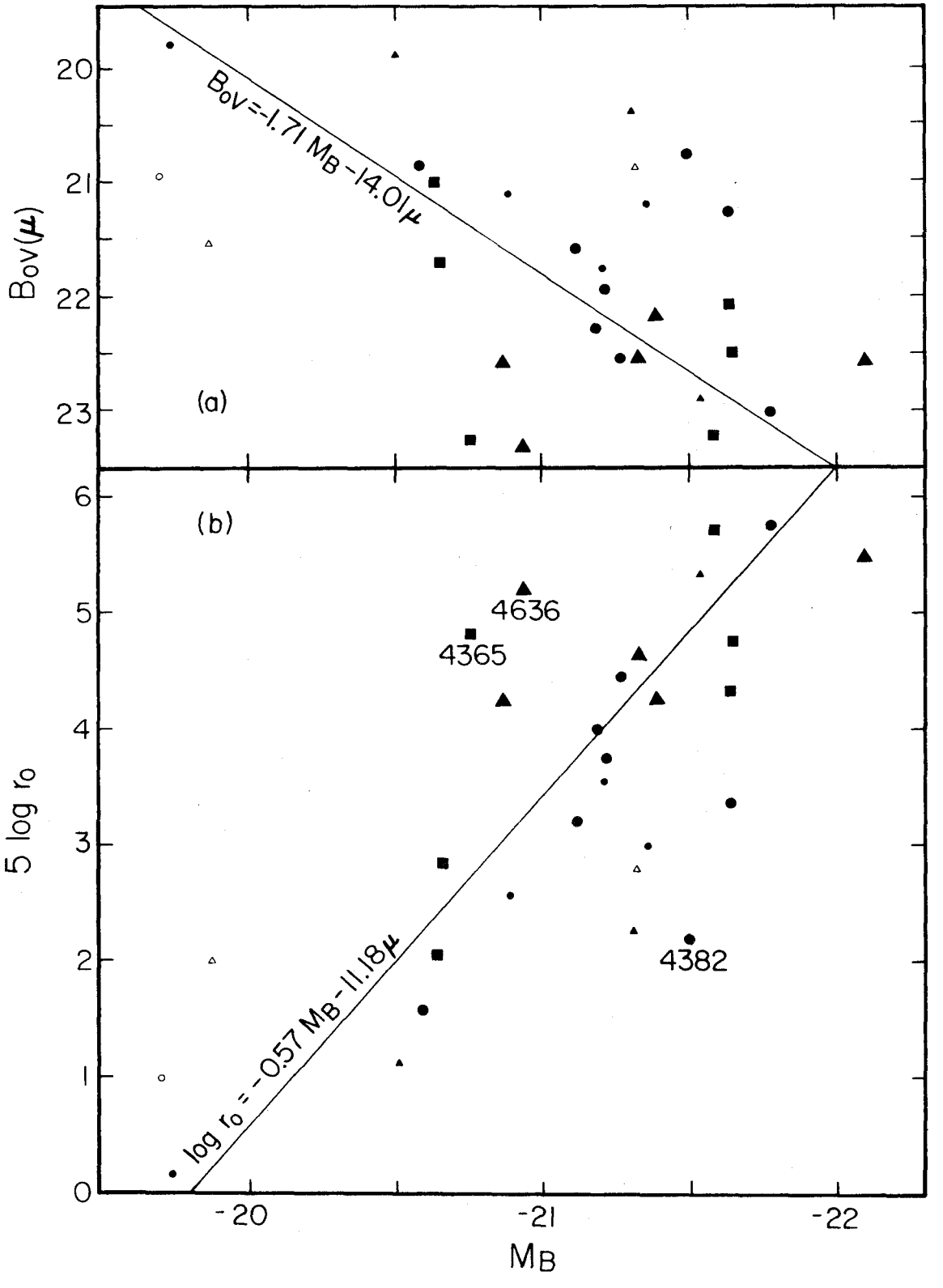
20
21
22
23
$B_{oV}(\mu)$
$B_{oV}=-1.71\,M_B-14.01\mu$
(a)
(b)
6
5
4
3
2
1
0
5 log r_o
4636
4365
4382
log $r_o=-0.57\,M_B-11.18\mu$
-20
-21
-22
M_B

The scatter in Figure 3 is the dispersion in observed models at constant magnitude. Unfortunately it also reflects any modelling or photometric errors. These are estimated below, and seem to be small. Part of the dispersion is due to the compacts, which were chosen for that purpose. However, some normal galaxies also deviate. NGC 4636 is discussed in the Appendix, where we suggest that it has a disk faint enough not to make the profile too different from an $r^{1/4}$-law, within the T1 classification, but strong enough to make the object appear diffuse. The presence of a disk was also suggested by Sandage (1961). In NGC 4365 we have probably included too much tidal halo in the model. Finally, NGC 4382 and 4649 are potentially the most tidally disturbed galaxies in the sample. If, as suggested earlier, these galaxies acquired abnormally strong halos[1] by tidal

---

[1]Note that NGC 4382 is an S0 galaxy. However, the profile is nowhere even close to exponential, so the disk is a small perturbation on the spheroid, as in NGC 524 (Paper I) and NGC 4636. Its existence should be kept in mind, but generally we have treated NGC 4382 like the ellipticals.

---

stretching or heating, the required light was presumably taken from just interior to the halo. This would produce a deviation like the one observed. Detailed studies of more objects are required to test this interpretation.

We have shown that neither de Vaucouleurs parameter determines M_B by itself. However, together they must define M_B very precisely, since no fit was tolerated unless it described the galaxy to $\lesssim$10%. Thus large deviations are generally of equal amounts and in opposite directions in Figures 3(a) and (b). The total magnitude of a de Vaucouleurs law is B_{0V} - 5log r_0 + constant. Figure 4 shows B_{0V} - 5log r_0 against M_B.

The expected good correlation is present. Twenty-four galaxies satisfy

$$M_B = 1.013\ (B_{0V} - 5\log r_0) - 39^m.53, \text{ or}$$
$$M_B = (B_{0V} - 5\log r_0) - 39^m.28, \qquad (5)$$

constraining the slope to be 1. The dispersion is only $0^m.18$. Thus B_{0V} - 5log r_0 is an excellent absolute magnitude indicator, and has been used to provide average M_B ticmarcs in Figure 2.

In the above, we have neglected NGC 3379, 4365, 4382 and 4636. Equation (5) holds only if $\varepsilon = \frac{1}{2} D(0)/r_0$ is the same for all objects; otherwise there is an additional small term in ε. The four neglected galaxies deviate mostly because they happen to have abnormal values of ε. We have chosen to omit the objects rather than complicate the discussion by using the correction explicitly.

FIGURE 4

The absolute magnitude of a de Vaucouleurs model is shown plotted against M_B. The meaning of the symbols is the same as in Figure 2.

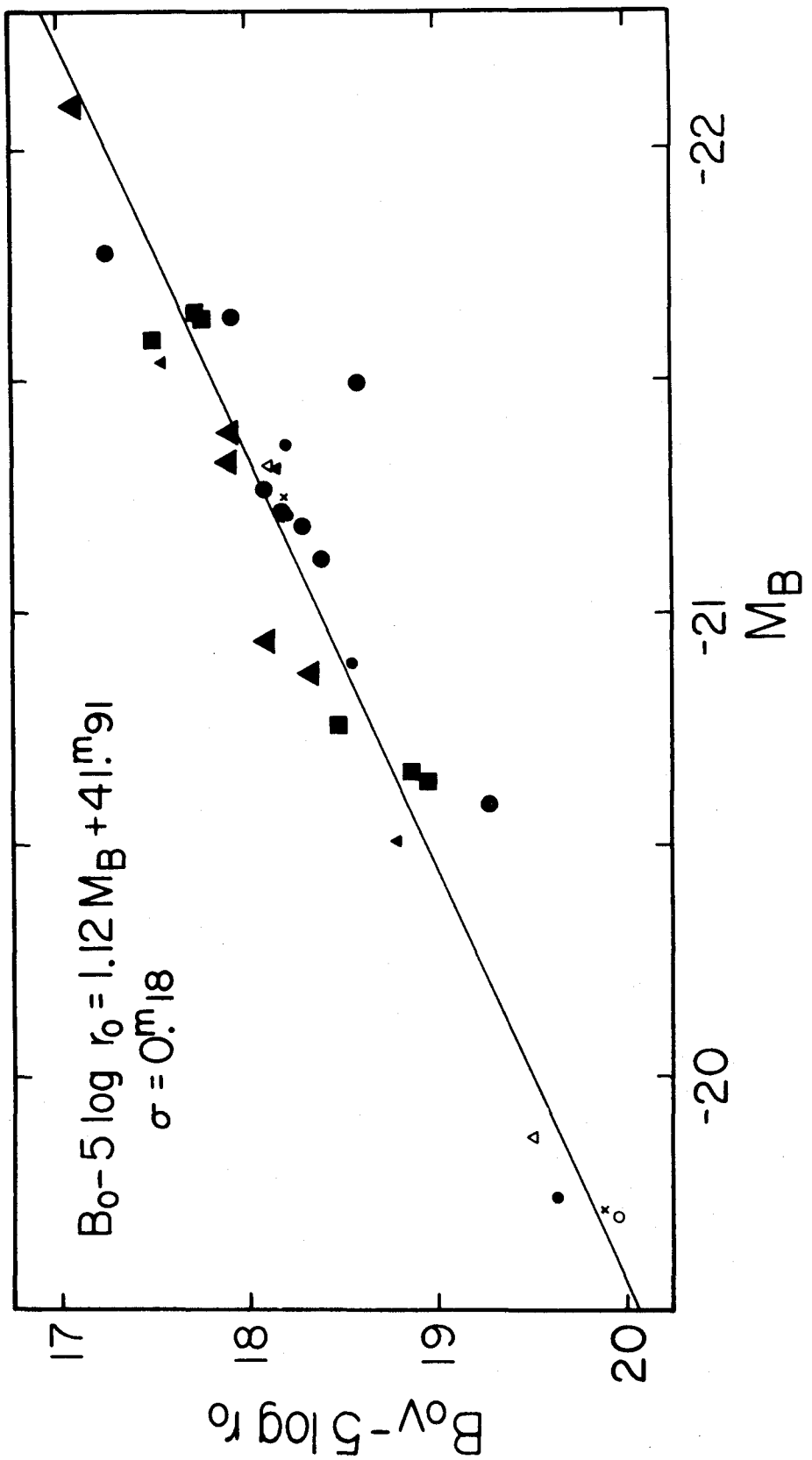
$B_{oV}-5\log r_o$
17
18
19
20
-20
-21
-22
M_B
$B_o-5\log r_o = 1.12\,M_B + 41.^m91$
$\sigma = 0.^m18$

Note in Figure 4 that $B_{0V} - 5\log r_0$ is systematically brighter for T1 than for T3 galaxies. As discussed in § II, this probably means that we should have allowed for some outer halo even in T1 objects. The difference between the two groups is $0^m.18$ in M_B (nearly the dispersion in the Figure, not surprisingly), corresponding to errors in $\log r_0$ of 0.10, and in B_{0V} of $0^m.30$. For example, normal galaxy triangles in Figure 2 should be shifted leftward, parallel to $B_{0V}(\log r_0)$, by this amount. This has no effect on any of the conclusions of either this or the next section. However, it does contribute slightly to the scatter in Figure 3.

A more serious limitation is the smallness of the absolute magnitude range. All the galaxies are within 2.3 mag of first-ranked cluster ellipticals like NGC 4472. The number of galaxies is also small. Thus the parameter relations derived here should be regarded as preliminary. They do not, however, depend on the particular nature of the de Vaucouleurs law. In the Appendix, similar relations will be derived using Hubble (1930) and King (1966) models, fully confirming the present results.

Remark: II Zw 67 and VII Zw 421 are included as crosses in Figure 4, only to show how they fit into the absolute magnitude range. Neither is very faint, and II Zw 67 is as bright as giant ellipticals. Thus, as stated in Paper I,

these are giant, early-type systems with spectra like metal poor or young stars.

IV. DISTANCE DETERMINATION USING $B_{0V}(\log R_0)$

Equation (3) can be used to determine relative distances, since B_{0V} is almost independent of distance while r_0 is proportional to it. For example, we can test claims of Gudehus (1973) and others that the Virgo cluster is closer than its redshift distance by ~ 30%, corresponding to a peculiar velocity of ~ 350 km s^{-1}. Eleven of the normal galaxies in Figure 2 are in Virgo. Eight others are not; seven of these have larger velocities than Virgo by factors of 1.6-3.5. Evaluating the mean deviations of these groups around $B_{0V}(\log r_0)$, we find,

for 11 Virgo galaxies, $\delta_V(\log r_0) = +0.005 \pm 0.039$

$(\sigma_1 = \sigma_{obs}/\sqrt{9})$, and

for 8 others, $\delta_o(\log r_0) = -0.009 \pm 0.024$

$(\sigma_2 = \sigma_{obs}/\sqrt{6})$.

Thus $$\delta_V - \delta_o = 0.015 \pm 0.046 \ (\sqrt{\sigma_1^2 + \sigma_2^2}) \ .$$

This means that Virgo is closer than its velocity distance by

$$\delta(m - M) = 0\overset{m}{.}07 \pm 0\overset{m}{.}23 \ , \qquad (6)$$

corresponding to a peculiar velocity of 39^{+107}_{-121} km s^{-1} in the direction suggested by Gudehus. Furthermore, this is an upper limit, since we have neglected the K-correction. The differential K-correction between the nearest

and farthest galaxy is $0^m.05$; if included, it would decrease $\delta(m - M)$. This null result supports Sandage and Tammann's (1974, 1975) claims that the Virgo cluster has no peculiar velocity, and that the local Hubble flow is very uniform. In fact, the method used is very similar to that of Gudehus. However, parameters are more accurately derived from actual profiles, and the groups being compared are treated exactly alike. In general, the method is similar to, but potentially more accurate than one used by de Vaucouleurs (1961) to determine relative distances in the direction of the Virgo cluster.

V. CONCLUSIONS

Our purpose has been to make a preliminary study of the brightness and size parameters of the spheroidal component of galaxies. Previous studies (Fish 1964, Gudehus 1973, 1975) were based on poor or less complete data such as mean surface brightnesses. Their reliability is uncertain. The major results of the present paper are listed below.

(1) Galaxies with close neighbors of comparable mass have extended outer halos with respect to a de Vaucouleurs law. These are absent or much reduced in isolated objects. Possibly this is tidal distension of the gravitational potential field. In bound pairs, the outer part of the potential well envelopes both objects, and stars are shared in complicated orbits; this halo will probably gain energy and grow at the expense of the galaxy orbits.

(2) The galaxy sample covers a range of 2.3 mag in M_B, downward from first-ranked cluster ellipticals. Over this range, the de Vaucouleurs half light radius r_0 varies from 1.0 to 14.1 kpc, and the brightness B_{0V} from 19.8 to 23.3 B μ.

(3) Over the above M_B range, there is a good correlation of B_{0V} with r_0, more luminous galaxies being more diffuse (larger r_0, fainter B_{0V}). For 19 normal galaxies, $B_{0V} = 3.02 \log r_0 + 19.74$ μ, with a dispersion of only $0^{\mu}.28$.

(4) There is a large range of models (B_{0V}, r_0) at each M_B. Large deviations from the M_B correlations can often be understood in terms of physical features such as unrecognized disks (NGC 4636), or tidal effects (NGC 4382, 4649). However, both parameters together necessarily determine the absolute magnitude well, to $0^{m}.18$.

(5) Most compacts are compact only because they have low luminosity; they satisfy the $B_{0V}(\log r_0)$ relation. A few are intrinsically compact in having abnormally small r_0 and bright B_{0V} for their absolute magnitude. These include the peculiar object II Zw 67 (see Paper I). This extends similar results reached in Paper I. On the other hand, most S0 compact spheroids seem abnormally diffuse.

(6) The $B_{0V}(\log r_0)$ relation can be used to determine relative distances, since B_{0V} is nearly independent of distance while r_0 is proportional to it. As an example, we can evaluate the error in the redshift/distance modulus for 11 Virgo cluster galaxies relative to 8 mostly more distant objects. Virgo is closer than its redshift distance by $\delta(m - M) \leq 0^m.07 \pm 0^m.23$. This corresponds to a peculiar velocity of $\leq 39^{+107}_{-121}$ km s^{-1}, supporting Sandage and Tammann's (1974, 1975) observations that the local Hubble flow is very uniform.

The above results are fully confirmed when a similar analysis is made using the Hubble (1930) and King (1966) brightness profiles (Appendix).

Our main limitation is the small and rather biased sample of galaxies. This may affect the statistics of the parameter correlations, which should be regarded as only preliminary. It also bases our judgement of how to do the model fitting on a few, possibly special objects. Similar problems have occurred previously. For instance, NGC 3379, the subject of considerable detailed dynamical modeling (Miller and Prendergast 1962, Prendergast and Tomer 1970, Wilson 1975), is suggested here to be strongly influenced by tidal effects.

The sample is also too small to allow an investigation of some of the most interesting aspects of spheroid structure. How do the parameter correlations behave when the magnitude range is extended, especially to very low luminosities? Do spheroids disappear by decreasing r_0, or the brightness, or both? How does the spheroid of an S galaxy compare quantitatively to an elliptical? Is there any difference between galaxies in different clusters? These problems are so well known and so fundamental that it seems surprising that they are so neglected. The greatest need is for more surface photometry, from the nuclei to the faint outer parts, and accurate enough to differentiate between models like tidal halos and faint disks. Hopefully the new generation of fast microphotometers will provide these data.

APPENDIX TO CHAPTER 2

ON THE HUBBLE (1930) AND KING (1966) PROFILE FITTING FUNCTIONS

Note: The Appendix will later be expanded into Paper III of the series on "Brightness Distributions in Compact and Normal Galaxies."

AI. INTRODUCTION

Our study of galaxy spheroids has so far been based completely on the de Vaucouleurs (1948, 1953) model of the brightness profile. Many other fitting functions have also been proposed (Hubble 1930, Baum 1955, King 1962, Abell and Mihalas 1966, King 1966), and used in specific cases. However, no detailed comparison of these functions has been made, so their physical differences and relative usefulness are poorly known. To make such a comparison, and also to investigate whether any of the present results depend on the particular nature of the de Vaucouleurs law, we will, in this Appendix, repeat much of the above discussion using the Hubble (1930) and King (1966) profiles.

AII. THE HUBBLE LAW

Hubble's (1930) well-known brightness relation

$$I = I_{0H}/(r/a + 1)^2 \qquad (A1)$$

was proposed to describe the average profile of 15 ellipticals which he had measured. I_{0H} is the central surface brightness in intensity units. We define B_{0H}, analogous to B_{0V}, by $B_{0H} = -2.5 \log I_{0H}$. The parameter a is the radius at which the brightness has decreased by a factor of 4 (= 1.505μ). Figure A1 shows a series of Hubble laws

FIGURE A1

A series of Hubble laws is plotted in a coordinate system in which a de Vaucouleurs law is a straight line. Starting at $r \simeq a$, the profiles are straight for $\sim 5\ \mu$.

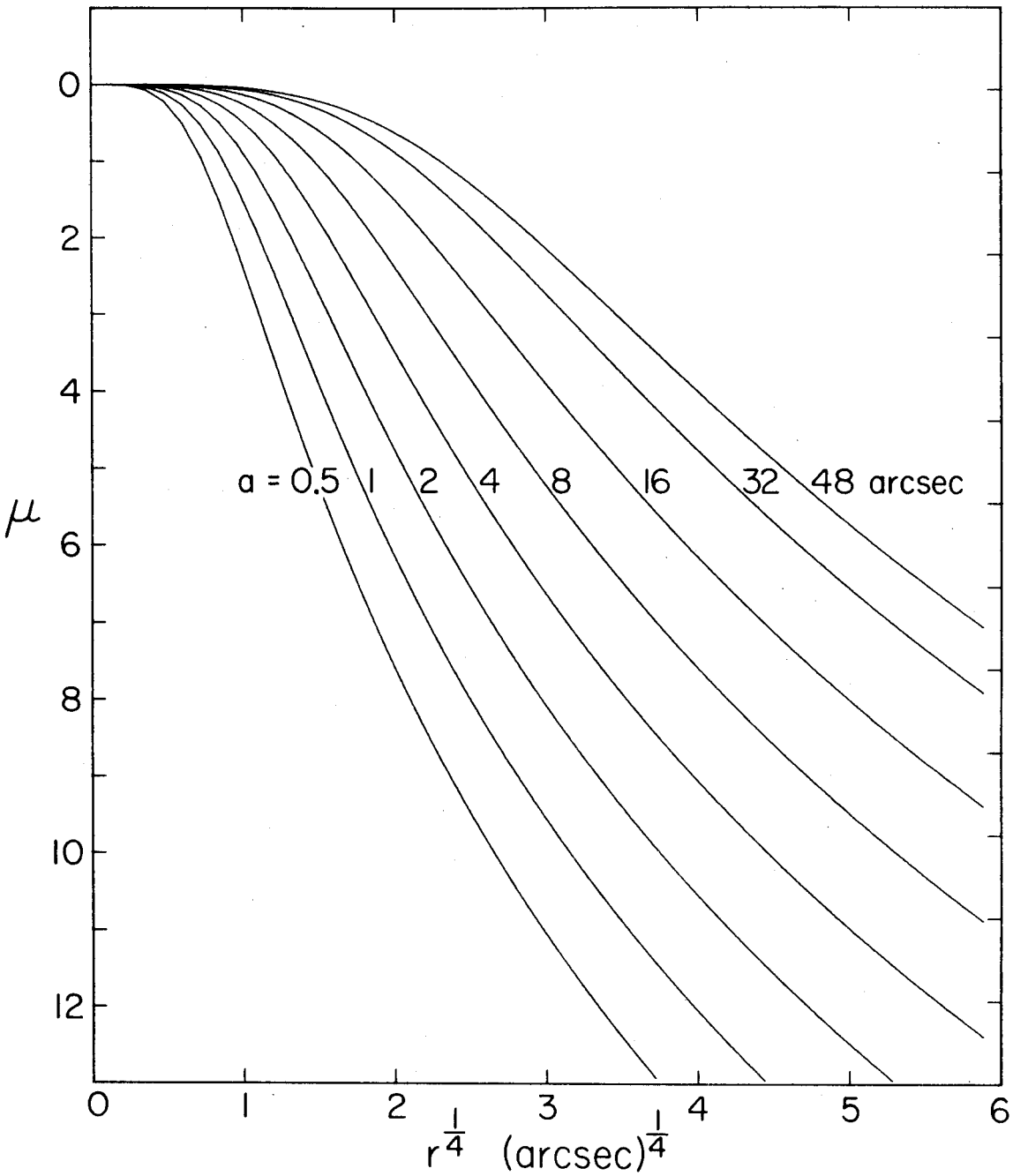
0
2
4
6
8
10
12
μ
a = 0.5 1 2 4 8 16 32 48 arcsec
0
1
2
3
4
5
6
r^1/4 (arcsec)^1/4

plotted against $r^{1/4}$. Starting just outside a central core, they are similar to de Vaucouleurs laws for ~ 5 μ. At larger radii, they have increasingly bright halos above a de Vaucouleurs law. (Recall that the $r^{1/4}$-law has finite total luminosity, while the brightness of a Hubble law diverges logarithmically.) Thus the two functions are very similar, with equation (A1) having the possible advantages of describing any central cores or tidal halos.

Hubble laws $\mu = B_{0H} + 5\log(r/a + 1)$ were fit to the King ellipticals using standard nonlinear least squares techniques. Table 1 lists the parameters. Since a is very small, typically 3-6 arcsec for giant ellipticals in the Virgo cluster, we will not discuss compacts, which are smaller and even farther away.

Figure A2 shows the galaxies, scaled to a single dimensionless Hubble law by adding $18-B_{0H}$ to the magnitudes and by dividing the radii by a. The T groups are separated by 3 μ. Figure A2 is the Hubble law version of Figure 1.

The profiles generally disagree with the model in the central 1-3 arcsec. Since no central cores are detected, and the seeing disk is ignored, this feature of equation A1 is not used. Rather, as we will show quantitatively below, the parameter a is used only to determine the profile slope in the $r^{1/4}$-region. This begins at 1/2 a - a, and extends over ≳ 5 μ to the start of a tidal halo. Over this

FIGURE A2

Profiles of the King ellipticals, scaled to have a common Hubble model (dashed lines) with B_{0H} = 18 B μ and a = 1 kpc. The T groups have been separated by 3 μ. The strongly deviant T1 galaxy is NGC 4636. Tidal halos in T2 and T3 galaxies are again evident.

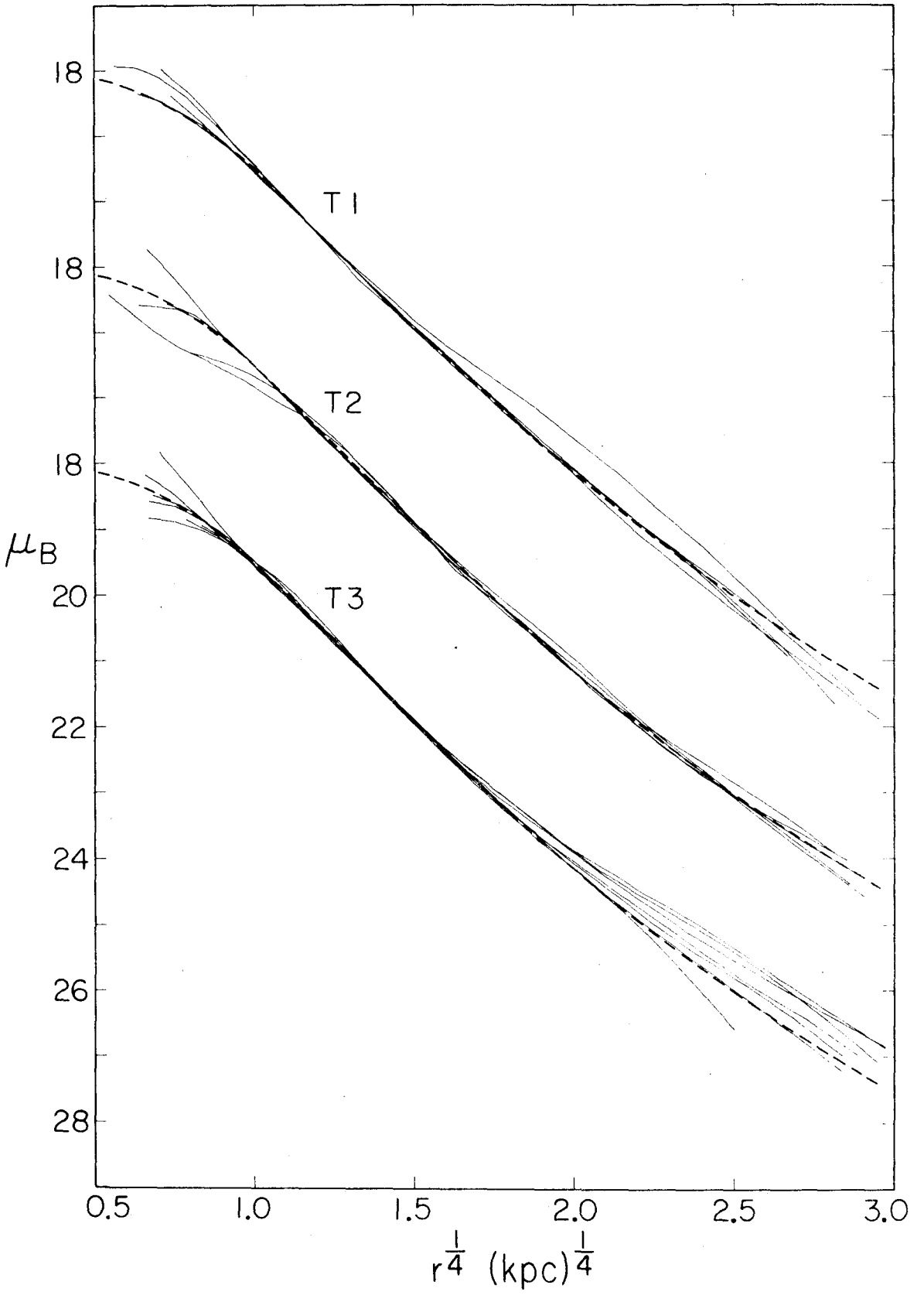
18
18
18
20
22
24
26
28
μ_B
T1
T2
T3
0.5
1.0
1.5
2.0
2.5
3.0
$r^{\frac{1}{4}}$ (kpc)$^{\frac{1}{4}}$

range, the Hubble law fits slightly better than a de Vaucouleurs relation, because the latter cannot reproduce the halo curvature. However, the amount of halo is variable from galaxy to galaxy, whereas the model halo is fixed, as defined by the outer r^{-2} power law. Thus all galaxies are not equally well fit. T1 objects have too little halo; they are generally intermediate between Hubble and de Vaucouleurs. Most T3 galaxies have far too much halo. The milder T2 galaxies, and especially M 87, are fit the best.

A comparison of Hubble and de Vaucouleurs parameters is shown in Figures A3 and A4. Both correlations are very good. Within the errors, and omitting NGC 4636 (discussed below),

$$a = 0.093\ r_0 + 0.00\ \text{kpc}, \quad \text{and} \tag{A2}$$

$$B_{0H} = B_{0V} - 5.27\ \mu\ . \tag{A3}$$

The scatter is 0.10 kpc (σ) about equation A2 and 0.24 μ about equation A3. These are essentially the simplest relations possible, and mean that the two models measure the same physical properties.

To show how closely the two models are in fact related, we will derive the above relationships. We know from Figure A1 that the similarity holds in the range $1 \lesssim \frac{r}{a} \lesssim 10$. The

FIGURE A3

Correlation between the radius parameters of the Hubble and de Vaucouleurs laws for King ellipticals. Circles, squares and triangles correspond to T3, T2 and T1 galaxies respectively. NGC 4636 has been omitted from the least squares solution.

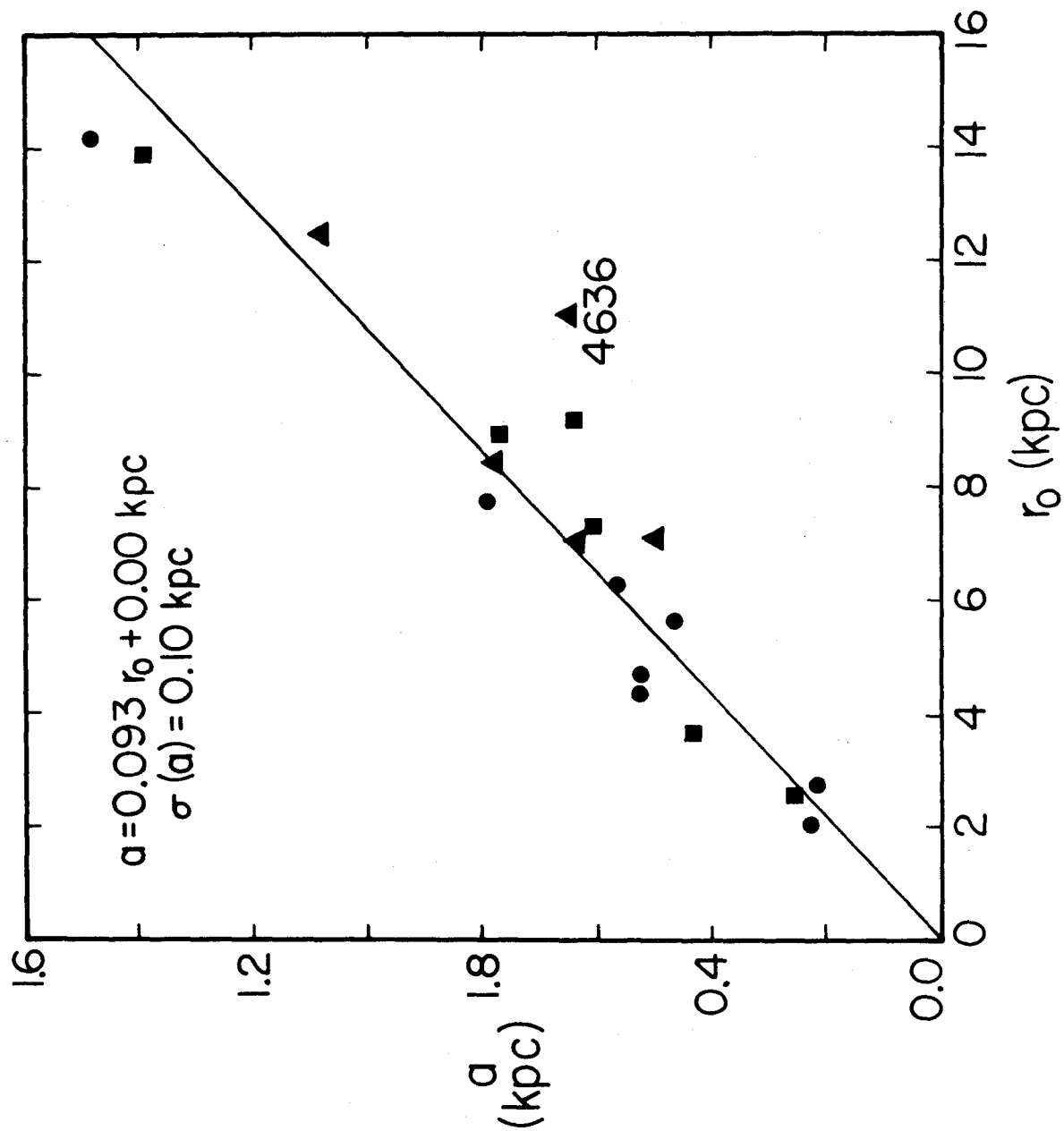
a=0.093 r₀ + 0.00 kpc
σ (a) = 0.10 kpc
4636
a (kpc)
r₀ (kpc)
0.0
0.4
1.8
1.2
1.6
0
2
4
6
8
10
12
14
16

FIGURE A4

Correlation between the surface brightness parameters of the Hubble and de Vaucouleurs laws. The meaning of the symbols is the same as in Figure A3.

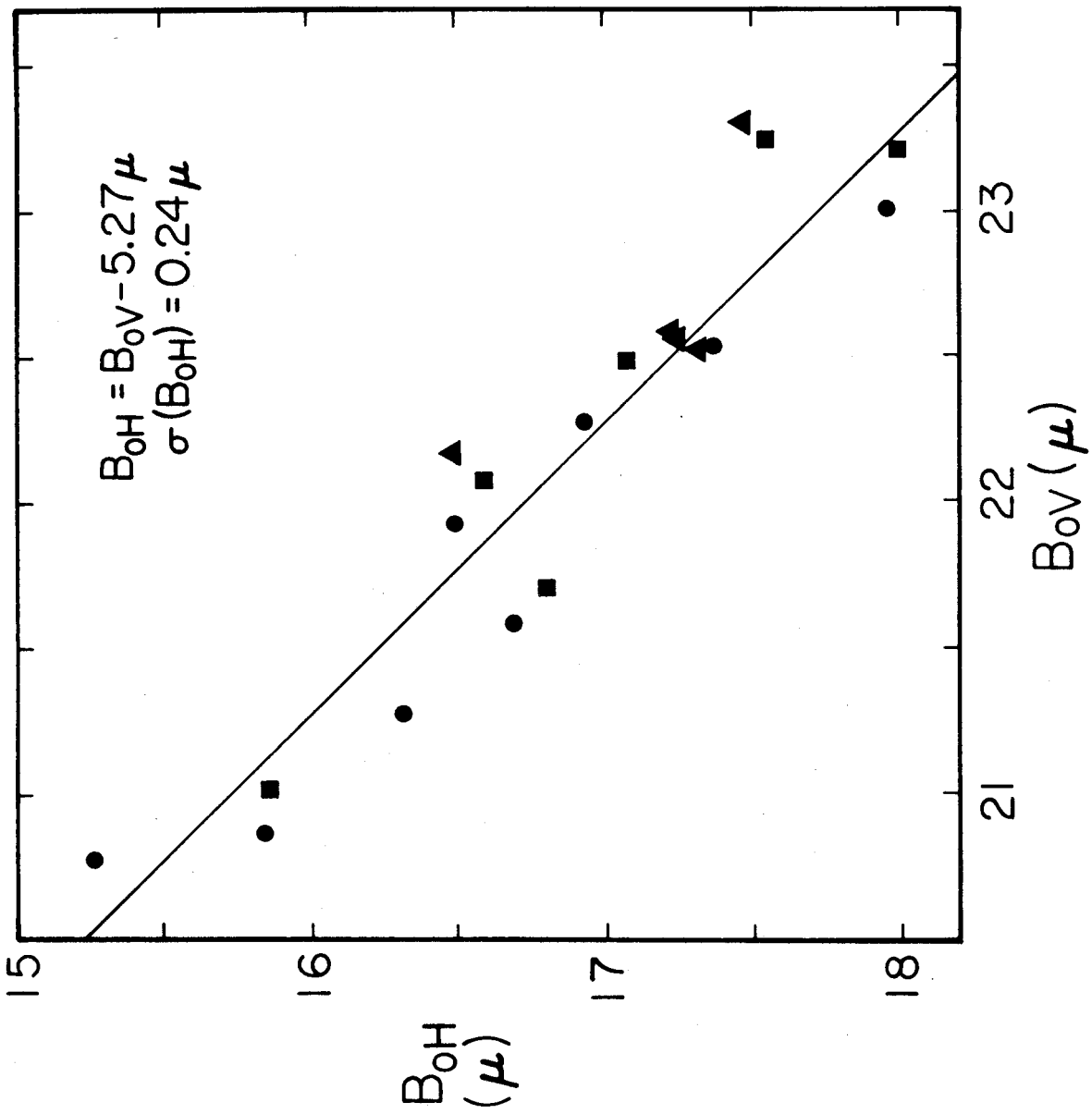
$B_{oH} = B_{oV} - 5.27\mu$
$\sigma(B_{oH}) = 0.24\mu$
15
16
17
18
21
22
23
B_{oH} (μ)
B_{oV} (μ)

slope of a Hubble law in de Vaucouleurs coordinates is

$$\frac{d\mu}{dr^{1/4}} = 8.686 \frac{r^{3/4}}{r + a} \quad . \tag{A4}$$

We want to relate this to the slope of the de Vaucouleurs law which we would fit to the Hubble profile. The above slope (A4) is largest at r = 3a. To minimize the deviations, we would use a slightly lower slope. However, for the moment we adopt the value at r = 3a:

$$\frac{d\mu}{dr^{1/4}} (r = 3a) = \frac{4.950}{a^{1/4}} \quad .$$

Equating this to the slope $-8.325\ r_0^{-1/4}$ of a de Vaucouleurs law yields $a = 0.125\ r_0$. This is close to the observed relation. Now suppose that $a \propto r_0$ also holds for the slightly less steep de Vaucouleurs law we would actually draw. Demand further that the models have the same absolute magnitude:

$$B_{0H} - 5\log a = B_{0V} - 5\log r_0 + \text{constant.}$$

Finally, use the fact that at r = a the Hubble law already satisfies de Vaucouleurs. Then a simple derivation gives

$$a = 0.087\ r_0 \quad , \text{ and}$$
$$B_{0H} = B_{0V} - 5.32 \quad . \tag{A5}$$

This is virtually identical to what was observed. The Hubble law has the same slope as its de Vaucouleurs model at r/a = 1.19 and 8.98, in excellent agreement with our requirements; i.e., there is a de Vaucouleurs model with $a \propto r_0$ which has almost the same slope as the Hubble law over the desired range a - 10a. Thus the only role of the parameter a is to determine the model slope in this part of the profile. The existence of a core is irrelevant for the present galaxies.

In view of the above discussion, B_{0H} and a must satisfy parameter correlations similar to those for B_{0V} and r_0. For example, Figure A5 shows the B_{0H}(log a) relation

$$B_{0H} = 2.93 \log a + 17.56 \text{ } \mu \text{ .} \qquad \text{(A6)}$$

The dispersion is again 0.28 μ. Equation A6 is entirely equivalent to equation (3). Thus all the conclusions about galaxy parameters derived earlier are confirmed here.

FIGURE A5

This correlation between B_{0H} and a is almost identical to the one between the de Vaucouleurs parameters (see Figure 2). Equations 3, A2 and A3 predict $B_{0H} = 3.02 \log a + 17.58$ $\underset{\sim}{\mu}$.

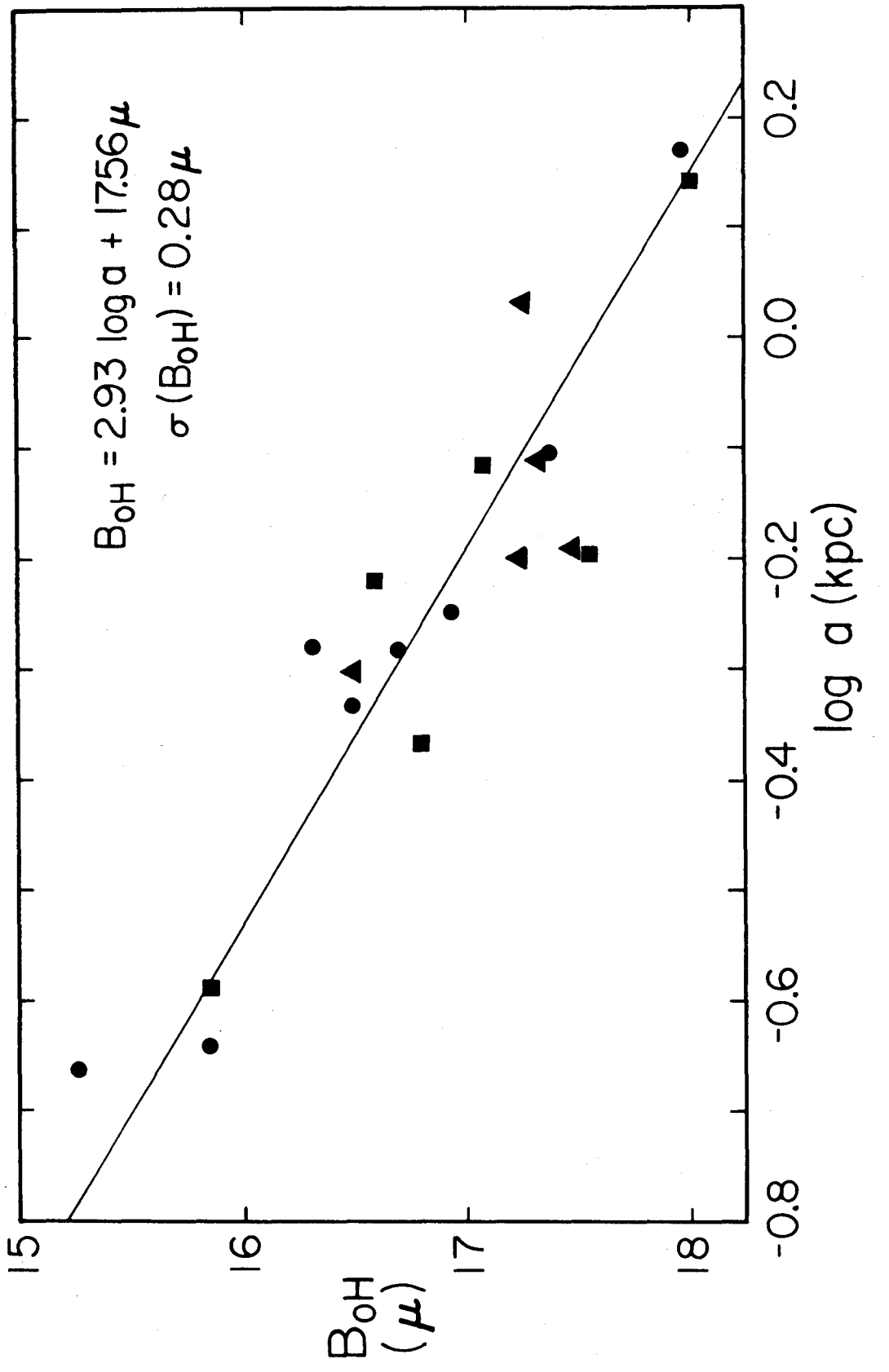
$B_{oH} = 2.93 \log a + 17.56\mu$
$\sigma(B_{oH}) = 0.28\mu$
B_{oH} (μ)
log a (kpc)
15
16
17
18
-0.8
-0.6
-0.4
-0.2
0.0
0.2

AIII. A MODIFIED HUBBLE LAW

We showed in Figure A2 that T3 galaxies have too much outer halo for a Hubble law. To produce a model with a variable halo, we can allow the power 2 to become a free parameter n:

$$I = I_{0M}/(r/a_M + 1)^n \quad . \tag{A7}$$

This function was least-squares fit to the King galaxies, over an enlarged fitting range which included all of the rising part of the halo. The parameters are again listed in Table 1.

The quality of the fit is very much improved. For example, the profile of the T3 galaxy NGC 2300 was much too shallow for a Hubble law, which held over only 3-1/2 μ. The modified Hubble law fits the whole galaxy to a few percent. In general, the fit is now excellent, through the rising part of the tidal halo to the beginning of any outer cutoff.

The parameter correlations for B_{0M} and a_M are very similar to those of the Hubble law. The scatter is slightly larger, because a_M is no longer the only parameter determining the profile slope. Otherwise they are equivalent.

The third parameter, n, approximately measures the amount of halo. Table A1 gives mean values of n for the different tidal groups. NGC 7626, known not to have an excess halo, is included with the T1's. NGC 4636 is omitted, for reasons discussed below. The quoted error ε is the rms deviation divided by the square root of the number of galaxies (in parentheses).

TABLE A1

MEAN HALO PARAMETERS

Tidal Class	<n> ε	(number)
T3	1.82 ± 0.04	(7)
T2	1.92 ± 0.05	(6)
T1	2.00 ± 0.06	(5)

Clearly, as T increases, n decreases to fit flatter halos. In the limit of unperturbed galaxies, our modified fitting function reproduces the normal Hubble law.

Another way to display the effects of T3 envelopes is to examine the correlation of a_M with n (Figure A6). Generally, T3 galaxies have small values of n and a_M compared to T1 objects. This probably results from a combination of several effects. There is a coupling of a_M and n in the sense that if n must be small to fit a

FIGURE A6

Correlation of a_M and n for modified Hubble law fits to normal galaxies. The meaning of the symbols is the same as in Figure A3. NGC 7626 should be considered as a T1 (triangle). Then T1 galaxies tend to have the largest, and T3's the smallest values of a_M and n. A prominent exception is NGC 4636, discussed in the text. Part of the dispersion is due to the absolute magnitude range; eg., the upper envelope of the distribution generally consists of the brightest objects.

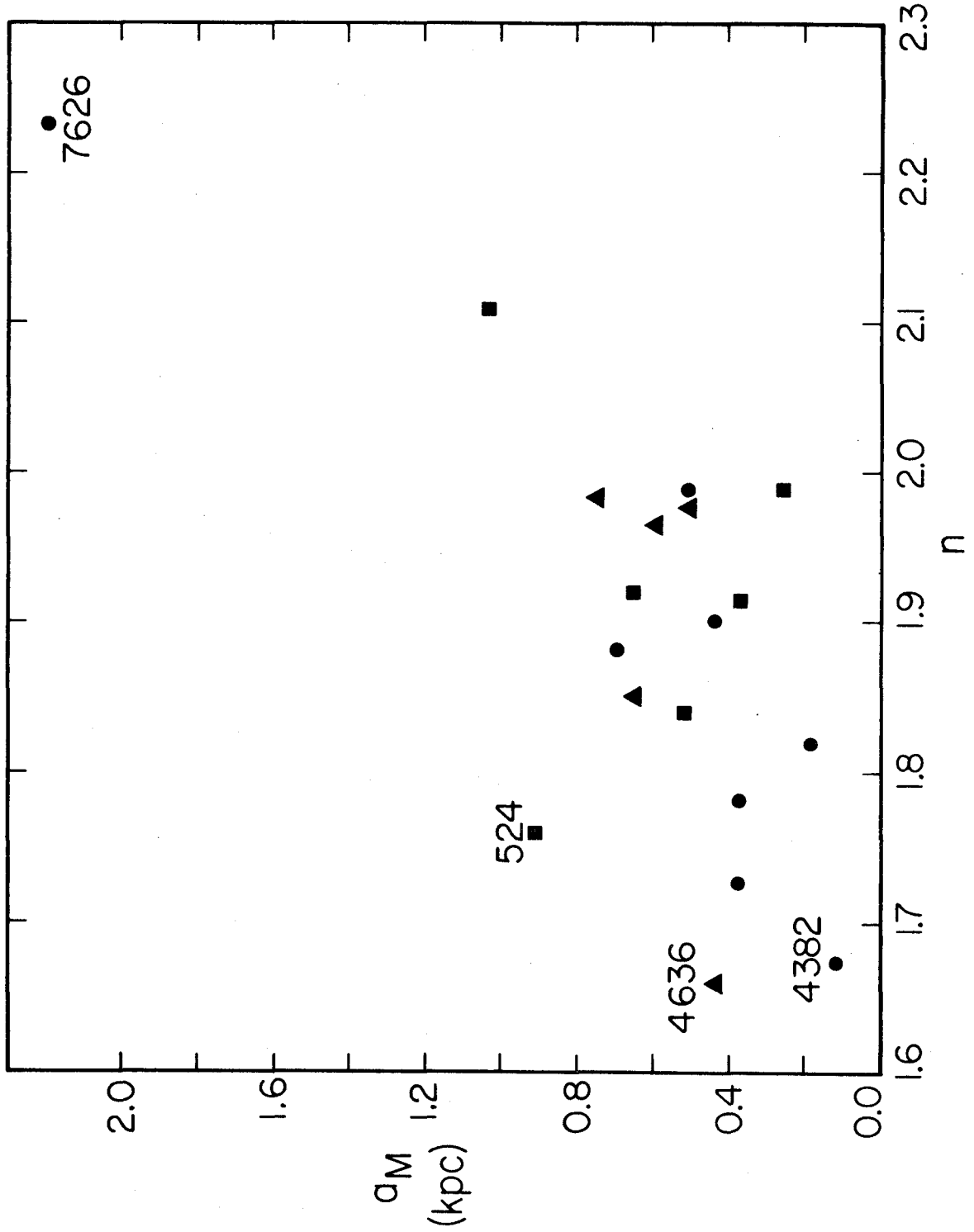
7626
524
4636
4382
2.0
1.6
1.2
0.8
0.4
0.0
a_M (kpc)
1.6
1.7
1.8
1.9
2.0
2.1
2.2
2.3
n

shallow halo, a_M must be made small to still fit a steep core. There may also be a dynamical effect; if stars for the halo were taken from the inner parts, those parts of the profile will be more compact. Finally, the present T1 galaxies happen to be more luminous than the T3's, making their a_M values relatively larger. In fact, this also tends to make the correlation worse; for example, the upper envelope of the distribution in Figure A6 mostly consists of the brightest objects.

NGC 4636 is once again a prominent exception to the correlation. In most of the discussion so far, it has behaved strangely. Figure A6 now suggests an explanation. The symptom is that n is unusually small for a T1 galaxy, smaller than for any other object. The reason is an outer halo, which is unusually faint, but which starts unusually close to the center. Only in NGC 4382, which is strongly tidally disturbed, and which has a disk, does the halo start at smaller radius. This suggests that NGC 4636 is an S0 galaxy with a strongly dominant spheroid. Similar galaxies are NGC 3115, whose disk would be difficult to detect if seen face-on, NGC 4382 and NGC 524 (Paper I). Sandage (1961) has independently stated that the galaxy has a disk.

The behavior of NGC 4636 would then be explained. The disk would make it abnormally diffuse for its M_B (see Figures A6, 2, and 3). It would account for the deviation in Figure A2, where NGC 4636 is the only T1 object poorly fit by a Hubble law. On the other hand, the purely spheroid region is so small, and the disk so faint, that the profile appeared acceptably $r^{1/4}$. Since the disk was included in the de Vaucouleurs fit, r_0 is abnormally large compared to a (Figure A3).

That the halo is not exponential is not an important objection. A relatively faint and/or small exponential added to a bright spheroid will produce only a small and non-exponential perturbation (cf. NGC 524 in Paper I; NGC 4382's disk is non-exponential, and see also Kormendy 1976b). NGC 4636 is more than a magnitude brighter than NGC 3115. Clearly there must exist many other elliptical galaxies with unrecognized faint disks.

We have shown that the Hubble law behaves very similarly to the de Vaucouleurs law, and confirms and extends the results of § II, III and IV. We conclude with a brief examination of the simplest of the dynamical models, that of King (1966).

AIV. THE KING MODELS

The King (1966) models were presented as a first step from the "gross empiricism" of fitting functions toward realistic dynamical models. They are based on a velocity distribution $f(\vec{r}, \vec{v})$ which is everywhere an isothermal gaussian minus a constant to make f reach zero at the local escape velocity. This cutoff produces a finite radius in what would otherwise be the well-known infinite isothermal. The models were designed for tidally truncated globular clusters, but also describe galaxies reasonably well.

There are three parameters. Two describe a core, much like the Hubble law does: B_{0K} is the central surface brightness, and r_c the "core radius" at which the brightness has dropped by approximately a factor of two (King 1966). If the limiting radius is r_t, then we can use as the third parameter $c = \log(r_t/r_c)$.

A set of numerical models with various c has kindly been made available by King (1975). They are compared to the de Vaucouleurs law in Figure A7. All have similar cores. The low-c models then cut off strongly, and are unlike most galaxies. Only strongly tidally limited objects like NGC 4486B (Paper I) and nearby dwarf ellipticals (cf. Hodge 1971, and references given there) have such profiles.

FIGURE A7

A series of King models is shown plotted against $r^{1/4}$. Globular clusters and tidally stripped ellipticals typically have c ~ 1.5. Galaxies with various amounts of tidal halo have c ~ 1.75 - 2.25. Compare Figure A1, showing various Hubble laws.

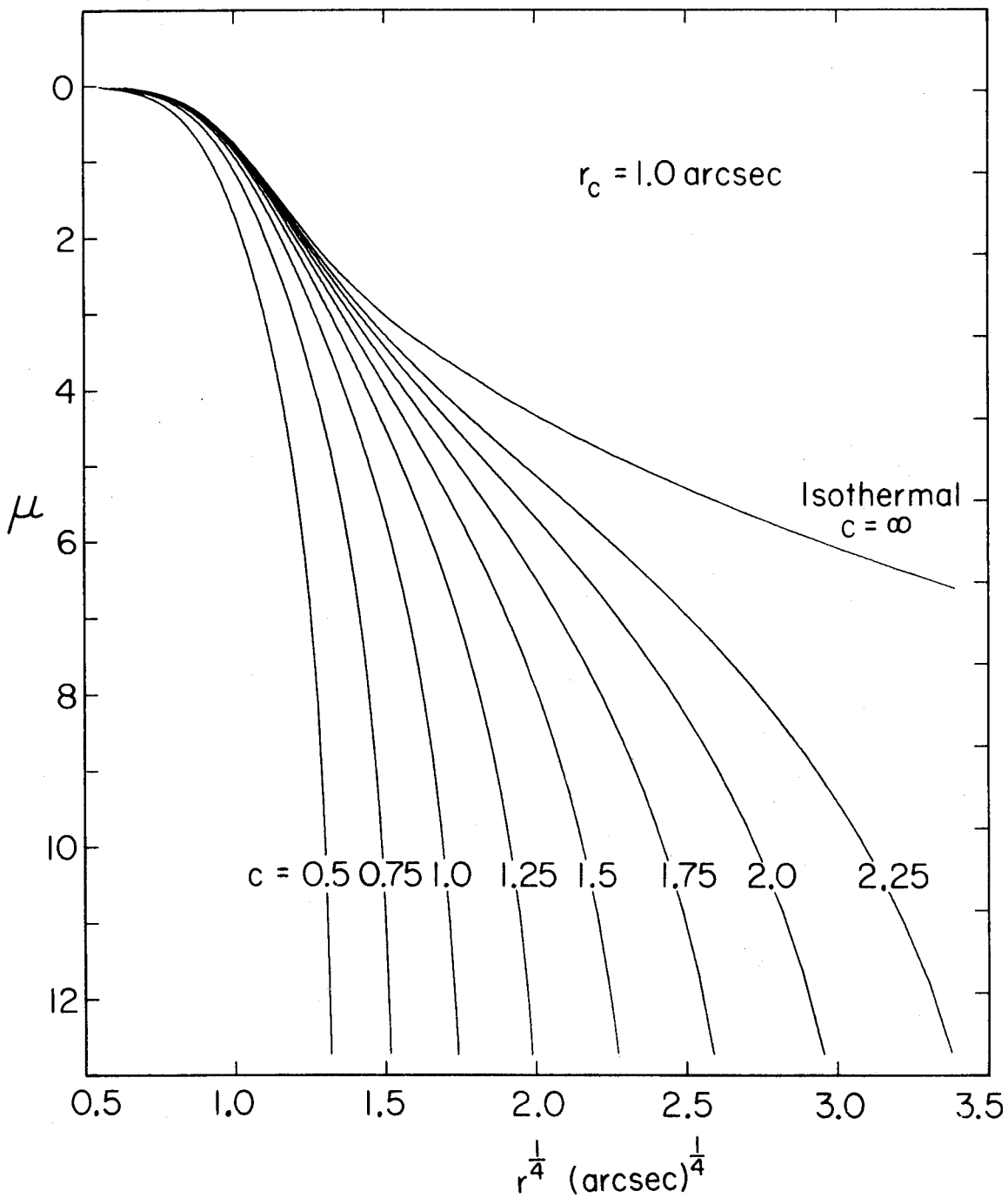
0
2
4
6
8
10
12
μ
r_c = 1.0 arcsec
Isothermal
c = ∞
c = 0.5 0.75 1.0 1.25 1.5 1.75 2.0 2.25
0.5
1.0
1.5
2.0
2.5
3.0
3.5
$r^{\frac{1}{4}}$ (arcsec)$^{\frac{1}{4}}$

These are the models that fit globular clusters (King 1966, Peterson and King 1975). In the range $1.5 \lesssim c \lesssim 2.0$ the models are de Vaucouleurs over $\gtrsim 6$ μ (see also King 1966, especially Figure 5). Finally, for $c > 2$, the central concentration becomes so great that an outer "halo" above a de Vaucouleurs law appears, as the profiles begin to approach the outer r^{-1} power law of an isothermal. Except for the eventual outer cutoff, King models are very similar to the modified Hubble law. Both have a core radius and brightness scale, and a parameter controlling the amount of halo.

Models were fit to the normal galaxies by eye, as discussed in King (1966) and Peterson and King (1975). The results are listed in Table 1, and illustrated in Figure A8. Only those galaxies are shown for which the $c = 2.25$ model was best. As a result, one object has been omitted from each T group.

T3 galaxies are fairly well described by King models, except for the outer parts of their halos. Here the models cut off too strongly. In these outer parts the assumptions of isothermal or even isotropic velocity distributions are likely to fail. Since tidal halos are presumably asymmetrical, the photometry is probably also in some doubt. In contrast, the fit to T1 galaxies is poor everywhere. The observed profiles are much too straight--too like a

FIGURE A8

Profiles of those King ellipticals which are best described by a c = 2.25 King model. The objects have been scaled to make r_c = 1 arcsec and B_{0H} = 18 B μ. As before, the T groups have been separated by 3 μ. This figure is the King model analogue of Figures 1 and A2.

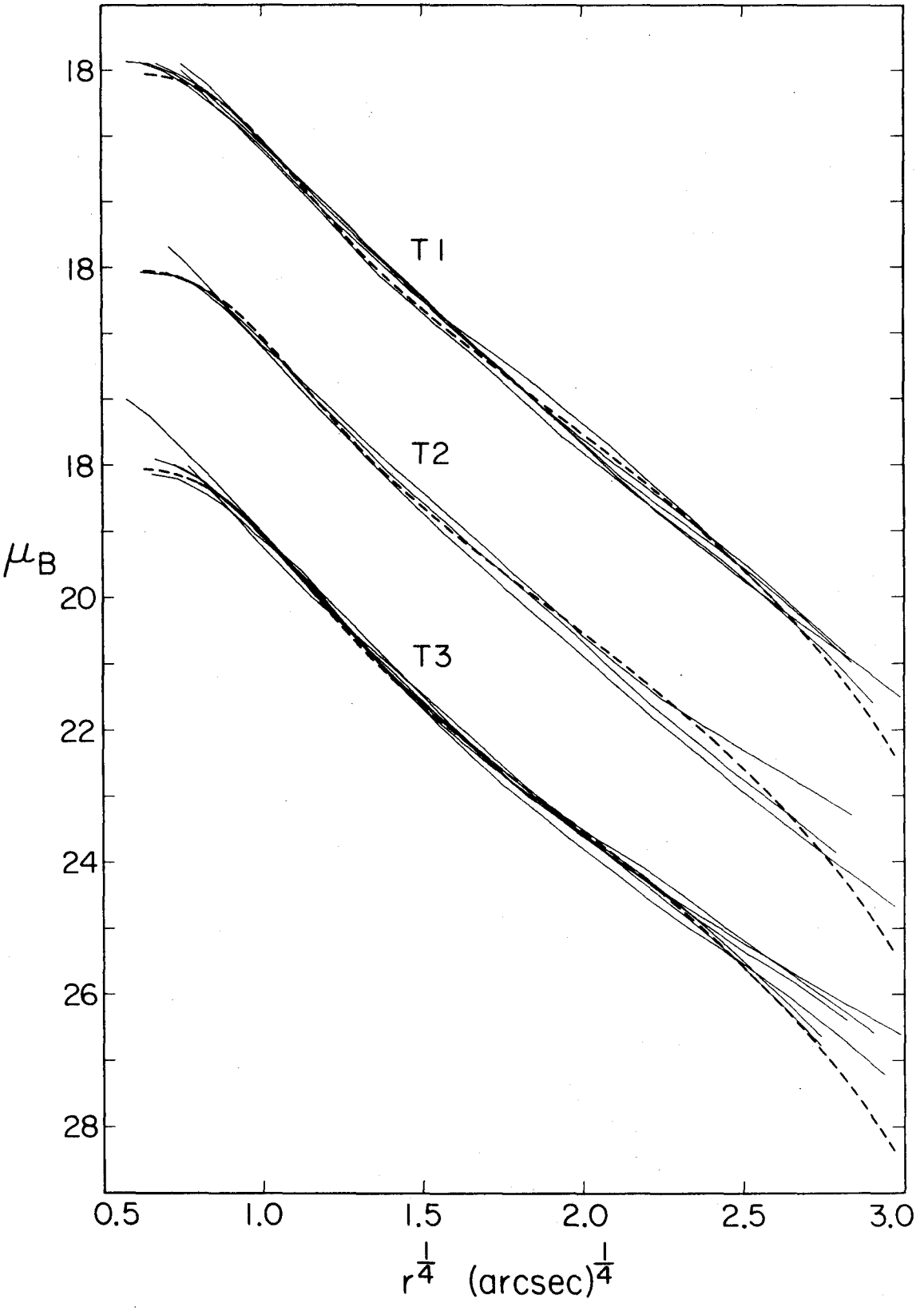
18
18
18
20
22
24
26
28
μ_B
T1
T2
T3
0.5
1.0
1.5
2.0
2.5
3.0
$r^{\frac{1}{4}}$ (arcsec)$^{\frac{1}{4}}$

de Vaucouleurs law--for the c = 2.25 model. Clearly a more complicated dynamical model is required. However, generally the behavior resembles that of the modified Hubble law.

Figure 8 also serves as a final check on the tidal halo hypothesis. Since the same model has been used for all the galaxies, the difference between T groups is minimized. However, the T3 objects turn out to be scaled in the same way as in Figure 1. That is, the family of curves looks similar. This is not true for the T1 objects. Since the c = 2.25 model has the wrong shape, the errors are larger, and so there is more freedom in how to do the fitting. As a result, the procedure produces as much halo (like the model) as possible. The fits are not very trustworthy. Still, despite being minimized, the difference between T1 and T3 galaxies is still quite noticeable. Thus both the Hubble and King models confirm the existence of tidal halos.

The above discussion suggested that King and modified Hubble laws behave similarly. Figures A9 and A10 show that this is true quantitatively. Both straight lines are least-squares fits to the unlabeled points.

$$r_c = 1.05\ a_M + 0.029 \text{ kpc}; \ (\sigma = 0.091 \text{ kpc}); \qquad \text{(A8)}$$

$$B_{0K} = 0.73\ B_{0M} + 5.23\ \mu\ ; \ (\sigma = 0.29\ \mu) \ . \qquad \text{(A9)}$$

FIGURE A9

Correlation between the core radii of the King and modified Hubble laws. The symbols have the same meaning as in Figure A3. Only the unlabeled points were used to define the straight line. Large fitting errors are expected for some objects which have profiles much different in shape than a King model.

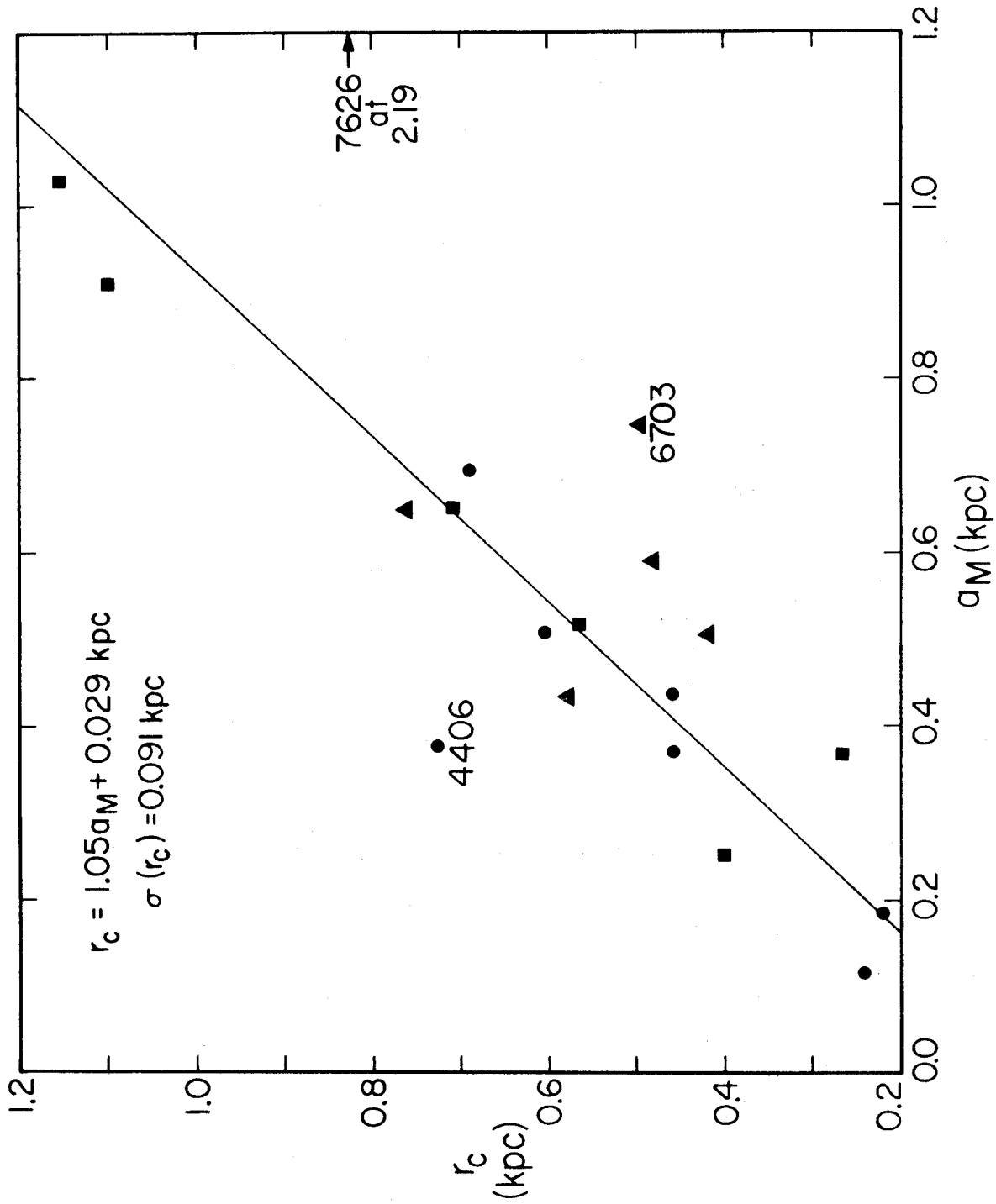
$r_c = 1.05 a_M + 0.029$ kpc
$\sigma(r_c) = 0.091$ kpc
7626 at 2.19
4406
6703
r_c (kpc)
a_M (kpc)
0.0
0.2
0.4
0.6
0.8
1.0
1.2

FIGURE A10

Correlation between the "central surface brightness" of King and modified Hubble models. The symbols have the same meaning as in Figure A3. NGC 7626 was not used in defining the line.

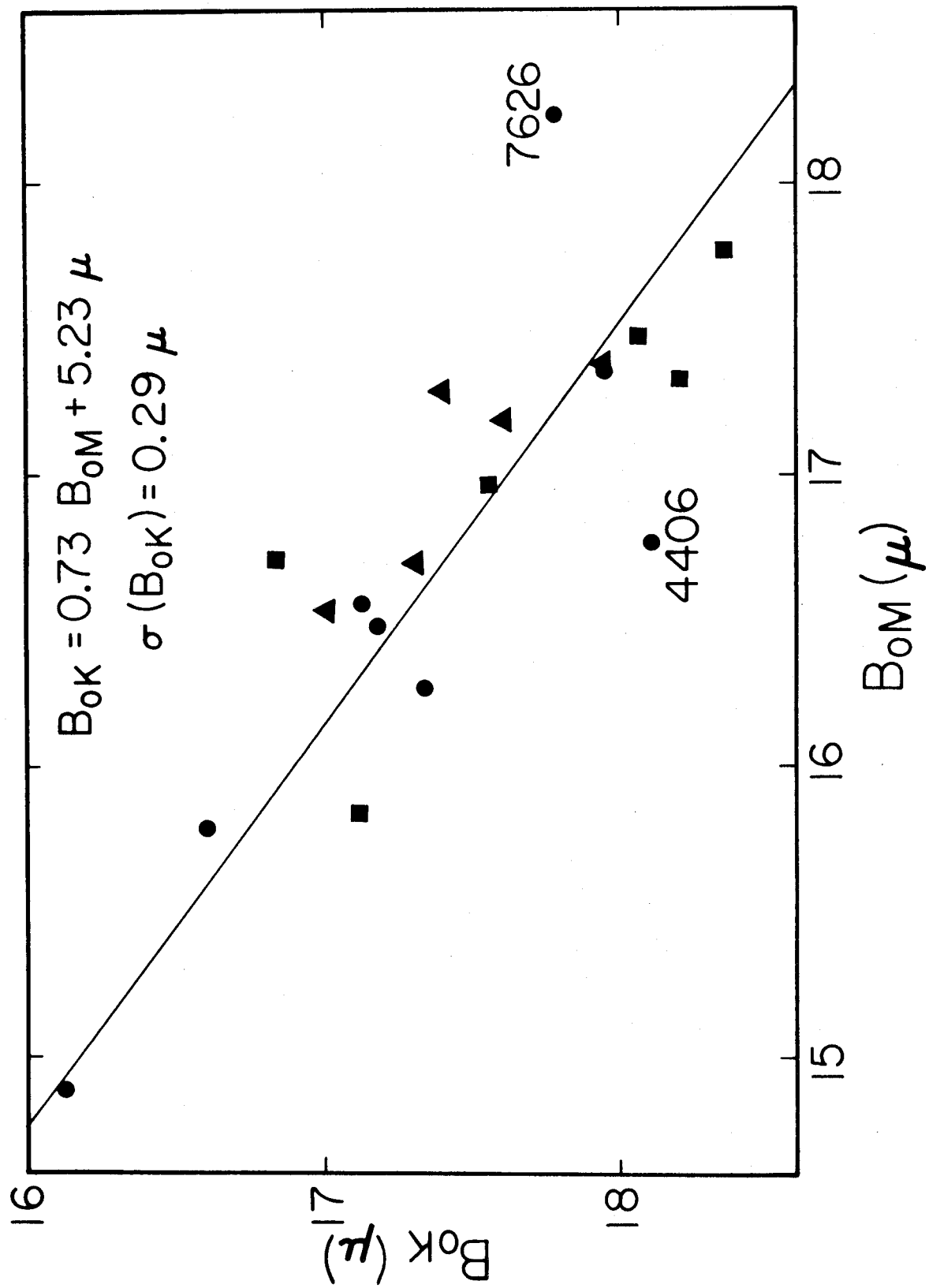
$B_{oK} = 0.73\ B_{oM} + 5.23\ \mu$
$\sigma(B_{oK}) = 0.29\ \mu$
7626
4406
$B_{oK}\ (\mu)$
$B_{oM}\ (\mu)$
16
17
18
15
16
17
18

Strongly discordant points are due to gross King-model fitting errors. For instance, in NGC 4406, large changes in r_c produced almost no change in the (poor) quality of the fit; the model simply has the wrong shape. These points have been omitted, above. The reason that $B_{0K} \neq B_{0M}$ is that the Hubble law core is sharper. Note that $r_c \simeq a_M$ despite the fact that at r_c, I has dropped by only a factor of 2, not 4. The sharp Hubble-law core fits the data badly; a small a_M is needed for the outer profile slope, but as a result B_{0M} and B_{0H} are much brighter than the real central surface brightness.

King parameter correlations such as $B_{0K}(\log r_c)$ are again similar to their modified Hubble law counterparts. As in § AIII, the scatter is larger than in the de Vaucouleurs and Hubble cases. Otherwise, the King parameters again confirm the conclusions reached using the Hubble law. These conclusions are apparently model independent.

To summarize, the King profile behaves like the modified Hubble law because both have similar parameters, two describing a central core, and one specifying the amount of halo relative to the core. The inner parts of tidally distended galaxies are fit fairly well. However, unperturbed galaxy profiles have shapes different from the models, suggesting that an isothermal velocity distribution cut off at the escape velocity is an oversimplification.

Considering the simple assumptions, the models work well. Nevertheless, well chosen but physically unfounded fitting functions still provide the best fits to galaxy profiles, and are probably the most useful in deriving physical scales.

REFERENCES

Abell, G. O., and Mihalas, D. M. 1966, A. J., 71, 635.

Arp, H., and Bertola, F. 1971, Ap. J., 163, 195.

Baum, W. A. 1955, Pub. A.S.P., 67, 328.

Burkhead, M. S., and Kalinowski, J. K. 1974, A. J., 79, 835.

Dennison, E. W. 1954, Ph.D. thesis, University of Michigan.

de Vaucouleurs, G. 1948, Ann. d'Astrophys., 11, 247.

_____. 1953, M.N.R.A.S., 113, 134.

_____. 1961, Ap. J. Suppl., 6, 213.

_____. 1974, in The Formation and Dynamics of Galaxies (IAU Symposium No. 58), ed. J. R. Shakeshaft (Boston: D. Reidel), p. 1.

de Vaucouleurs, G., and de Vaucouleurs, A. 1964, Reference Catalogue of Bright Galaxies (Austin: University of Texas Press).

Faber, S. M. 1973, Ap. J., 179, 423.

Fish, R. A. 1964, Ap. J., 139, 284.

Gudehus, D. H. 1973, A. J., 78, 583.

_____. 1975, Pub. A.S.P., 87, 763.

Hodge, P. W. 1971, Ann. Rev. Astr. and Ap., 9, 35.

Hubble, E. 1930, Ap. J., 71, 231.

King, I. 1962, A. J., 67, 471.

_____. 1966, ibid., 71, 64.

_____. 1975, private communication.

King, I. R., and Kiser, J. 1973, Ap. J., 181, 27.

Kormendy, J. 1976a,b, in preparation.

Kormendy, J., and Bahcall, J. N. 1974, A. J., 79, 671.

Kormendy, J., and Sargent, W. L. W. 1974, Ap. J., 193, 19.

Miller, R. H., and Prendergast, K. H. 1962, Ap. J., 136, 713.

Peterson, C. J., and King, I. R. 1975, A. J., 80, 427.

Prendergast, K. H., and Tomer, E. 1970, A. J., 75, 674.

Richstone, D. O. 1975, Ap. J., 200, 535.

Rood, H. J. 1965, A. J., 70, 689 (A).

Rood, H. J., Page, T. L., Kintner, E. C., and King, I. R. 1972, Ap. J., 175, 627.

Sandage, A. 1961, The Hubble Atlas of Galaxies (Washington: Carnegie Institution of Washington).

Sandage, A., and Tammann, G. A. 1974, Ap. J., 194, 559.

_____. 1975, ibid., 196, 313.

Wilson, C. P. 1975, A. J., 80, 175.

Zwicky, F. 1971, Catalogue of Selected Compact Galaxies and of Post-Eruptive Galaxies (Guemligen: F. Zwicky).

Zwicky, F., and Herzog, E. 1968, Catalogue of Galaxies and of Clusters of Galaxies, Vol. 4 (Pasadena: California Institute of Technology).

CHAPTER 3

DECOMPOSITION OF OBSERVED PROFILES INTO SPHEROID AND DISK COMPONENTS

I. INTRODUCTION

In a previous paper (Kormendy 1976a, hereafter Paper I), we began a study of galaxy luminosity distributions by qualitatively discussing sixteen red compact and four normal galaxies. Subsequently, we made preliminary studies of spheroid parameters (Paper II, Kormendy 1976b), and fitting functions (Paper III, Kormendy 1976c). We will continue here by discussing the disks of compacts, commenting also on several more general aspects of disk structure.

Freeman (1970) has made a pioneering investigation of disk parameter systematics, reaching the following conclusions. (1) For unknown reasons, the profile is usually exponential, $I(r) = I_o\, e^{-\alpha r}$, confirming results of de Vaucouleurs (1959). (2) Sometimes the exponential cuts off toward smaller radii before the spheroid becomes dominant ("Type II profile"). (3) The scale length is $2 \leq \alpha^{-1} \leq 10$ kpc in S0-Sbc galaxies, and $2 \leq \alpha^{-1} \leq 5$ kpc in Sc-Im galaxies. (4) The corrected central disk brightness is constant at $B(0)_c = 21.65 \pm 0.30(\sigma)$ B_{μ} for 28 of 36 galaxies. Seven have brighter values; only one dwarf irregular is fainter. (5) The fractional contribution of the spheroid is only weakly correlated with morphological type.

More recent work has largely confirmed these results (eg., de Vaucouleurs and Freeman 1972, Schweizer 1976, and many others). However, in each case an exponential was fit to the profile as observed. This may introduce errors if the spheroid contribution is significant in the region studied.

There are strong reasons for believing that spheroids continue largely unchanged into the disk. Figure 1a shows exponential and de Vaucouleurs law fits to the major axis profiles of five compacts. The extrapolated spheroids are never faint compared to the disk. This is equally true in a great many galaxies studied by previous authors. In Figure 1a the transition from spheroid to disk is so sharp that the observed profile is much less than 0.75 μ (= 2.5 log 2) brighter than the models at their crossing point. Clearly, the contribution of the spheroid to the exponential parameters is large. This is not surprising, in view of the extended halos of edge-on galaxies (Kormendy and Bahcall 1974; Spinrad and Ostriker 1974), local observation of the galaxy's spheroid (eg., Eggen, Lynden-Bell and Sandage 1962; Schmidt 1975), and theoretical requirements for massive halos (Ostriker and Peebles 1973).

Therefore, in this paper we will explore the de-

composition of galaxy profiles into intrinsic spheroid and disk components (cf. de Vaucouleurs 1958, 1975). We will consider the implications on profile shapes, particularly in the transition region between the components, and on parameter systematics. The objects studied will mostly be S0 compacts from Paper I.

We will also fit exponentials to the observed disks to derive parameters for comparison to normal galaxies (§ II).

The profile decompositions are made in § III. Motivated by the effects on the parameters, the constancy of $B(0)_c$ is considered in more detail in § IV. Conclusions are listed in § V. A Hubble constant of H_o = 50 km s^{-1} Mpc^{-1}, and a galactic absorption of $0^m.2$ csc b^{II}, are used throughout.

II. PARAMETERS OF THE DISKS OF COMPACTS

We showed in Paper I that many disks in compact galaxies were really lenses (Sandage 1961), and not exponentials. These clearly require a complicated overall fitting function. However, the major shallow parts of the profile can be fit very well by exponentials, thus allowing a comparison to normal disks. Figure 1 illustrates these fits, and Table 1 lists the parameters. VII Zw 352 is not shown in the Figure; it would appear almost identical to V Zw 257.

Figure 1b illustrates well the difference between lenses and exponential disks. NGC 7457 is exponential for at least three scale lengths, and shows no sign of an outer cutoff. In contrast, in VII Zw 793, which has a very strong lens, the model holds over only ~ 1/2 scale length, and is far from compelling. For all the compacts, the range of validity is short, but the quality of the fit is clearly good enough to adequately define the parameters.

In Table 1, the first column gives the Zwicky (1971) designation, and the second the adopted distance (Paper I). Column 3 is the probable disk classification, using L for lens and E for exponential. A question mark means that the existence of a disk is uncertain. The next five columns give the parameters of the de Vaucouleurs laws, μ_V =

FIGURE 1

Model fits to the major axis profiles (heavy lines) of six compacts and the normal galaxy NGC 7457. The straight line is the exponential. The light curved line is a de Vaucouleurs law, which is identical to the one used in Paper II for the round galaxies I Zw 21, VII Zw 303, and V Zw 114. In VII Zw 793, the major axis is contaminated by light from the bar, so the minor axis is used.

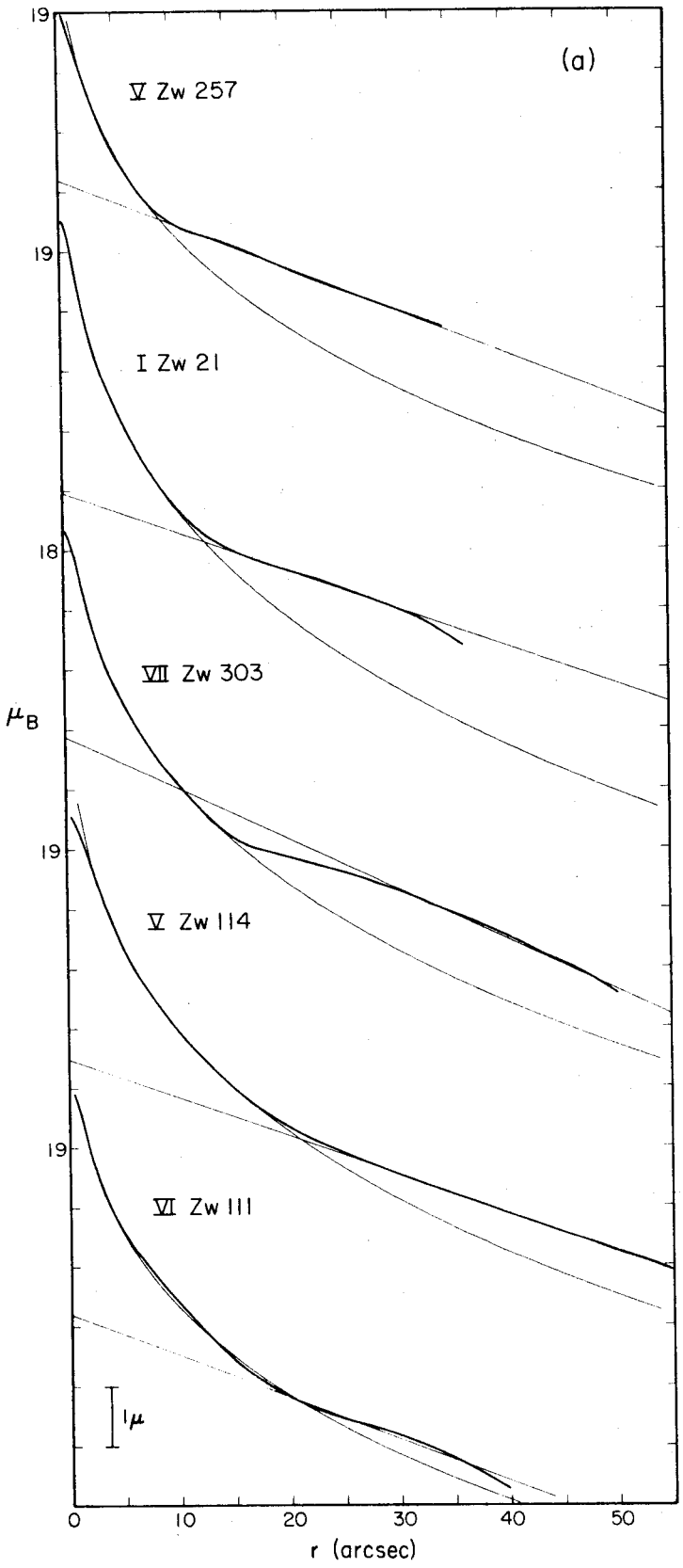
(a)
V Zw 257
I Zw 21
VII Zw 303
V Zw 114
VI Zw 111
19
19
18
19
19
μ_B
1μ
0
10
20
30
40
50
r (arcsec)

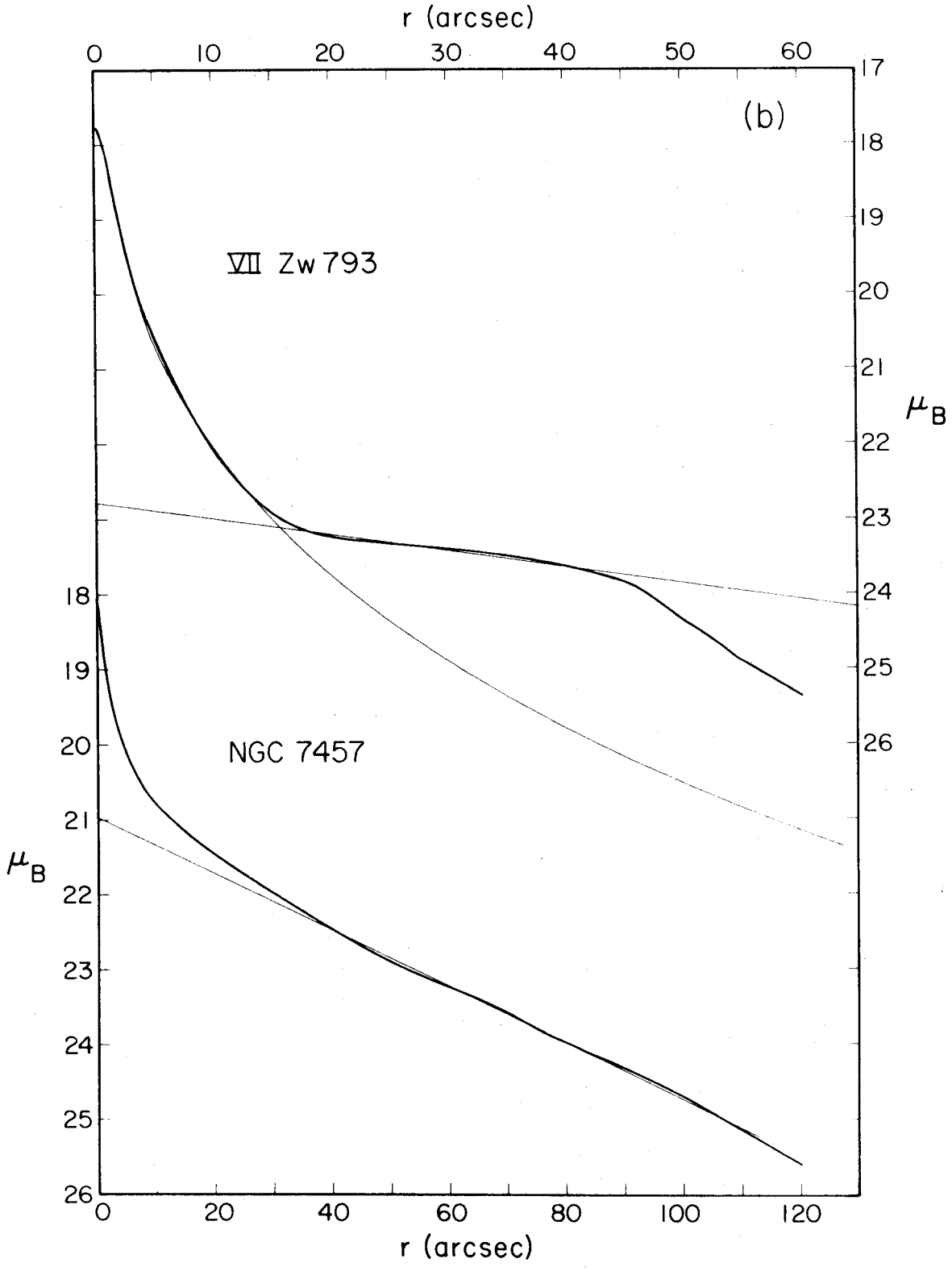
r (arcsec)
0
10
20
30
40
50
60
(b)
VII Zw 793
NGC 7457
μ_B
17
18
19
20
21
22
23
24
25
26
0
20
40
60
80
100
120
r (arcsec)

TABLE 1

STRUCTURE PARAMETERS*

Galaxy	Distance (Mpc)	Disk Type	Model†	B_o	r_o (kpc)	$B(0)_c$	α^{-1} (kpc)	β (kpc)
V Zw 114	103	?	O	20.90	3.6	22.06:	8.3:	
			IF	19.83	2.1	22.8::	9.8::	
			LS	19.95	2.2	22.9::	10.0::	
			C	20.80	3.5	22.49::	7.9::	12.6::
VI Zw 111	90	?	O	21.88	5.8	21.50:	6.8:	
			IF	21.89	5.8	23.2::	7.7::	
			LS	22.02	6.3	23.2::	6.6::	
			C	21.84	5.7	...	...	...
V Zw 257	89	E or L	O	22.34:	4.4:	21.83	6.4	
			IF	21.4::	2.2::	22.27	7.5	
			LS	21.5::	2.3::	22.30	7.6	
			C	22.32:	4.4:	22.11	6.3	5.2
I Zw 21	98	L	O	21.53	2.5	22.78	8.0	
			IF	20.88	1.7	23.4::	10.4::	
			LS	21.03	1.9	23.6::	11.6::	
			C	21.49	2.5	22.90	7.8:	7.8
VII Zw 303	46	L	O	20.94	1.7	20.81:	2.8:	
			C	20.83	1.6	20.29	2.3	5.1
VII Zw 352	182	L or E	O	19.20:	0.9:	21.76	4.9	
			IF	...	...	21.95:	5.2:	
			LS	...	...	21.98:	5.3:	
			C	19.00:	0.9:	21.87	5.0	4.2
VII Zw 793‡	30	L	O	20.87	1.0	22.68	7.4	
			IF	20.35	0.75	23.4::	34::	
			LS	20.37	0.76	23.5::	100::	
			C	20.72	0.95	22.73	7.3:	2.7
NGC 7457	15	E	O	...	...	21.20	2.1	

*Colons mean uncertainty; a double colon means the fit was indicative only. For example, in the second and third rows for VII Zw 793, the disk is essentially flat, so that any α^{-1}, positive or negative, but with $|\alpha^{-1}| \gtrsim 30$ kpc would work well. See Figure 4.

†The parameters given are for fits (O) of the observed profile, (IF) using iterative fitting to make a decomposition into a de Vaucouleurs law and a full exponential; (LS) using least squares similarly, and (C) using a third-order cutoff exponential. The latter three models are described in § III.

‡Minor axis.

$B_o + 8.325\ [(r/r_o)^{1/4}-1]$, and exponentials, $\mu_E = B(0)_c + 1.0857\ \alpha r$. In the above, r is the radius, and all brightnesses μ and B are in B mag arcsec^{-2} (Bμ). We will define β in § III. Surface brightnesses have been corrected for galactic absorption, and $B(0)_c$ has been corrected to a face-on value as in Freeman (1970).

Before making the comparison to normal galaxies, we should note a problem with Freeman's analysis. Unfortunately, much of the data used are inaccurate. In particular (King 1975), this includes the large sample of Liller (1960, 1966). Normally, her photometry is most accurate below ~ 22 Bμ, where scattered light and calibration problems are smallest. Nevertheless, many of Freeman's Type II profiles are so classified only because of a small change in slope at ~ 25 Bμ. This feature is probably not well established. If a fit is made to the inner region, which is equally exponential and long in radius range, most profiles become Type I. $B(0)_c$ becomes fainter, often going down to ~ 21.65 Bμ. Three profiles remain strongly Type II. However, two of these, NGC 4270 and NGC 4343 are clearly almost edge-on on Sky Survey prints. They were included because they have enough central bulge to satisfy an axial ratio test. But edge-on galaxies can easily have Type II profiles for geometrical

reasons (see also Burstein 1976). The other galaxy, NGC 4659, seems definitely to be Type II. This look at the Liller data suggests that Type II profiles are much rarer than Freeman's analysis indicates.

Despite the above remarks, the parameter plots remain largely unchanged. In particular, $B(0)_c$ still usually equals 21.65 B_{μ}. We will therefore use Freeman's results as published.

Figure 2 shows $B(0)_c$ against morphological type for compact and normal galaxies. Most compacts do not appear unusual. Four of seven have $B(0)_c = 21.79 \pm 0.23(\sigma)$ B_{μ}. VII Zw 303 has a brighter value, 20.81 B_{μ}, like other Type II objects, but this depends rather strongly on the chosen fitting range. The two other galaxies with very flat lenses, I Zw 21 and VII Zw 793, have faint values of 22.78 and 22.44 B_{μ} respectively. They begin to confirm the general suspicion (e.g., de Vaucouleurs 1974a) that there exist faint disks, which selection effects have mitigated against in the past.

Figure 2 also shows $B(0)_c$ values for formal exponential fits to two elliptical compacts, and to T3 ellipticals from Paper II. These are generally normal, or faint if the galaxy is very luminous, or the surface photometry

FIGURE 2

Extrapolated central disk brightness $B(0)_c$ against morphological type for compact and normal galaxies. Compacts are shown as filled circles (Type I profiles) and open circles (Type II profiles). Similarly, normal galaxies are plotted as crosses and plus signs respectively. Data for most normal galaxies come from Freeman (1970); but formal values have been added for some ellipticals from Paper II. The straight line denotes $B(0)_c = 21.65$ B_{μ}.

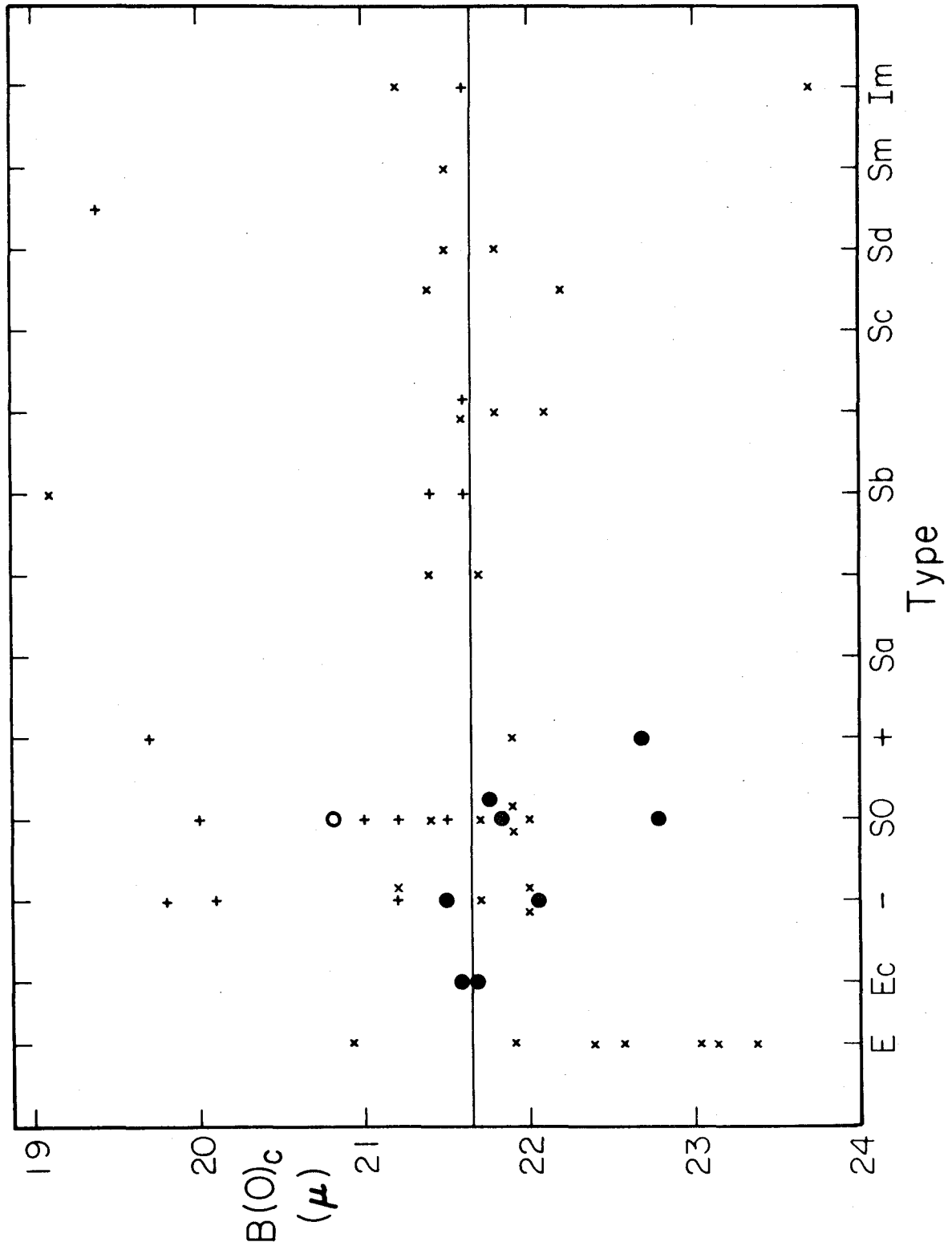
19
20
21
22
23
24
B(O)c
(μ)
E Ec - SO + Sa Sb Sc Sd Sm Im
Type

very deep (see also Freeman 1970). This will be important in § IV.

Similarly, we can consider the scale lengths. Table 1 shows that α^{-1} is 6-1/2 - 8-1/2 kpc for five of the seven galaxies. This is at the long end of the range observed by Freeman. Thus there is a strong contrast between these disks and the bright, short-scale-length spheroids discussed in Paper II. This quantifies Zwicky's (1971) description of galaxies with "compact cores and large, nearly uniform brightness halos."

III. PROFILE DECOMPOSITION

a) Calculation Methods

We have shown that the lenses of compacts mostly have normal parameters. In this §, we wish to find spheroid and disk models which add up to fit the observed profile. We are interested primarily in two questions. How do the parameters of the underlying distributions compare with those derived above? And, how do the component shapes change in this process?

We showed in Papers II and III that the de Vaucouleurs (1948) law best fits tidally unperturbed ellipticals. As shown in Figure 1, it also describes compact galaxy spheroids very well. Since it is also mathematically very well behaved, we will use it here to model spheroids. The parameter values naturally depend strongly on the chosen fitting function (and on photometric errors), but we will show that other functions lead to similar results.

The fitting range is usually divided into two parts, one covering the region where the observations follow the $r^{1/4}$ law, the other covering the exponential. In between is a gap where we do not demand that the model profile fit the data. This allows an investigation of the profile shapes in the transition region. We will verify that no errors are introduced (i.e., no solutions are missed) by

frequently also using an overall fitting range that excludes only the seeing disk.

Two calculation methods are used.

1. Iterative Fitting: Begin by making a least squares fit of (say) an exponential in the disk range. Extrapolate it into the spheroid range, and subtract from the observations to get a first estimate of the underlying spheroid. Fit to this a de Vaucouleurs law. Extrapolate it into the disk range, and subtract from the observations to get an underlying disk. Fit this disk profile, and iterate. In 8-10 iterations both underlying profiles are determined to ≤ 0.01 μ. The calculation can begin with either the spheroid or the disk, resulting in (very different) convergence from opposite directions. However, the solutions agree. In fact, the algorithm is very reliable. Nevertheless, to help define the uniqueness of the results, a more statistically well-defined method is also desirable.

2. Standard Nonlinear Least Squares: Find I_{oV}, r_o, I_{oE} and α^{-1} so that $\mu(r) \equiv -2.5 \log I(r)$, with

$$I(r) = I_{oV}\, 10^{-3.33[(r/r_o)^{1/4}-1]} + I_{oE}\, e^{-\alpha r} ,$$

in obvious notation,

is least squares closest to the observed profile, within the fitting ranges. The disk and spheroid are fit simultaneously. The disadvantage is the (I_{oV}, r_o) and (I_{oE}, α^{-1}) are very strongly coupled. That is, the minimum in the 4-dimensional χ^2 hypersurface is a steep-walled, narrow, diagonal valley, with only a shallow minimum. This means that the relative contribution of spheroid and disk can be varied considerably without very much affecting the quality of the fit. We will discuss this further below. However, the two calculation methods always produce very similar solutions, and the qualitative behavior of the profiles is always well determined.

b) Results: De Vaucouleurs Spheroid and Full Exponential Disk

i) I Zw 21

I Zw 21 has the most accurately measured spheroid-disk transition region of any of the compacts. Since its behavior is also typical, we will discuss it in detail. Most of our comments apply equally well to the other galaxies.

Figure 3 shows the results. Naturally, both spheroid and disk become fainter. The spheroid also becomes steeper, reducing r_o slightly. Meanwhile B_o becomes brighter,

FIGURE 3

Decomposition of I Zw 21 using the iterative fitting algorithm. The various lines are explained in the key. The underlying spheroid profile, which is almost identical to the spheroid model, is not shown. The spheroid fitting range is from 1.2 to 8.4 arcsec, and the disk range from 20 to 32 arcsec. The dotted lines show a decomposition using a fitting range of 1.2 to 32 arcsec. In this and all subsequent figures, μ_B has been corrected for galactic absorption. Since I Zw 21 is also seen face-on, the exponential intercepts are just $B(0)_c$.

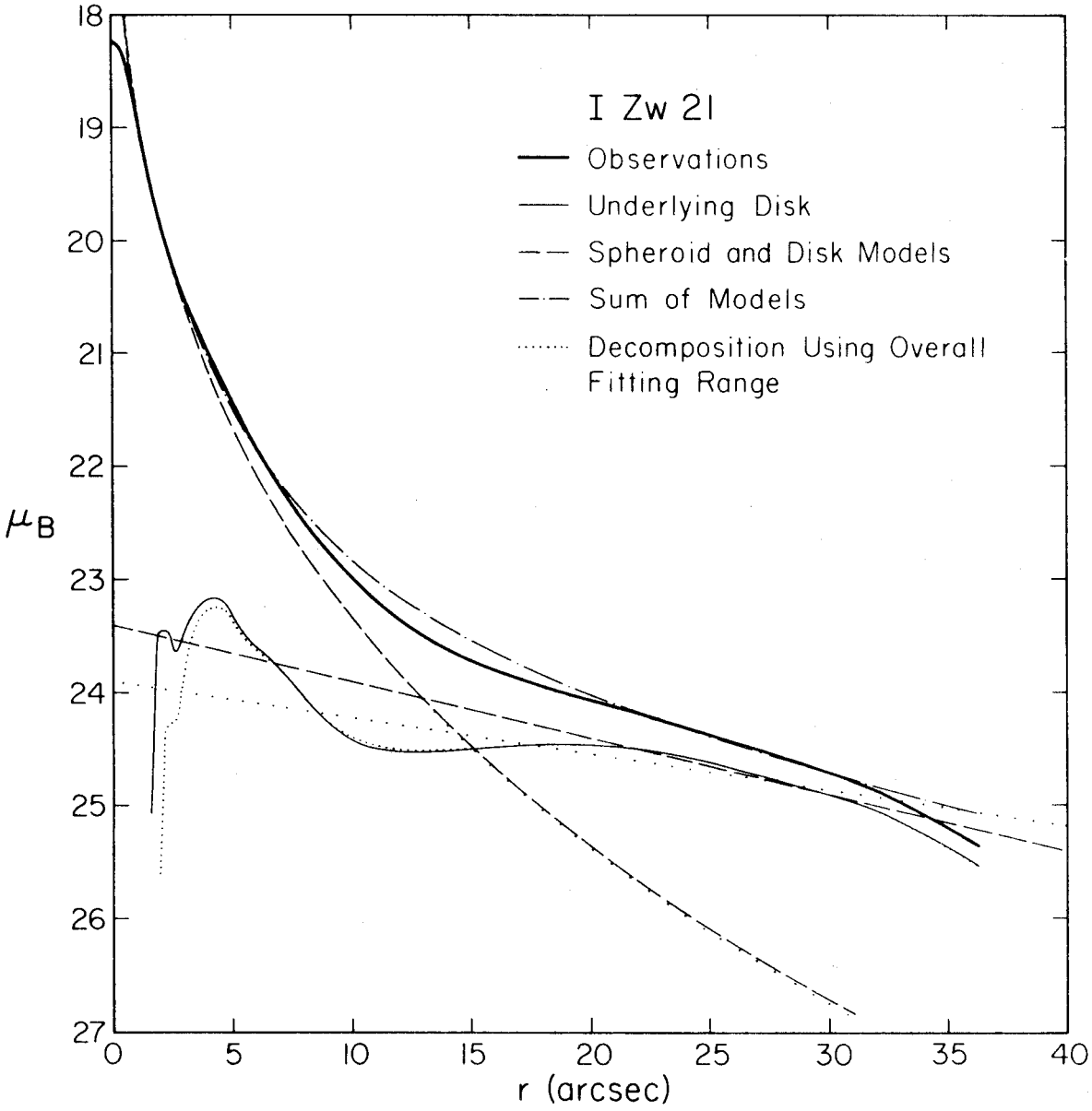
I Zw 21
Observations
Underlying Disk
Spheroid and Disk Models
Sum of Models
Decomposition Using Overall Fitting Range
μ_B
r (arcsec)
18
19
20
21
22
23
24
25
26
27
0
5
10
15
20
25
30
35
40

because the upper part of the spheroid profile is almost unchanged, so that the de Vaucouleurs law intercept is brighter. The new parameters are given in Table 1; we see that the change is only moderate. In contrast, the disk becomes considerably shallower and fainter, and much less exponential. As a result, α^{-1} is very large, essentially indeterminate, and $B(0)_c$ is fainter. Most interesting is the behavior in the transition region. The underlying disk profile has a brightness cutoff as it enters the dominant part of the spheroid.

Before proceeding, we will try to justify the assumption that the cutoff is in the disk.

1. The observationally strongest cases are S0 compacts with strong lenses (I Zw 21, VII Zw 303, and VII Zw 793). But lenses sometimes have cutoffs toward smaller radii which are already obvious without decomposition. Examples include VII Zw 303 (below, see also Paper I), and NGC 1553 (Freeman 1975). The ESO Sky Survey plate shows that NGC 1553 has a bright ring, apparently unresolved by Freeman, with a fainter zone immediately inside it.

2. Exponentials may have similar obvious cutoffs, in Type II profiles.

3. Stars in disks move in nearly circular orbits, while spheroids have hot, nearly isotropic velocity distributions. Thus it is much easier to create sharp features such as edges (or spiral arms!) in disks.

4. We noted earlier that there are observational reasons for believing that spheroids do not stop where disks start.

How strongly do the observations imply a cutoff? For no cutoff, the profile would have to agree with the dot-dashed curve in Figure 3. The maximum deviation is 0.2 μ, which is excluded by the observations. For some other galaxies, a similar deviation could be reduced by changing the way the profile segments were fit together in Paper I. However, in I Zw 21, the transition region and disk were almost completely determined by a single deep Schmidt plate. This was measured three times, with different slit sizes, and on both the Berkeley PDS and the Caltech microphotometer. Thus there was no human intervention in determining the profile shape, from well within the spheroid to the limit of the photometry. With a noise of only a few percent, the observations seem definitely different from the model. The cutoff is real.

Further confirmation comes from making a decomposition with a fitting range that covers the whole galaxy (dotted

lines in Figure 3). The disk profile is virtually unchanged. Only the exponential fit is worse, since the parameters must now recognize the drop in μ at $r^{1/4} \simeq 2.0$. Given a de Vaucouleurs law as the spheroid model, there is very little freedom for the disk shape.

On the other hand, the exact amount of cutoff is not well determined. With much noise, the calculated disk profile is forced to converge on the exponential in the spheroid range, because it is always easy to take the required small amount of light away from the spheroid. This is only an artifact of the calculation. But it fills in any cutoff, so we can tell only that the disk profile must drop by $\gtrsim 1/2\ \mu$ in the transition zone. We will show in c), below, that a complete cutoff is allowed.

Finally, we consider the accuracy of the parameters. The possible tradeoff between the components produces an allowed parameter range which is two or three times as large as the difference between the results of the two calculation methods. However, this is only a formal error, since it does not include errors in the photometry, and since the quantitative results depend on the spheroid model (cf. § III d)). We will use the parameters only in a very approximate way, and for this they are entirely adequate.

ii) VII Zw 793

This was one of the most peculiar galaxies discussed in Paper I. It has an extraordinarily strong, almost completely uniform lens. Figure 4 shows that the shape of this underlying lens is again very nonexponential. As in I Zw 21, it is a broad, nearly uniform plateau in brightness, with strong cutoffs on both sides. The measurements are again accurate enough to be fairly conclusive.

iii) VII Zw 303

The halo of this galaxy is a lens which already has a Type II-like profile before decomposition (see § II and Paper I). It is even more extreme in its requirement for a disk cutoff than the above objects. A decomposition using a full exponential is impossible. However, we will see below that a fully cut off exponential is as successful here as in the other galaxies.

iv) Other Objects

All the other profiles also formally require a disk cutoff. However, for these the data are poor enough that errors might account for the behavior. A typical example is V Zw 257, illustrated in Figure 5. With some difficulty, the profile segments in Paper I could be averaged to remove about half of the difference between the obser-

FIGURE 4

Least squares decomposition of VII Zw 793. The underlying spheroid profile is again omitted since it is nearly the same as the de Vaucouleurs model. The spheroid fitting range is from 1.2 to 8.4 arcsec, and the disk range from 25 to 38 arcsec.

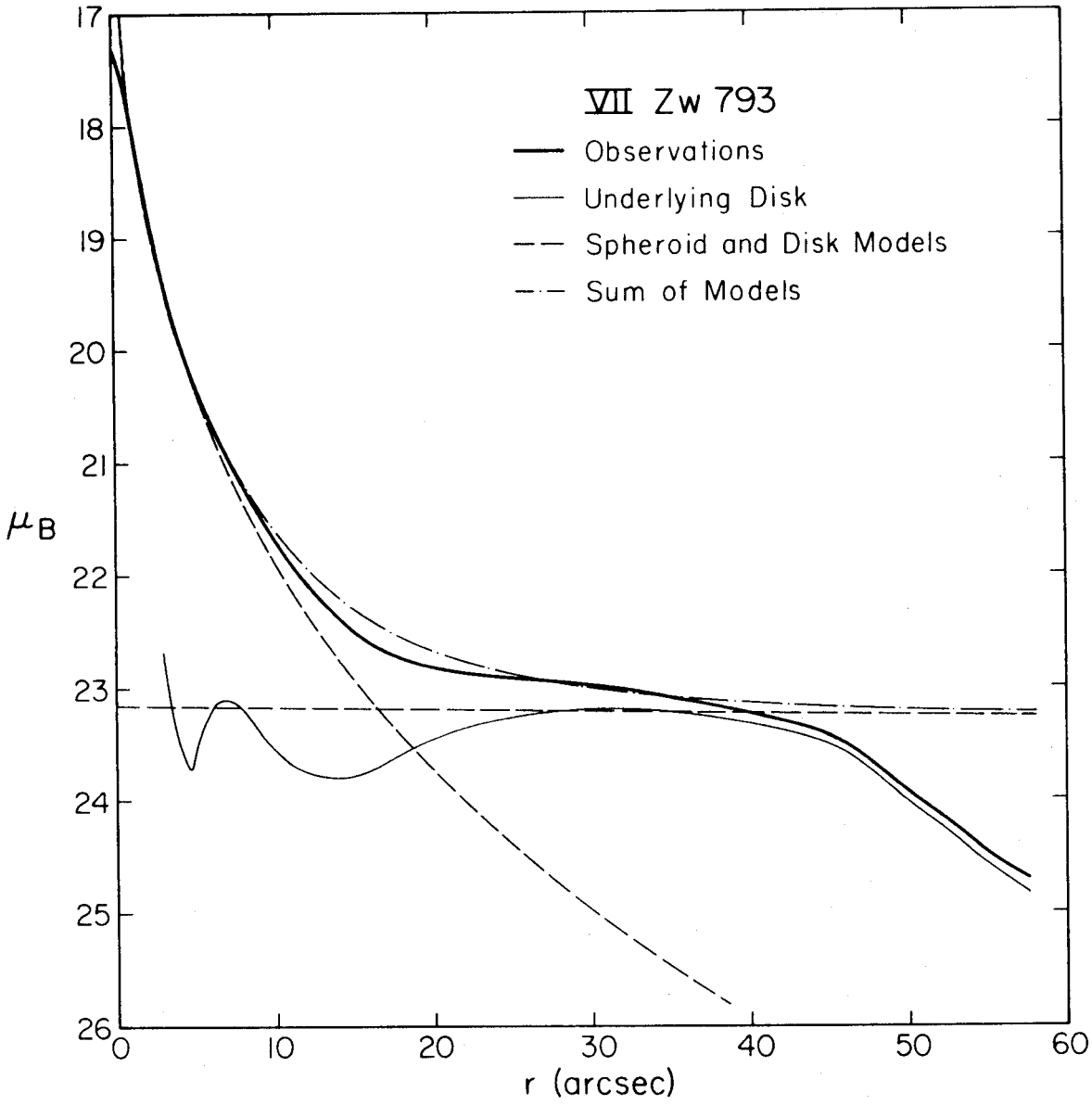
VII Zw 793
Observations
Underlying Disk
Spheroid and Disk Models
Sum of Models
μ_B
17
18
19
20
21
22
23
24
25
26
0
10
20
30
40
50
60
r (arcsec)

FIGURE 5

Iterative fitting decomposition of V Zw 257. The spheroid and disk fitting ranges are 1.7 - 6.6 and 14 - 35 arcsec respectively. A decomposition using a fitting range of 1.7 - 35 arcsec (dotted) again confirms the need for a cutoff. Note that both underlying disk profiles remain very exponential until the cutoff begins. This galaxy may have an exponential rather than a lens disk.

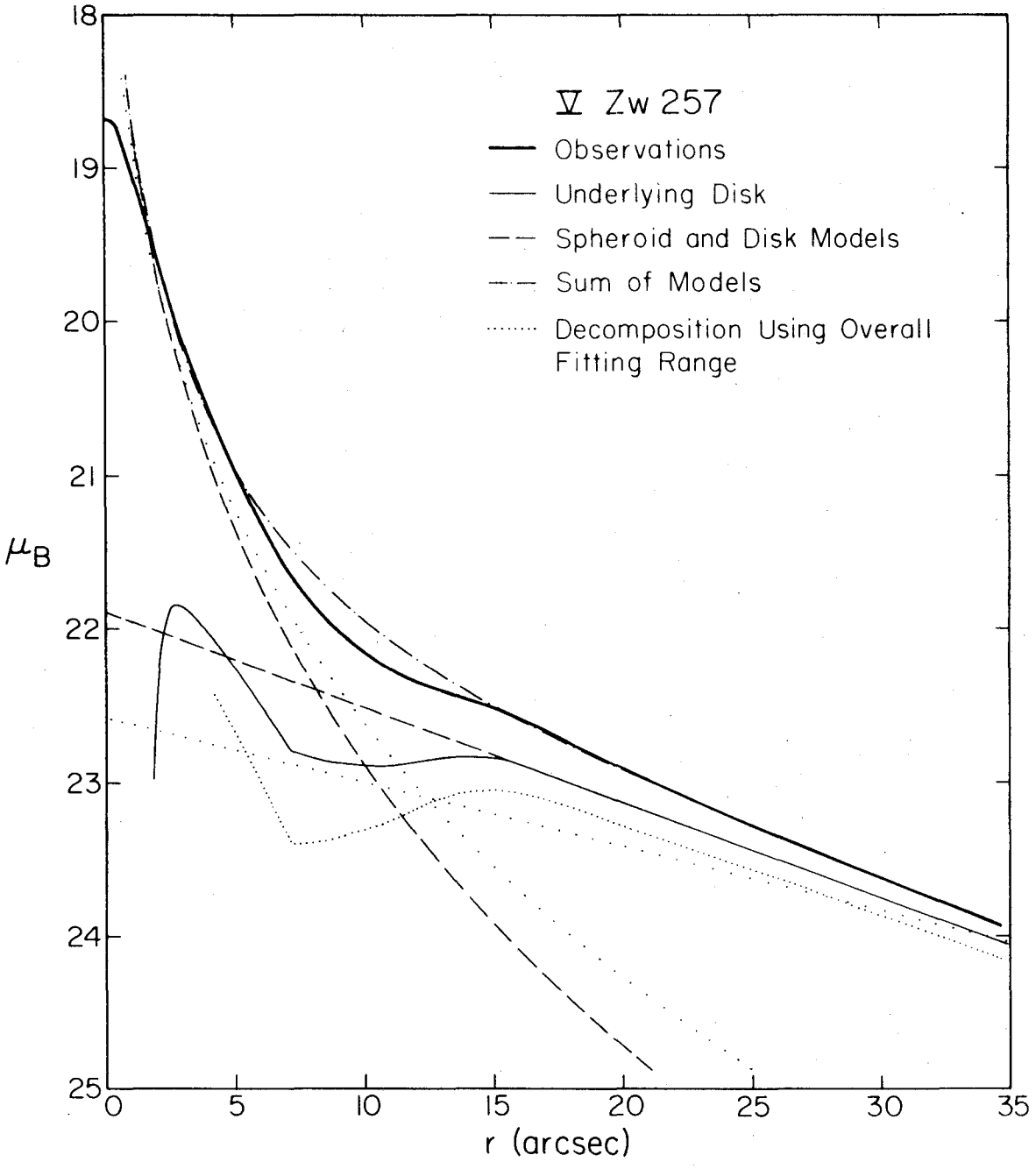
V Zw 257
Observations
Underlying Disk
Spheroid and Disk Models
Sum of Models
Decomposition Using Overall Fitting Range
μ_B
r (arcsec)
18
19
20
21
22
23
24
25
0
5
10
15
20
25
30
35

vations and the dot-dashed curve. Photometric errors might account for the rest. However, the similar behavior of all the galaxies provides additional support for the existence of cutoffs.

c) Results: De Vaucouleurs Spheroid and Cutoff Exponential Disk

We have shown that lens disks tend to cut off by a large but unknown amount as they enter strong spheroids. We would now like to know if they can disappear completely. This requires our choosing a new disk fitting function which has a sharp and complete cutoff at a specifiable radius β, but which is similar to an exponential for $r >> \beta$. A convenient such function is

$$I(r) = I_o \, e^{-(\alpha r + \beta^n/r^n)} \quad , \qquad (1)$$

where n determines the sharpness of the inner edge. A little experimentation shows that n = 3 works well, without making the β^n/r^n term too important for $r > \beta$. It should be emphasized that the above is only a convenient fitting function, like the de Vaucouleurs law, and is not physically meaningful, as an exponential may be.

Figure 6 shows the results for I Zw 21, and Table 1 lists the parameters. The quality of the decomposition is

FIGURE 6

Decomposition of I Zw 21 using a cutoff exponential disk. The spheroid and disk fitting ranges are 1.2 - 8.4 and 11.5 - 32 arcsec respectively. The dot-dashed model is covered almost everywhere by the curve for the observations.

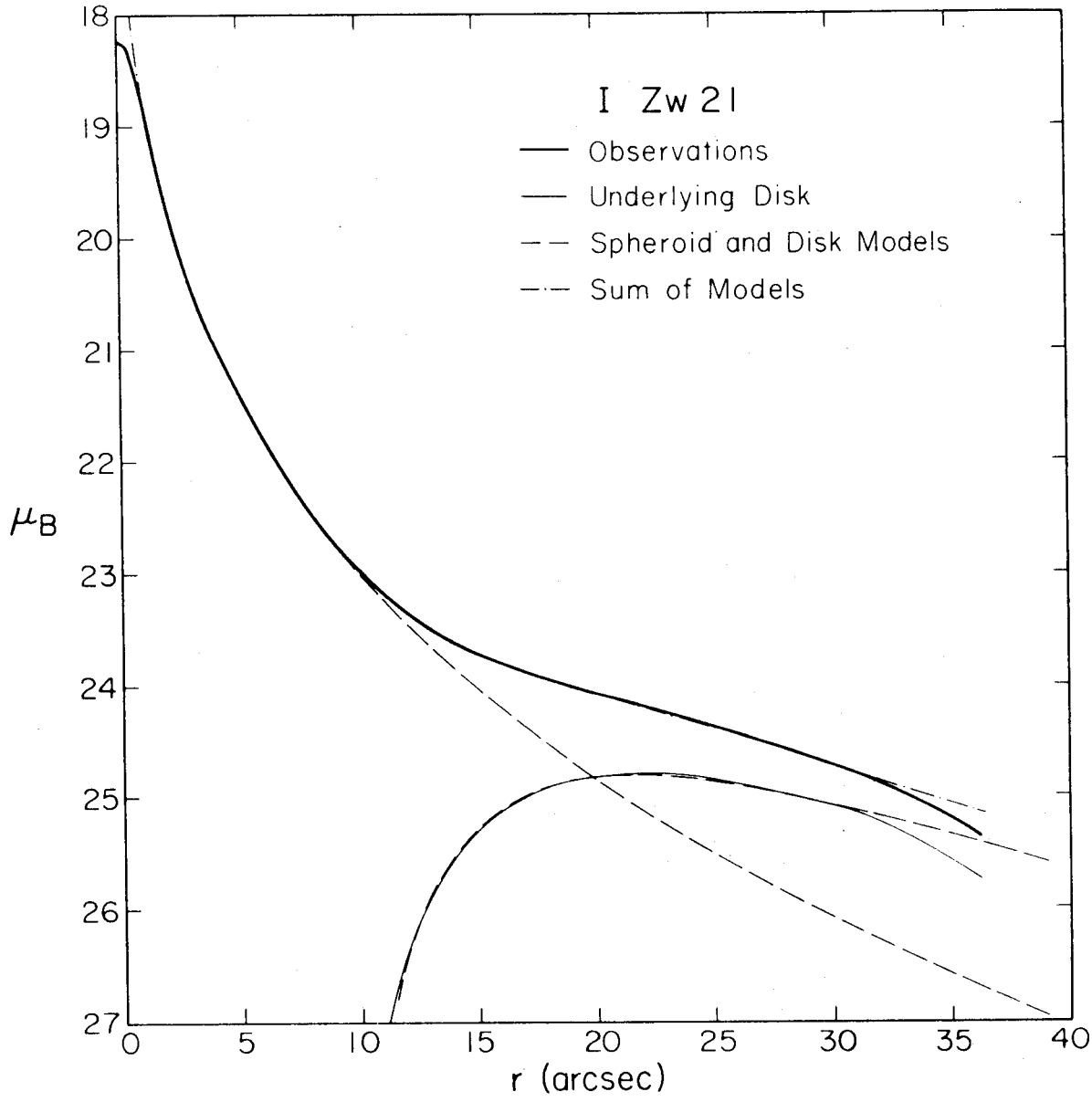
I Zw 21
Observations
Underlying Disk
Spheroid and Disk Models
Sum of Models
μ_B
18
19
20
21
22
23
24
25
26
27
0
5
10
15
20
25
30
35
40
r (arcsec)

excellent; the model reproduces the data to $\leq 0.03\ \mu$ between 1.1 and 32 arcsec. The spheroid is almost completely unchanged in the process, so the disk is somewhat fainter than before. The curved lens profile would be equally well fit with an n = 2 cutoff, and probably a wide variety of other functions.

VII Zw 303 is shown in Figure 7. A full-disk decomposition was impossible for this object, but the cutoff disk succeeds to $\sim 0.02\ \mu$ throughout the galaxy. The difference from I Zw 21 is that β is relatively larger, and the disk brighter, compared to the spheroid. This rather diminishes the difference in principle between Type I and II profiles. The latter may only require a spheroid relatively small and faint enough to uncover a cutoff which exists in many galaxies anyway. Whether this statement, made here for lenses, is also true for real exponentials requires further investigation.

The other galaxies are similarly well decomposed using (1). We have thus shown that there exists an exponential disk model with a complete inner cutoff which allows an excellent decomposition even in the spheroid-disk transition region.

FIGURE 7

Cutoff disk decomposition of VII Zw 303. The spheroid and disk fitting ranges are 1.5 - 13.0 and 15 - 51 arcsec respectively.

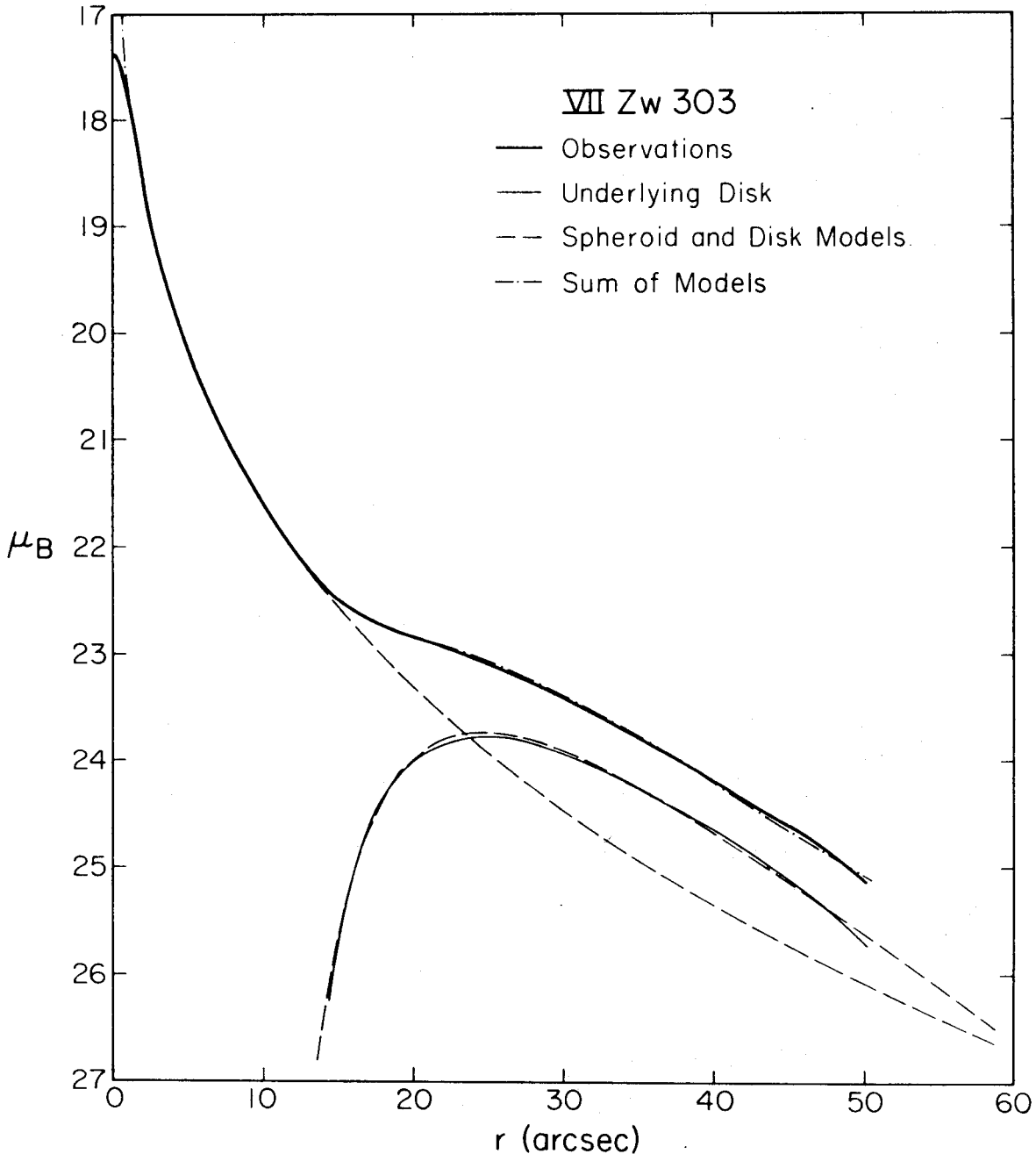
VII Zw 303
Observations
Underlying Disk
Spheroid and Disk Models
Sum of Models
μ_B
17
18
19
20
21
22
23
24
25
26
27
0
10
20
30
40
50
60
r (arcsec)

d) Other Spheroid Models

The discussion so far has all been based on the de Vaucouleurs $r^{1/4}$-law. The shapes of the profiles strongly suggest that this is appropriate. However, to explore the dependence of the results on spheroid models, we will consider here the effect of using the Hubble (1930) law, and the King (1966) model.

A Hubble law decomposition of I Zw 21 is shown in Figure 8. All the other galaxies behave similarly. The inner part of the spheroid fit is largely unchanged. The main difference is at larger radii, where a Hubble profile always drops less steeply than the $r^{1/4}$-law (see Paper III). Thus the extrapolated spheroid is even brighter than before, and so the disk becomes even fainter. It also cuts off very strongly. In essence, the Hubble law fits most of the transition zone without help from the disk, so the latter is forced to disappear completely.

The King (1966) profile is a dynamical model based on an isothermal velocity distribution cut off at the local escape velocity. It was designed to produce a finite limiting radius r_t, and thus fit tidally limited globular clusters. Elliptical galaxies are also moderately well described, with larger values of $c = \log (r_t/r_{core}) \simeq 2.2$ (King 1966, Paper III). We showed in Paper III that the

FIGURE 8

Hubble law decomposition of I Zw 21. The extrapolation of the spheroid is brighter than in the de Vaucouleurs case, and forces the disk to disappear in the transition region. The fitting ranges are the same as in Figure 3.

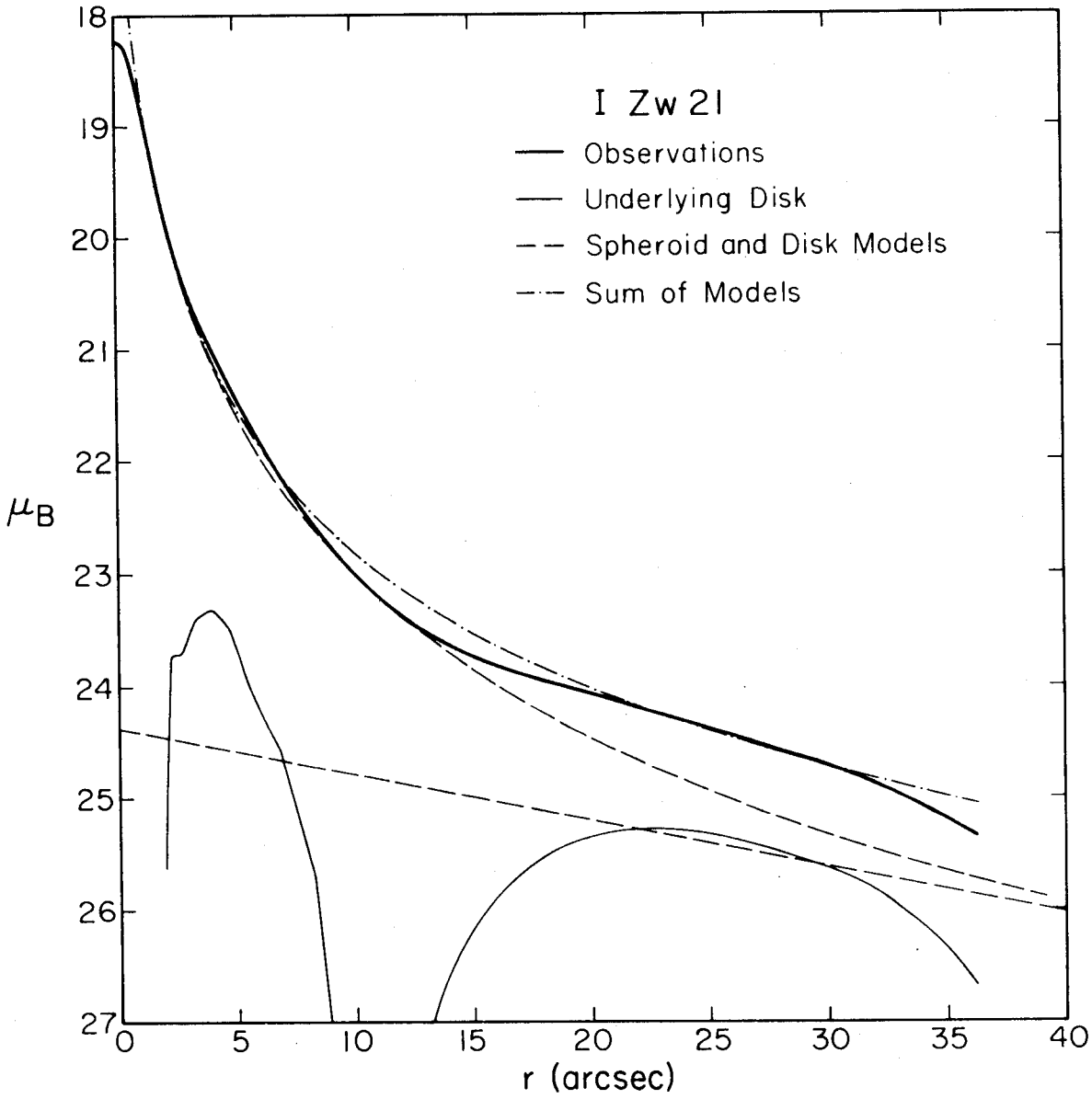
I Zw 21
Observations
Underlying Disk
Spheroid and Disk Models
Sum of Models
μ_B
r (arcsec)
18
19
20
21
22
23
24
25
26
27
0
5
10
15
20
25
30
35
40

King model, like the Hubble law, is brighter than the de Vaucouleurs law at large radii. A normal King model thus requires a disk cutoff at least as strongly as a Hubble law. Only if c is small ($c \sim 1$) does it cut off strongly enough to allow the disk to remain exponential. But such a model is physically very implausible, implying a strong cutoff in the velocity distribution in dynamically isolated objects.

Thus, although the disk parameters can be greatly affected (contrast Figure 8 with Figure 3), the requirement for a disk cutoff is largely model independent.

e) Effect of Decomposition on Parameter Systematics

Consider first the spheroid parameters in Table 1. After decomposition, r_o is smaller and B_o brighter than before. If the disk is required to be everywhere exponential, r_o decreases by $\sim$ 20 - 50%, and B_o by $\sim$ 0.2 - 1 μ. However, a plot of B_o against r_o shows that the points move almost parallel to the B_o (log r_o) relation derived in Paper II. It therefore remains unchanged. Also, we showed that other spheroid models are even less affected by decomposition. And if the disk has an inner edge, as suggested by the data, there is essentially no change in the spheroid parameters (row C in Table 1). Therefore, to good accuracy the conclusions

reached in Paper II are quantitatively unchanged.

The situation is rather different for disks. The spheroid contributes significantly at all radii, so the underlying disk is faint. Often, disks which seemed to have brightness scales near the favored value of 21.65 B_{μ} are intrinsically much fainter. This is especially true when the disk is weak (V Zw 114, VI Zw 111), but it is even important in objects like V Zw 257. If the spheroids were actually Hubble or King models, the effect would be even larger. This suggests that we also investigate the spheroid contribution to the disk brightness scale in normal galaxies (§ IV).

The scale lengths α^{-1} become somewhat larger in decomposition, but do not greatly change Freeman's (1970) parameter distribution. The qualitative effects are more important here. The lenses all become very non-exponential, with broad, rather uniform brightness tops, and inner as well as outer cutoffs. Any distinction between Type I and II profiles is much reduced. Since the profiles of the present objects are so non-exponential, the parameter α^{-1} has little meaning.

IV. ON THE UNIVERSALITY OF $B(0)_c = 21.65$

The remarkable uniformity of the brightness scale of exponential disks, $B(0)_c = 21.65 \pm 0.30(\sigma)$ Bμ for 28 of 36 galaxies (Freeman 1970), has been a puzzle ever since its discovery. We have shown that for several compact galaxies, values of $B(0)_c$ near 21.65 Bμ are produced by the contribution of the spheroid to much fainter disks. In this §, we will investigate whether a similar effect could be important in normal galaxies.

We will consider the distribution of $B(0)_c$ for a series of model galaxies. Each model is the sum of an $r^{1/4}$-law spheroid and an exponential disk. Spheroids are assumed to follow the $B_o(\log r_o)$ relation derived in Paper II, with values of r_o of 0.5, 1, 2, 3, 4, 6, 8 and 10 kpc. This covers the range from very compact objects to giant ellipticals. The disk scale lengths used are α^{-1} = 2, 4 and 8 kpc, covering the range observed by Freeman. For each α^{-1} we use values of the intrinsic $B(0)_c$ which bracket 21.65 μ, namely, 20, 21, 22, 23, 24, 25 Bμ, and ∞ (no disk at all).

A model was constructed for each combination of parameters. The resulting 168 profiles were plotted, and examined to find the most exponential radius range. To

mimic the procedure used with real data, a limiting magnitude of 26 B_{μ} was adopted. An exponential was then fit to the composite model in the chosen range. Figure 9 shows $B(0)_c$ for this fit against the intrinsic brightness of the underlying disk.

The behavior of the points in Figure 9 is very striking. Bright disks tend to dominate, and produce bright values of $B(0)_c$. Seven of the eight Freeman (1970) galaxies with $B(0)_c \neq 21.65$ B_{μ} were similarly bright. However, for nearly any intrinsic $B(0)_c \gtrsim 22$ B_{μ}, the models produce values near 22 B_{μ}. Even spheroids alone have normal parameters. This was noted already in § II. All this suggests that the observed universality of $B(0)_c = 21.65 \pm 0.3$ B_{μ} is largely due to the contribution of the spheroid. Real underlying disks can be much fainter.

Let us consider Figure 9 in more detail. The preferred disk brightness is ~ 22.1 B_{μ}, slightly fainter than Freeman's value. However, it depends rather strongly on the limiting magnitude. If the limit is 25 - 25.5 B_{μ}, which is more reasonable for many of Freeman's galaxies, than $B(0)_c \simeq 21.7$ B_{μ}.

Giant elliptical galaxy spheroids, shown as crosses, tend to have the faintest $B(0)_c \simeq 22.2$ B_{μ}. If there is

FIGURE 9

$B(0)_c$ for composite model galaxies against the real brightness of the underlying disk. The symbol sizes and shapes refer to the model parameters, as described in the key. Filled symbols indicate that the profile was moderately exponential in the fitting range, as in real disk galaxies. Open symbols refer to profiles which were clearly curved in the fitting range. A horizontal line is shown at 21.65 $B_{\odot}$.

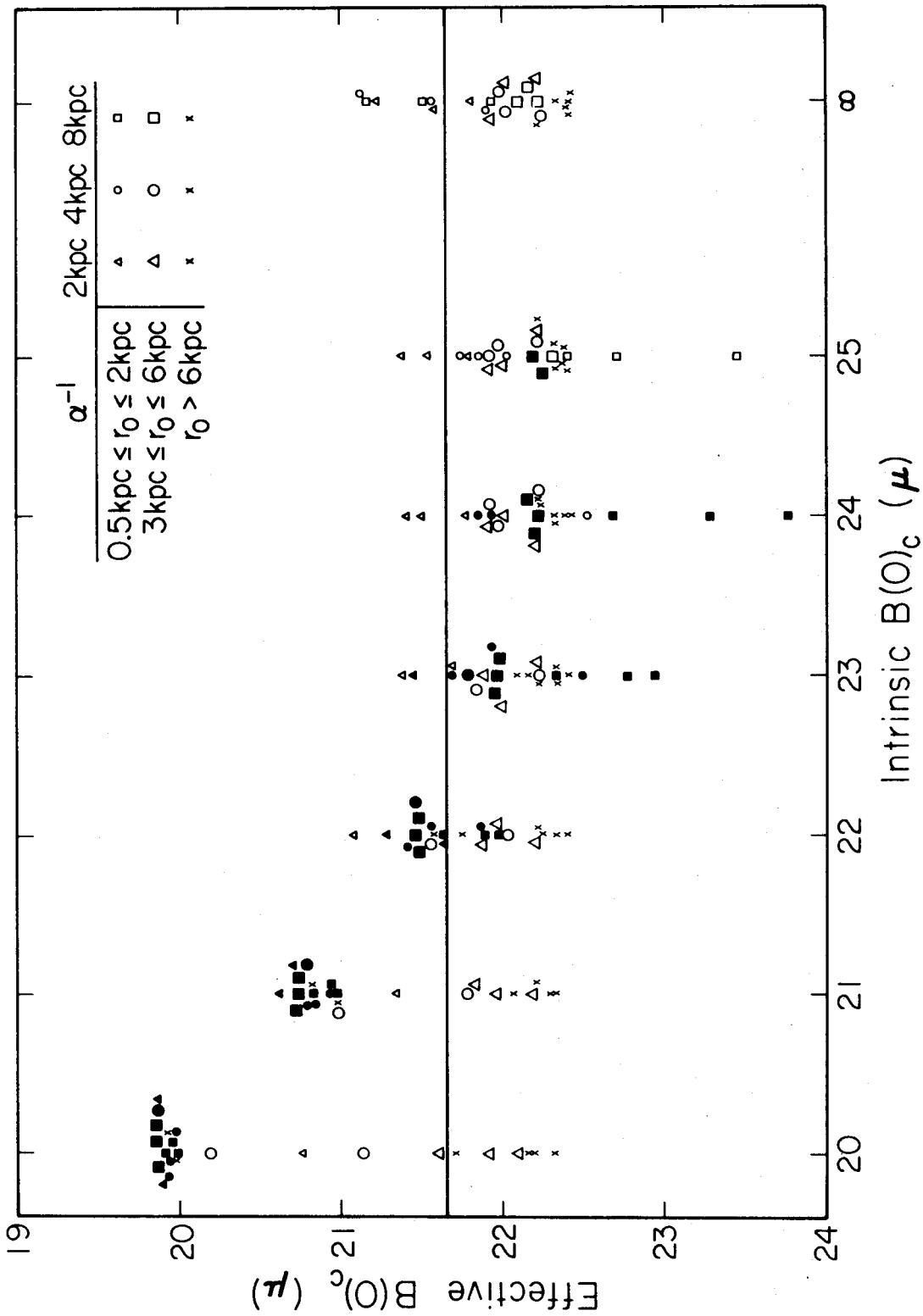
α⁻¹
2kpc 4kpc 8kpc
0.5kpc ≤ r₀ ≤ 2kpc
3kpc ≤ r₀ ≤ 6kpc
r₀ > 6kpc
Effective B(O)c (μ)
Intrinsic B(O)c (μ)
19
20
21
22
23
24
20
21
22
23
24
25
∞

even a slight tidal halo, α^{-1} is increased so much that the disk scale appears even fainter (cf. Figure 2). If an exponential with a scale length of 2 or 4 kpc is added to such a spheroid, it produces only a small ring-like enhancement over a de Vaucouleurs law, usually at small radii compared to any halo. Often the profile is not exponential. Such features have been observed in NGC 524 (Paper I), which seems to have a lens and a disk interior to a tidal halo. I Zw 118A and NGC 4636 (Paper III) may be similar.

Several models in Figure 9 have disk scales near 23-1/2 B_{μ}, much fainter than the normal values. These have the largest disks, which dominate over the shortest scale length spheroids even if they are faint. However, they mostly represent late-type galaxies with large α^{-1}, a combination not found by Freeman. Galaxies later than Sbc all had $\alpha^{-1} \lesssim 4$ kpc, not 8 kpc as in the above models. Thus there is no conflict with previous observations. When galaxies with compact spheroids and disk scales near 8 kpc are found, then faint values of $B(0)_c$ are in fact seen (I Zw 21 and VII Zw 793, in § II).

Thus the models are quite unambiguous in predicting the behavior Freeman observed. They have two shortenings

which prevent them from being completely definitive. We will now show that, while these are not negligible, they probably do not seriously affect the conclusions of this §.

First, we have assumed that spheroids satisfy a de Vaucouleurs law at all radii. For reasons discussed earlier, this should be a good approximation. In fact, deviations tend to occur in the favorable direction of even brighter halos, whether for tidal reasons (Paper II), or because a Hubble (1930) or King (1966) model is appropriate (Paper III). Nevertheless, it would be useful to have direct confirmation, by measuring edge-on galaxies with essentially normal spheroids (eg., NGC 4565 and NGC 4594).

It should also be noted that there exist edge-on galaxies with very peculiar spheroids. Whether these have cutoffs, or even whether they follow a de Vaucouleurs law at all, is unknown. A fairly common feature is a "box-shaped" central bulge, seen with varying strength in objects like NGC 4565, NGC 7332, and especially NGC 128 (Sandage 1961). These objects have been discussed, eg., by de Vaucouleurs (1974b), but are not yet understood. Peculiarities like these might be important in the present context. However, in their more extreme form they might

also be recognizable. For instance, one might expect barred galaxies to look "box-shaped" when seen edge on. The same is true for spheroid-like lenses such as those discussed in Paper I, especially when the lens has a bright outer rim. Probably disks also affect spheroids, as suggested by de Vaucouleurs (1974b) and others. Clearly, these subjects require further investigation, but the peculiarities are usually small enough, or else rare enough, that they seem unlikely to be a problem here.

The second problem is the possible number of galaxies with $B(0)_c = 21.65$ B_{μ} and no spheroid at all. If there are too many, and almost none have fainter values, then there is still an unexplained universality of disk scales.

A partial literature search has been made for galaxies unaffected by a spheroid. It turns out that there are strong selection effects in most of the data, favoring bright disks (see also de Vaucouleurs 1974a). For instance, several galaxies measured by Schweizer (1976) have little or no spheroid, and $B(0)_c \simeq 21.67$ μ, but they are all van den Bergh (1960) luminosity class I. In contrast, Ables (1971) measured low luminosity objects, but most were highly obscured. In fact, Ables found many central disk brightnesses between 22.5 and 23.5 B_{μ}. When corrected for ~ 2 mag of galactic absorption, though,

almost all of these turn out to have abnormally bright $B(0)_c$. Only the two objects with $A_B < 1$ mag have brightness scales fainter than 21 B_{μ}, and one of these has $B(0)_c = 23.96$ μ (IC 1613, see also Freeman 1970). Certainly there are observations of a number of disks with the favored value of 21.65 B_{μ}, and no spheroid. But there are also many which are brighter, and at least one measured one which is fainter. A careful investigation, allowing both for selection effects and spiral structure (Schweizer 1976), is required to see whether disks unaffected by spheroids also prefer $B(0)_c = 21.65$ μ. In the present data, selection effects seem sufficient to account for the behavior.

It should be noted that even a small spheroid can be important (see V Zw 257 in Table 1). Thus it is very difficult to estimate the fractional contribution to the total light of the various components. Since it was not corrected for the spheroid contribution, Freeman's (1970) k greatly overestimates the disk importance. For instance, formal k values for the present galaxies are increased by 0.3 - 1.6 mag by decomposition with a full exponential. With a cutoff exponential the change would be greater. Thus $k \simeq 0$ for any of Freeman's galaxies is not necessarily sufficient to imply that the spheroid contribution is

negligible. This emphasizes again the difficulty in deducing precise parameters for disks in strongly composite systems.

V. CONCLUSIONS

We have examined the problem of decomposing galaxy brightness profiles into their underlying spheroid and disk components. This was suggested by Figure 1, and arguments which imply that each component contributes significant light where the other dominates. The main conclusions are listed below.

(1) Before decomposition, the lenses of compacts are very exponential over short ranges, and have mostly normal parameters. However, I Zw 21 and VII Zw 793 have brightness scales $B(0)_c >> 21.65$ B$_{\mathcal{Y}}$, confirming a general suspicion that there exist galaxies with faint disks. The scale lengths α^{-1}, typically 6-1/2 - 8-1/2 kpc, are at the long end of the range observed by Freeman (1970) for normal galaxies (cf. Zwicky's [1971] description of "large, nearly uniform brightness halos.")

(2) A re-examination of the interpretation and accuracy of the data used suggests that Type II profiles are much rarer than suggested by Freeman (1970).

(3) Decomposition of S0 compacts suggests that the disks must cut off in the transition zone between the two components. Thus lenses seem intrinsically to be

broad, non-exponential brightness plateaus, with cutoffs on both sides. It would be of interest to see if true exponentials have similar inner cutoffs.

(4) The strength of the inner cutoff is poorly determined, but a completely cutoff function of the form $I \propto \exp\{-(\alpha r + \beta^3 r^{-3})\}$ works very well.

(5) The Type II profile of VII Zw 303 look similar, after decomposition, to the other galaxies (see [3]). The difference between Types I and II may not be great. Type II behavior may only require a spheroid which is small and faint enough to uncover a cutoff which exists in many disks anyway.

The relationship between Type II profiles and lenses is unclear. Probably a lens is not just a strong Type II, because a steep drop is often observed in the profile before a shallower exponential begins (cf. NGC 1553 in Freeman (1975), and VII Zw 421 and II Zw 67 in Paper I). However, a Type II profile might result from adding a weak lens to a normal exponential. More data are needed.

(6) The effect of profile decomposition on the spheroid parameter studies of Paper II is small. On the other hand, compact disks which had $B(0)_c \simeq 21.8$ μ

become considerably fainter.

(7) Motivated by this, a series of spheroid and disk composite models was constructed having a large range of parameters. In particular, the disks used had brightness scales of 20 - 25 B_{μ}. Exponential fits were then made to the summed profiles. The brightest disks are dominant, and produce effective $B(0)_c$ which are bright, but almost any disk with intrinsic $B(0)_c \gtrsim 22$ B_{μ} produced a value near 21.65 μ. Thus the observed universality of $B(0)_c \simeq 21.65 \pm 0.30(\sigma)$ B_{μ} (Freeman 1970) is largely due to the contribution of the spheroid. The real disks can be much fainter.

Photometry of galaxies with no spheroid at all is found to be consistent with this conclusion. There are strong selection effects in much of the data, favoring bright disks. Of course, 21.65 B_{μ} will always be near the center of the range of observed values, because disks much fainter than the sky are very hard to find and measure (cf. de Vaucouleurs 1974a). But it no longer seems necessary to explain a compelling universality in disk brightness scales.

REFERENCES

Ables, H. D. 1971, Pub. U. S. Naval Obs., Ser. II, 20, 3.

Burstein, D. 1976, to be published.

de Vaucouleurs, G. 1948, Ann. d'Astrophys., 11, 247.

_____. 1958, Ap. J., 128, 465.

_____. 1959, Hdb. d. Phys., 53, 311.

_____. 1974a, in The Formation and Dynamics of Galaxies (IAU Symposium No. 58), ed. J. R. Shakeshaft (Boston: D. Reidel), p. 1.

_____. 1974b, ibid, p. 335.

_____. 1975, Ap. J. Suppl., 29, 193.

de Vaucouleurs, G., and Freeman, K. C. 1972, in Vistas in Astronomy, Vol. 14, ed. A. Beer (Oxford: Pergamon Press), p. 163.

Eggen, O. J., Lynden-Bell, D., and Sandage, A. R. 1962, Ap. J., 136, 748.

Freeman, K. C. 1970, Ap. J., 160, 811.

_____. 1975, in Dynamics of Stellar Systems (IAU Symposium No. 69), ed. A. Hayli (Boston: D. Reidel), p. 367.

Hubble, E. 1930, Ap. J., 71, 231.

King, I. R. 1966, A. J., 71, 64.

_____. 1975, private communication.

Kormendy, J. 1976a,b,c, in preparation.

Kormendy, J., and Bahcall, J. N. 1974, A. J., 79, 671.

Liller, M. H. 1960, Ap. J., 132, 306.

_____. 1966, ibid, 146, 28.

Ostriker, J. P., and Peebles, P. J. E. 1973, Ap. J., 186, 467.

Sandage, A. 1961, The Hubble Atlas of Galaxies (Washington: Carnegie Institution of Washington).

Schmidt, M. 1975, Ap. J., 202, 22.

Schweizer, F. 1976, submitted to Ap. J. Suppl.

Spinrad, H., and Ostriker, J. P. 1974, Bull. A.A.S., 6, 332 (A).

van den Bergh, S. 1960, Ap. J., 131, 215.

Zwicky, F. 1971, Catalogue of Selected Compact Galaxies and of Post-Eruptive Galaxies (Guemligen: F. Zwicky).